"Durable Catalysts for Fuel Cell Protection during Transient Conditions"

DOE/3M Company Award DE-EE0000456

Radoslav Atanasoski, Principal Investigator

Subcontractors and Federally Funded Research and Development Centers:

Dalhousie University, Halifax, Nova Scotia, Canada
Oak Ridge National Laboratory, Oak Ridge, TN
AFCC Automotive Fuel Cell Cooperation, Burnaby, BC, Canada
Argonne National Laboratory, LeMont, IL

Final Report

Authors: Radoslav Atanasoski; rtatanasoski@mmm.com
Dennis van der Vliet; dfvandervliet@mmm.com
David Cullen; cullenda@ornl.gov
Ljiljana Atanasoska; llatanasoska@mmm.com

Duration of Effort: August 01, 2009 – June 30, 2014 (59 Months)

Executive Summary

The objective of this project was to develop catalysts that will enable proton exchange membrane (PEM) fuel cell systems to weather the damaging conditions in the fuel cell at voltages beyond the thermodynamic stability of water during the transient periods of start-up/shut-down and fuel starvation. Such catalysts are required to make it possible for the fuel cell to satisfy the 2017 DOE targets for performance and durability.

The project addressed a key issue of importance for successful transition of PEM fuel cell technology from development to pre-commercial phase. This issue is the failure of the catalyst and the other thermodynamically unstable membrane electrode assembly (MEA) components during start-up/shut-down and local fuel starvation at the anode, commonly referred to as *transient conditions*. During these periods the electrodes can reach potentials higher than the usual 1.23 V upper limit during normal operation. The most logical way to minimize the damage from such transient events is to minimize the potential seen by the electrodes. At lower positive potentials, increased stability of the catalysts themselves and reduced degradation of the other MEA components is expected.

This project was built on the already recognized durability of 3M's nano-structured thin film (NSTF) catalyst, by further advancing its usability for transient conditions. Our approach for enabling fuel cell systems to endure/mitigate the damaging starvation conditions was to develop and implement catalysts with high activity towards the oxygen evolution reaction (OER) from water. We have modified both the anode and the cathode catalysts to favor the oxidation of water during transient conditions and to maintain the potentials close to the thermodynamic onset for water oxidation. To avoid the complexity of system-related approaches (cell voltage monitoring, gas purging, *etc.*) and improve the reliability, our method is materials based. As such, the protection is from within the MEA and is therefore always "ON".

During the course of the program we developed a highly active OER catalyst that allowed us to accomplish the program milestones by adding marginal amounts of platinum group metals (PGM). This paves the way for the 2017 DOE target for durability and for 0.1 mg/cm^2 of PGM loading to be achieved.

The OER enabled catalyst was successfully scaled up and its effectiveness was proven by several major automotive manufacturers both in their laboratories as well as in their more realistic 'real life' simulated testing in over two dozen short fuel cell stacks.

Glossary of Acronyms

AFCC	Automotive Fuel Cell Corporation
ANL	Argonne National Laboratory
BE	Binding Energy
BF	Bright Field
BOL	Beginning of Life
BOT	Beginning of Test
CCM	Catalyst Coated Membrane
COR	Carbon Oxidation Reaction
CR	Cell Reversal
CV	Cyclic Voltammogram
DC	Direct Current
ECSA	Electrochemical Surface Area
EDS	Energy dispersive X-ray spectroscopy
EOL	End of Life
EOT	End of Test
FC	Fuel Cell
GDL	Gas Diffusion Layer
GS	Gas Switching
HAADF	High-Angle Annular Dark Field
HOR	Hydrogen oxidation Reaction
LC	Load Cycle
LCGS	Load Cycle - Gas Switch
MEA	Membrane Electrode Assembly
MPL	Micro porous Layer
NMR	Nuclear Magnetic Resonance
NOC	Normal Operating Condition
NSTF	Nanostructured Thin Film
OEM	Original Equipment Manufacturer
OER	Oxygen Evolution Reaction
ORR	Oxygen Reduction Reaction
ORNL	Oak Ridge National Laboratory
PEM	Proton Exchange Membrane
PGM	Platinum Group Metals
PR	Perylene Red
PVD	Physical Vapor Deposition
RDE	Rotating Disk Electrode
RF	Radio Frequency

RRDE	Rotating Ring-Disk Electrode
SE	Secondary Electron
SHE	Standard Hydrogen Electrode
SIROF	Sputtered Iridium Oxide Films
STEM	Scanning Transmission Electron Microscopy
SU/SD	Start-up Shut Down
XAFS	X-Ray Absorption Fine Structure
XPS	X-Ray Photoelectron Spectroscopy
WDS	Wavelength Dispersive Spectroscopy
WUP	Warm-up Condition

Table of Contents

1. Introduction 6
   1.1. Project Justification, Original hypotheses and Approaches 6
   1.2. Technical Concept 6
   1.3. Innovation and novelty of the concepts 17
   1.4. Work Plan 17
2. Task 1: Efficient Oxygen Evolution Reaction Catalysts 20
   2.1. Initial assessment of OER activity of individual elements on Pt/NSTF 20
   2.2. OER activity of binary Ir – Ru Catalyst on Pt/NSTF 26
3. Task 1: Start up/ Shutdown 38
   3. 1. Accomplishments 38
   3. 2. Test Protocol 38
   3. 3. Go/No go Requirements 43
4. Task 1: Cell Reversal 49
   4.1. Go/ No Go CR testing 53
   4.2. Independent and comparative evaluation 57
5. Task 2: Oxygen Reduction Suppression on Anode 61
   5.1. Selective catalysts for the hydrogen oxidation and oxygen reduction reactions 62
   5.2. Oxygen Reduction Suppression by IrRu on low Pt loading 65
   5.3. ORR Suppression with "Mixed" Anode Catalyst 67
   5.4. Independent evaluation 68
6. Task 3: OER Capable Anode Scale up 69
   6.1. AFCC OER/NSTF Evaluation of the NSTF anode + OER concept 70
7. X-ray Photoelectron Spectroscopy and Scanning Transmission Electron Microscopy 77
   7. 1. Nature of sputter-coated Ir, Ru, and Ti films on Pt-NSTF 77
   7. 2. Effect of loading on structure of $Ir_{0.9}Ru_{0.1}$ OER catalysts 80
   7. 3. Stability and Impact in Start-up/Shutdown and Cell Reversal Tests 82
   7. 4. Understanding extraordinary stability of OER catalysts 84
8. Cell reversal durability of the anode during Start-up/Shutdown via gas switches 89
   8. 1. Technical Targets 89
   8. 2. Gas Switching 90
   8. 3. Durability under Load Cycle + Gas Switch (LCGS) 102
   8. 4. Location/Site Separation of the OER Catalyst from Pt 103
9. Conclusion: Summary of Major Accomplishments 105
10. Publications, Presentations, Websites and Inventions 108
   10. 1. Publications 108
   10. 2. Invited Presentations 109
   10. 3. Presentations 110
   10. 4. Web sites 111
   10. 5. Presentations to DOE 112
   10. 6. Inventions 113
11. References: 114

1. Introduction

1.1. Project Justification, Original hypotheses and Approaches

The objective of this project was to develop catalysts that will enable proton exchange membrane (PEM) fuel cell systems to weather the damaging conditions in the fuel cell at voltages beyond the thermodynamic stability of water during the transient periods of start-up/shut-down and fuel starvation. Such catalysts are required to make it possible for the fuel cell to withstand tens of thousands start-up/shut-down cycles and satisfy the DOE targets for performance and durability.

In order to compare the actual accomplishment of the project with the goals and the objectives as originally proposed, an extensive overview of the proposal will be presented. Thus, this section will also serve as the *technical background* to the work performed during the project. Because the assumptions upon which the proposal was based were confirmed, and as a result remained the same throughout of the project duration, sufficient details will be also included.

One major unforeseen but positive divergence from the work plan was the orientation towards the 'real life' application. This necessitated a quicker path towards the scale up phase, which sprouted many innovative approaches driven by the 'real life' evaluation feedback.

1.2. Technical Concept

1.2.1. Overall Relevance, Applicability and Approach

In the proposal for this project we have addressed one of the key issues of importance for successful transition of PEM fuel cell technology from the development to a pre-commercial phase (2010 - 2015). The issue, which is still actual, is failure of the catalyst and the other thermodynamically unstable membrane electrode assembly (MEA) components during start-up/shut-down and local fuel starvation at the anode, hereafter referred to as *transient conditions*. During these periods the electrodes can reach potentials much higher than usual 1-1.2 V during normal fuel cell operation. The most logical way to minimize the damage from such transient events is to minimize or limit the potential seen by the electrodes. At lower positive potentials, increased stability of the catalysts themselves and reduced degradation of the other MEA components is expected. The goal of this project was to develop catalysts that would reduce the potentials experienced during transient conditions. In order to achieve the above goal we worked on two major concepts:

- *Catalysts with high oxygen evolution reaction activity*
- *Anode catalysts with low oxygen reduction reaction activity.*

1.2.1. a. Catalysts with high oxygen evolution reaction activity

In this task we had to identify catalysts with high oxygen evolution reaction (OER) activity in order to maintain the lowest possible potential above the thermodynamic potential (1.23 V at Room Temperature) required for the decomposition of water during high voltage transients. A highly active OER catalyst will be able to satisfy high oxidative current demands at potentials close to the OER thermodynamic potential, thereby minimizing carbon corrosion and platinum oxidation. It is likely that these catalysts will not be good oxygen reduction reaction (ORR) catalysts. Therefore, the OER catalyst had to be integrated with the ORR catalyst in such a way that the catalytically active ORR sites are not blocked. Our early evidence suggested that depositing discrete particles with high OER activity on top of the ORR catalyst on the cathode could be the best approach, as contact of particles with the catalyst will block only a very small fraction of the ORR active surface area. Because the anode can undergo high positive potential excursions as well, particles of this kind can also be applied to the surface of the anode catalyst, without significantly impacting its hydrogen oxidation activity (HOR).

1.2.1. b. Anode catalysts with low oxygen reduction reaction activity

For this concept, the aim was to develop and modify an anode catalyst to have very low ORR activity without loss of activity for the HOR. Suppressing the ORR at the anode will lower the oxidative current demand on the cathode during transient events. This will in turn reduce the potential on the cathode during such events. The concept of ORR inhibited anode catalysts is based on the difference in reactivity of oxygen reduction, which is known to be a very demanding reaction, and the facility with which hydrogen oxidation proceeds. Blocking the reactive sites on the anode catalyst will inhibit the ORR disproportionately more than the HOR. This can be achieved either by adding or alloying the anode catalyst with an ORR inhibiting component, *i.e.* by co-deposition during the physical (or reactive) physical vapor deposition (PVD) process, or by over-coating the anode catalyst.

1.2.2. General background

This project was built on the already recognized durability of 3M's nano-structured thin film (NSTF) catalyst by further advancing its usability for transient conditions [1, 2]. We have also shown that NSTF catalysts are significantly more stable during high voltage operation than carbon supported catalysts [2]. However, even with such a stable catalyst support system there is a need to minimize the high potential excursions in order to protect other cell components, especially the carbon-based gas-diffusion layer (GDL) and bipolar flow field plates, and to further reduce Pt surface area loss (albeit already low with NSTF-coated catalysts) due to oxidation/dissolution. Technology that results in lower voltage excursions during transients will also benefit fuel cells that utilize dispersed, carbon-supported catalysts in their MEAs as lower potentials will reduce the

carbon support corrosion rate. As a result, this project has broad applicability across a wide range of PEM fuel cell technologies.

New catalysts were developed by adding to and/or modifying the existing PVD processes used for NSTF catalyst fabrication [3]. These processes are flexible and amenable to structural and compositional modifications of the catalyst for desired properties to be achieved and they encompass techniques such as reactive DC magnetron sputtering. The catalysts were deposited onto the same inert substrate and support structures used in 3M's large scale MEA production process. The deposition techniques allow for straightforward scale-up. The above approaches require a detailed examination of the interface between the existing NSTF catalyst and the newly implemented modifications, from both practical and fundamental points of view. Appropriate provisions were included in the work plan to study the nature of the modified catalysts from a more fundamental perspective. Since the catalyst development involves discrete nanometer-scale particles and/or clusters, characterization of individual particle compositions, atomic-structures, morphology, and sizes must be closely examined before, during and after transient events. Thus, high-resolution electron microscopy, including high-angle annular dark field (HAADF) scanning transmission electron microscopy (STEM), was a critical tool for the sub-nanometer-scale characterization of the new catalyst compositions and resulting NSTF structures [4,5].

In order to control MEA costs, the total platinum group metal (PGM) loading was kept low, taking into consideration that the PGM content of the durable catalyst for transient conditions satisfies the DOE stated term target.

1.2.3. Technical background and prior results

As evidenced by the patent literature, catalyst durability during transient periods of Fuel Cell (FC) operations defined as start-up/shut-downs (SU/SD) and fuel starvation has been recognized as an issue by the system integrators and stack manufacturers for quite some time (see, for example, [6]). In 2005 SU/SD came to prominence in the open literature with the appearance of the UTC paper by Reiser *et al.* [7]. As illustrated in Figure 1.1, an indication of how serious and widespread the problem was, this publication was almost simultaneously followed by a number of reports from industry and academia which presented ample experimental evidence and modeling results testifying to its importance.

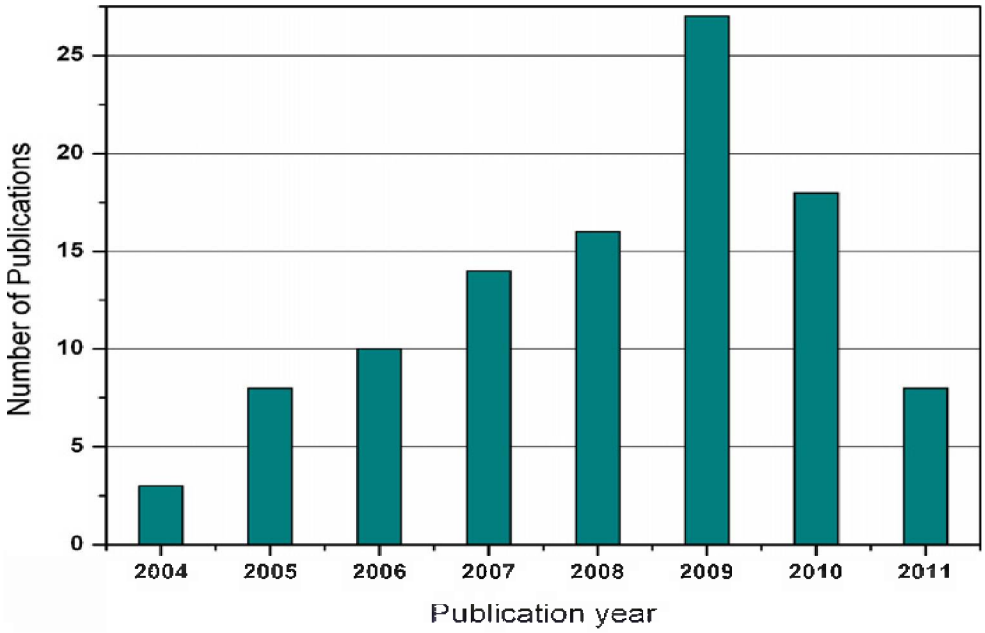


Figure 1.1. Publication history of articles after 2004 on the startup and shutdown processes of PEMFCs. After Y. Yu *et al.*, Journal of Power Sources *205 (2012) 10– 23*

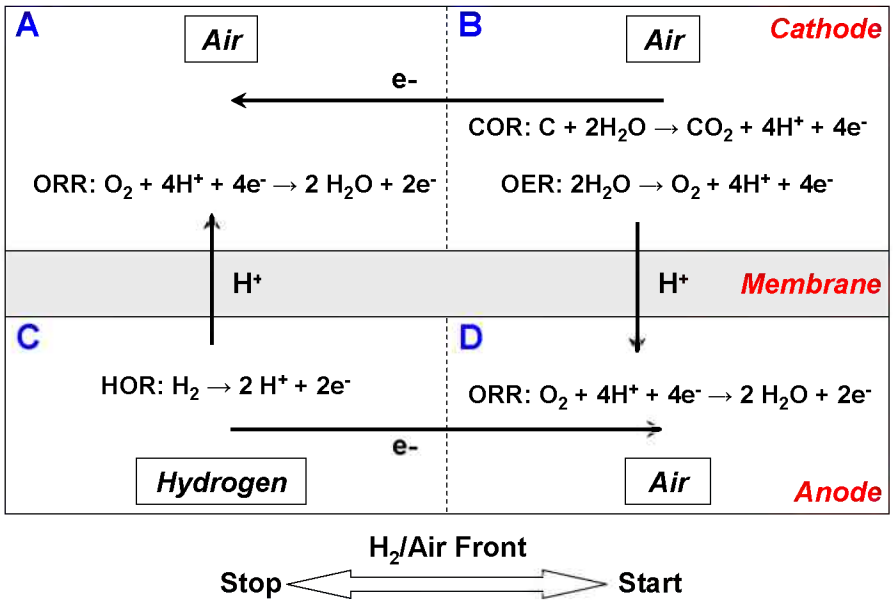


Figure 1.2. Schematic representation of a PEMFC experiencing a H_2/air-front during start-up/shut-down and accompanying major electrochemical reactions [8]. A, C; normal FC operation; B, D; operation in fuel starved region.

Figure 1.2 illustrates the problems arising from reactions taking place during the transient phenomena. As indicated in this figure, the reactions occurring on the part (B) of the cathode facing any anode area (D) depleted of hydrogen are oxidation of carbon (COR) and oxidation of water (OER). In both reactions, protons are produced to satisfy the ORR demand on the fuel deprived part of the anode side (region D). Corrosion of carbon is thermodynamically favored, but the

kinetics and mechanism of this reaction are such that the cathode potential quickly moves up to more positive values initiating the oxidation of water. The OER is not a facile reaction, requiring a high overpotential to proceed at a given rate (see [9] for overview). The best catalyst for the OER, unlike for the ORR, is not platinum. At voltages above 1.2 V, platinum is covered with oxides that are not catalytically active for the OER. As a consequence, the high overpotentials increase the rate of corrosion of the carbon-containing components of the MEA; any carbon catalyst supports, the micro-porous layer (MPL) of the GDL, even the bipolar plate materials.

In summary, the two directions that we have proposed to mitigate the problems during the transient regimes can be rationalized as follows (with reference to the schematic in Figure 1.2): First of all, the presence of a highly active OER catalyst on the cathode will reduce the cathode overpotential in region B for a given current demand. Secondly, inhibition of the ORR on the anode side will lower the ORR current in region D. This then lowers the OER current on the cathode (region B) through reduced proton demand and thus further reduces the overvoltage at the cathode.

1.2.4. Concept #1: Catalyst with high activity towards oxygen evolution

The purpose of developing catalyst with high activity towards OER is to maintain the cell voltage as low as possible during transient periods. The main challenge here is to add an OER catalyst component to the existing, highly active ORR catalyst without compromising this activity. Therefore, the goal is to produce a catalyst that will maintain the cathode potential as close as possible to the thermodynamic potential required for the oxidation of water. The proposed approach was based on:

- Our own fundamental understanding and practical experience with the materials and the processes involved in catalyst synthesis, both within and outside the fuel cell area;
- Full awareness of new developments outside our organizations (open and patent literature and input from 3M's customers);
- The encouraging results of our preliminary experiments done in a FC environment.

There is a wide agreement in the literature that RuO_2 is one of the most active OER materials (Figure 4). According to Trassati and O'Grady [10], at 1 mA/cm^2, a typical value for oxygen cross-over, the OER runs at ~ 1.42 V on RuO_2 films, a potential which is more than 400 mV lower than on bulk platinum. It also has a low Tafel slope (40 mV/decade of current density) and thus it can sustain 100 mA/cm^2 before reaching 1.5 V. RuO_2 is therefore much more active towards the OER than Pt. However, at 1.4 V, it transforms from RuO_2 to RuO_4 [11], which in an acidic environment is released as gas. RuO_2 therefore needs to be stabilized. The stabilizing components usually come from the family of MO_2 that are isomorphous to rutile RuO_2. IrO_2 is a PGM oxide that, in addition to having a stabilizing effect on RuO_2, is itself, a very active OER catalyst. Previously, we have studied the surface properties of a mixed IrO_2/RuO_2 catalyst and have found that iridium surface enrichment occurs after prolonged electrolysis. Simultaneously, the Tafel slope shifts from 40

mV/decade to 60 mV/decade for 100% IrO_2 (see Figure 1.4) [12 -14]. Depending on the catalyst preparation method and the degree of mixing of these two components, the 40 mV/decade slope is preserved with 75% Ir present at the surface, indicating the amount of Ru to be targeted in future studies. Nonetheless, the segregation problem can be eliminated with different synthesis methods. If complete dispersion of the two components is achieved, for example by depositing RuO_2 and IrO_2 by reactive sputtering in vacuum, no surface segregation or preferential dissolution of the components is observed [15].

We have also studied the stability and the interaction of RuO_2 with TiO_2, another well known stabilizing component for RuO_2. However, TiO_2 is not OER active. The mixed RuO_2 + TiO_2 system has been very widely studied ever since the introduction of this catalyst in the chlor-alkali industry (known as DSA^R; for general ref. see [16]). Our prior work has direct relevance to this project because we have generated the RuO_2/TiO_2 interface by PVD in vacuum before, a method that we have proposed for the catalyst fabrication here. We have found that TiO_2 increases the temperature of RuO_2 decomposition in vacuum from 400 °C to above 600 °C [17]. TiO_2 also acts as non-PGM diluents. Up to 80% of the catalyst content can be TiO_2 without loss of the desired catalytic properties (see *e.g.* [16]). The same applies to oxides with similar properties to TiO_2, such as oxides of tantalum, zirconium etc.

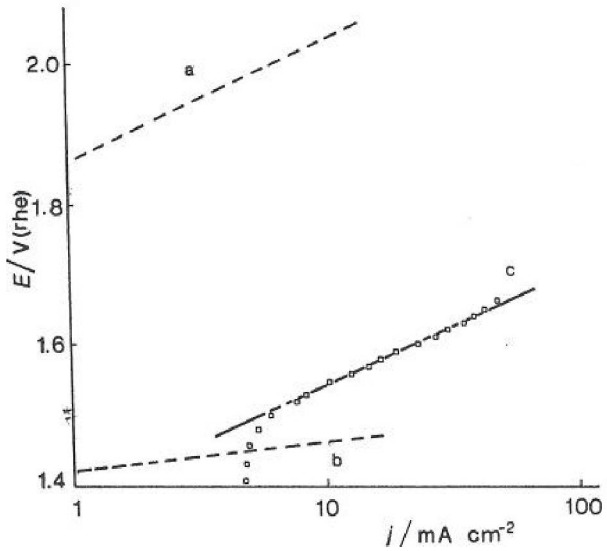


Figure 1.3. Polarization curves for oxygen evolution on (a) Pt, (b) RuO_2 single crystal, and (c) RuO_2 film. 1M $HClO_4$ at 25 oC [11].

Before the start of this project, the literature for sputtered PGM catalysts came mainly from two different areas of application. The medical device industry focuses mostly on sputtered IrO_x films (SIROF) as the charge delivery vehicle for a variety of stimulations (*i.e.* defibrillator leads) with high stability and high charge capacity. Both features are of direct interest for this project, the stability being the more obvious. The SIROF related papers pay close attention to the structure and morphology of the IrO_x film coatings, providing a lot of background information on how the

processing conditions impact the resulting product properties. For instance, Wessling *et al.* have compared RF and DC magnetron reactive sputtering on cold or hot substrates and showed that DC deposition on a cooled substrate generates an IrO_x morphology most appropriate for stimulation purposes [18].

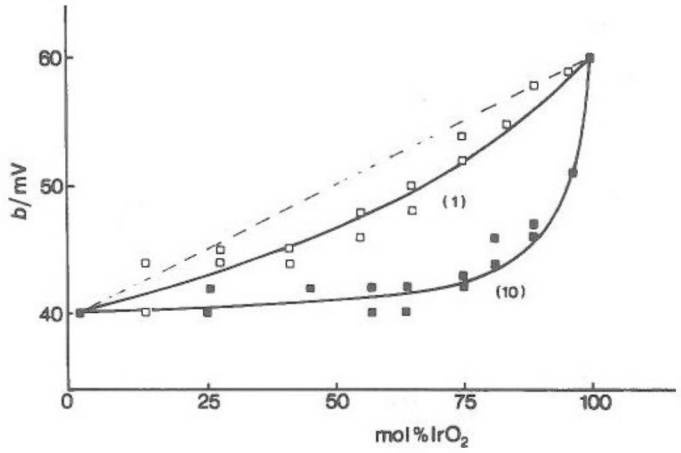


Figure 1.4. Dependence of Tafel slopes for OER on the surface composition of two $RuO_2 + IrO_2$ electrodes [12]; PGM precursors in aqueous (open) and non-aqueous solvents (closed). PGM content by XPS [13, 14]].

The other area with relevant data is either a part of or is closely related to FC technology. Vacuum deposition processes have been employed for better PGM utilization and improved stability for water electrolysis and/or for reversible fuel cell systems. In general, valuable compositional and structural information on a range of materials can be extracted from the work published in this area. Slavcheva *et al.* have recently reported on the characterization and electrochemical performance of IrO_x deposited by reactive magnetron sputtering [19, 20]. They reported 1.8 V at 0.86 A/cm^2 with only 0.2 mg/cm^2 Ir, an order of magnitude lower loading than the usual in this area [20].

While different from a processing point of view, chemical and thermal routes provide a wealth of information related to new materials and compositions that can be used for the OER. Mallouk's group used a combinatorial approach to show that the best bi-functional FC catalyst is 1:1 PtRu [21]. This catalyst is, however, anodically unstable. Adding ~ 5% Ir to the mix provides stability without loss of the catalytic activity. With microelectrodes as a testing vehicle, Dokoutchaev *et al.* [22] used a combinatorial approach for studying water oxidation on all six PGM elements. Ruthenium was found to be the most active but at the same time the least stable. Adding some of the other PGMs improved the Ru stability substantially.

The results of our own initial OER experiments were very encouraging. We have sputter-deposited and over-coated an NSTF PtCoMn cathode catalyst (0.1 mg Pt/cm^2) with 0.5, 1.5 and 6.0 nm of iridium per geometric area (Ir/NSTF) or, in terms of loading, 1.1, 3.4, and 14 μg/cm^2 Ir. OER polarization curves were measured in a 50 cm^2 cell. As evident from Figure 1.5, depositing

only 1.1 µg/cm^2 Ir decreased the cathode potential by 100 mV at 1 mA/cm^2. Further gains of ~ 20 mV and 35 mV were achieved for the samples containing 3.3 and 14 µg/cm^2 Ir respectively. It is interesting to compare this performance with that reported in the patent literature [23]. A catalyst containing two physically mixed components, 40 µg/cm^2 Ir and 0.4 mg/cm^2 Pt, gave a water oxidation current of 10 mA/cm^2 at 1.58 V, an improvement of 150 mV over pure platinum. In comparison, our material with 33 times less Ir, deposited on 0.1 mg/cm^2 Pt/NSTF, produced the same anodic current at 40 mV less positive voltage, 1.54 V. Therefore, the goal of this sub-task was to exploit our initial finding further and deeper.

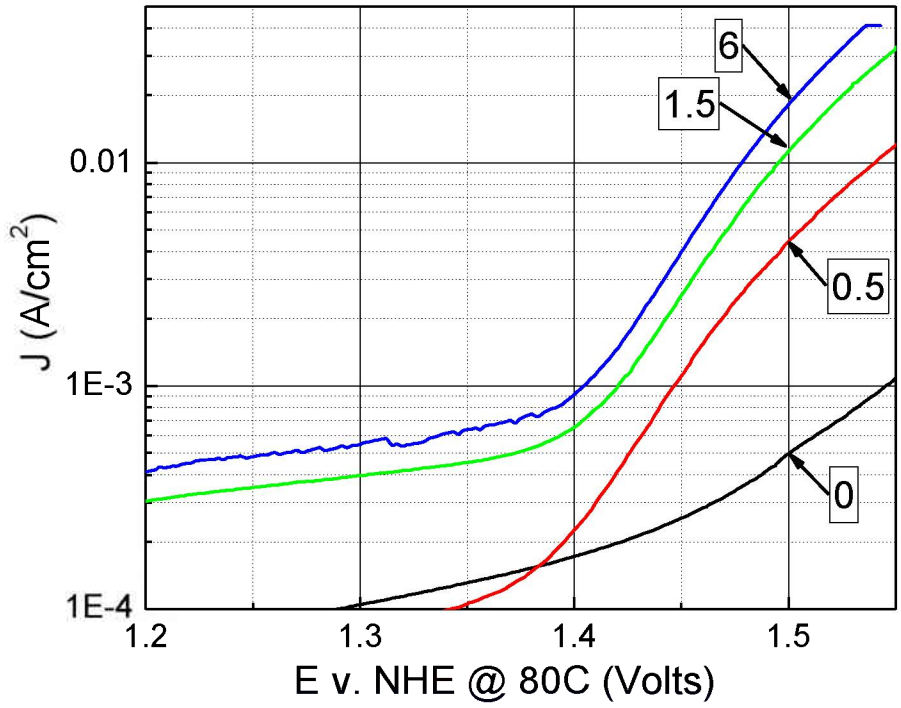


Figure 1.5. OER polarization curves in 50 cm^2 FC on PtCoMn (0.1 mg$_{Pt}$/cm^2)-NSTF catalyst over-coated with 0.5, 1.5 and 6 nm/cm$^2_{geo}$ Ir. Counter electrode: same as working without Ir. Test conditions: FC 80 °C, Working: N_2; Counter/reference: 1% H_2 in N_2 ; 1000 sccm, 0 psig, 100% RH; Potential scan rate: 1 mV/s.

1.2.4. a. Oxygen evolution reaction catalyst structures

While the PGM oxides are the most active OER catalysts, these oxides are in principle not active for the ORR [24]. We expected that the main interference with the ORR would be through physical blockage of the surface of the ORR catalyst. Therefore, the amount of OER catalyst needed to exhibit a specified activity and the impact of its presence on the ORR was carefully studied. We have assumed that the OER catalyst will be a distinct phase and that it will deposit as separate particles on top of the ORR catalysts. A simplified calculation was made to determine the fraction of the ORR surface sites that might be blocked by the OER catalyst particles. The

calculation was based on the amount of the RuO_2 catalyst needed to obtain 1 cm^2 OER active area per 1 cm^2 FC electrode surface area with particles 3 nm in size.

Rather than taking spherical particles, which would ideally have a point contact, we have performed the calculations with cubes of 3 nm (typical catalyst particle size) side lengths with the assumption that the contacting face of each particle will block 9 nm^2 of the available ORR catalytic surface area. With these assumptions, 2.2 $x10^{12}$ particles per cm^2 of geometric surface area are needed and these particles will block 0.2 cm^2 of the ORR catalyst surface area per cm^2 of substrate. The entitlement surface area for NSTF is ~ 40 cm^2/cm^2 which means that only 0.5% of the ORR active catalyst will be blocked. The amount of RuO_2 in the particles is 0.41 $\mu g/cm^2$, which equates to only 0.31 $\mu g/cm^2$ of Ru metal. According to Figure 1.3, an OER current of 1 mA/cm^2 on RuO_2 film is obtained at 1.42 V, a value similar to our experimental measurement on iridium overcoated catalyst with 14 $\mu g/cm^2$ Ir (see Figure 1.5). This was a strong incentive to develop a stable RuO_2-based catalyst. Stabilizing the RuO_2 with TiO_2, and setting the RuO_2 content at 30 % by weight, which is the upper limit of Ru content in the DSA^R anodes, would increase the number of particles needed by slightly more than a factor of 3. This would still cover only 1% of the ORR active surface area with a total PGM content below 1 $\mu g/cm^2$. Based on these numbers, it was clear that there is latitude to increase the OER activity by adding Ru + Ir with only minimal impact on both the total PGM loading and the fraction of blocked ORR surface area.

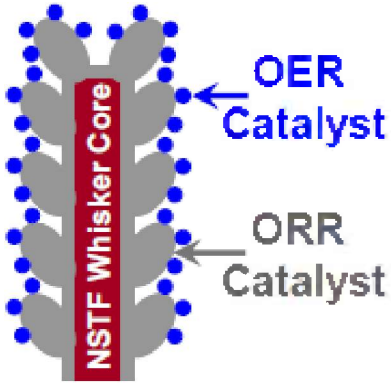


Figure 1.6. Schematic diagram illustrating the proposed mixed ORR/OER catalyst concept.

By adjusting the partial pressure and target powers during sputter deposition, a variety of grain sizes and discontinuous deposition with relatively large clusters can be obtained. Sub-monolayer coverage can produce sufficient OER activity and can result in nano-aggregates with a small cumulative footprint on the ORR catalyst surface area. This is illustrated in Figure 1.6.

High-resolution HAADF-STEM imaging of the NSTF layered-catalyst structures were used to correlate performance with OER catalyst characteristics such as morphology, size, and placement within NSTF and relationship with underlying ORR catalyst.

1.2.5. Concept #2: Anode catalyst with low oxygen reduction reaction activity

As discussed in 1.2, oxygen reduction will occur on the air side of the hydrogen/air front in the anode during SU/SD or fuel deprivation. The aim of this task is therefore to prepare catalyst systems that have high HOR activity (at least as good as Pt) but low ORR activity (at least an order of magnitude lower than Pt).

We have considered two main approaches to develop such catalyst systems. The first was to study series of Pt-M alloys and characterize their HOR and ORR activities. The second approach was to study the impact of a range of overlayer coatings on HOR and ORR performance.

1.2.5. a. Pt-M Intermix catalysts

There is an extensive body of literature on Pt-M alloys. However, for the most part, researchers are looking to develop high ORR activity catalysts. We did not find recent information describing hydrogen oxidation and oxygen reduction performance on the same Pt-M catalysts. To demonstrate the potential viability of this approach, however, we referred to two Dalhousie University-3M publications on compositions in the $Pt_{1-x}Ta_x$ binary composition range [25]. The employed sputter deposition technique gives, in principle, intimate mixing on the atomic scale in the as-deposited films. With 12 atomic % Ta, Figure 1.7 (Left), the performance as assessed with rotating ring disk electrode (RRDE) techniques, was measurably lower than that of pure Pt, exhibiting a half-wave potential shift ($E_{1/2}$) of 30 mV. X-Ray Photoelectron Spectroscopy (XPS) spectra suggested that the loss in catalytic activity may have been partially caused by passivation of surface Ta, as well as higher Ta contents in the first few surface layers as compared to the bulk composition.

In the second study [26], we measured the hydrogen oxidation activity of a series of $Pt_{1-x}M_x$ binary composition spreads, with emphasis on CO tolerance. The composition spreads, including $Pt_{1-x}Ta_x$ were prepared by sputter coating 3M's whisker support with gradients of Pt and M, in a manner designed to give intimate mixing of the as-deposited films. Figure 1.7 (Right) shows the HOR overpotential for a current density of 500 mA/cm^2, as a function of Ta content in $Pt_{1-x}Ta_x$. These data suggested that the HOR catalytic activity was essentially unchanged out to ~ 30 at.% Ta. Comparing the trends in ORR and HOR with composition leads to the possibility that there is indeed a range of Ta between 12 – 30 at.% where the ORR activity is significantly lower than Pt, while HOR activity is maintained.

It is important to note that these experiments were completed as two separate studies with completely different aims. Here they are combined for the first time. The studies were performed with different substrates (glassy carbon disks vs. NSTF) in different environments (RRDE station at room temperature in liquid electrolyte *vs.* fuel cell at 80°C with solid polymer electrolyte). Prior to this project, HOR and ORR performance were not measured on the same samples concurrently, to determine whether this composition window could be effectively exploited in a fuel cell environment and whether it would achieve the intended aim of increasing fuel cell durability. In

addition, there is a wide range of other elements and compounds that could feasibly be mixed in with Pt to produce a catalyst composition that is much more highly selective towards HOR compared to ORR than monometallic Pt.

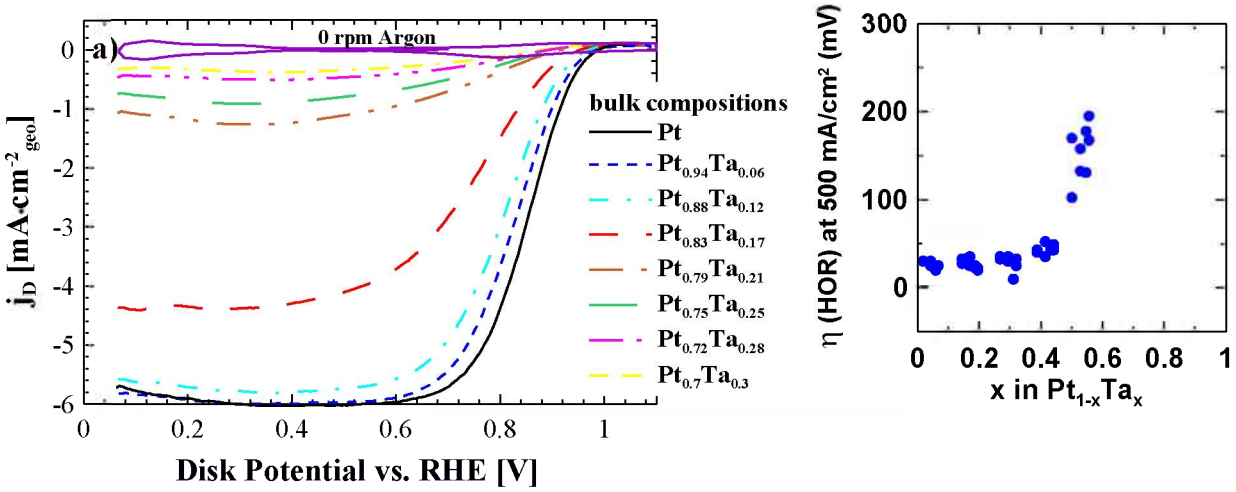


Figure 1.7. Left: ORR curves for $Pt_{1-x}Ta_x$ measured at 1600 rpm, 30°C in 0.1 M $HClO_4$. The samples were sputter-deposited onto glassy carbon electrodes [25].Right: Hydrogen oxidation overpotentials at 500 mA/cm² for $Pt_{1-x}Ta_x$ at 80°C in a 64-electrode "segmented" fuel cell [26].

1.2.5. b. Catalysts with an inert overlayer coating

The concept of an inert overlayer coating that impedes ORR kinetics to a much greater extent than HOR kinetics was proposed as an alternative means for improving the selectivity of the anode catalyst for the HOR. Prior to this project, we have studied the impact of some overlayer coatings (prepared by sputter depositing the overlayer material over standard Pt NSTF) on the performance of NSTF-coated Pt, with specific emphasis on catalyst surface area determination.. There was essentially no difference in ECSA between standard Pt-coated electrodes and electrodes with the same Pt thickness overcoated with 75-100 nm (planar equivalent; *i.e.* ~ 7.5-10 nm thick) of, for example, SiO_2 or Al_2O_3. ORR measurements suggested that the ORR performance of the overcoated Pt was lower than for the uncoated Pt, especially at high current densities. There was also a small impact on HOR performance, again most obvious at high current densities, suggesting that the overlayer also influenced HOR transport. Therefore, the platinum surface was still accessible to gas transport and thus the overlayer was likely deposited as either discrete particles or a porous film over the top of the Pt. Special attention was paid to the stability of the overcoated material.

In addition to the approach discussed above, it was hypothesized that the ORR activity will likely be reduced when the PGM content on the anode is reduced significantly, *e.g.* to 0.02 mg/cm^2, because of a reduction in the number of catalytic sites. This will reduce current densities for a given over-voltage (or conversely will increase overpotentials for a given current density) for both the HOR and ORR. As we have already emphasized, the HOR is very fast relative to the ORR and

thus the impact on HOR current densities at a given potential from reduced platinum loadings will be much smaller than the impact on ORR current densities. Our experience from the previous 3M/DOE projects has shown that the HOR polarization curves down to 0.05 mg/cm^2 are very similar, and thus there is negligible loss in fuel cell performance when the anode Pt loading is reduced. There are, however, other issues associated with low PGM loadings [27], specifically loss of Pt due to dissolution, lack of continuity of the thin film, and primary particle size of thin whisker coatings etc. Only selected samples with satisfactory long term performance and degradation from those previous 3M/DOE programs were subject to the modifications described in this section.

1.3. Innovation and novelty of the concepts

This project introduced two major novel approaches to solving durability issues during transient periods of FC operation that to our knowledge had not been reported thus far. These new concepts are original both in the *materials* that we are introducing into the catalysts and the *processes* through which we are incorporating these materials into the existing catalyst:

1. Incorporating OER active particles onto/into the structure of the cathode (and anode) catalyst without interference with its basic function, the ORR on the cathode and HOR on the anode.
2. Over-coating or intimately mixing the anode catalyst with inert material that will selectively inhibit the ORR without interfering with the HOR.

We emphasize the fact that the additives to the existing anode and cathode NSTF catalysts are fully integrated and as such act as one catalyst. This is in contrast to approaches that have been proposed elsewhere, *e.g.* [6], where OER catalysts more active than platinum have been introduced as additional layers or a mechanical mixture of two separate catalysts. The new catalyst should be equally applicable for transient conditions in both automotive and stationary applications.

1.4. Work Plan

The work was organized in three tasks, based on the previously introduced concepts:

- Task 1. Efficient Oxygen Evolution Reaction Catalysts (Sections 2 through 4)
- Task 2: Low Oxygen Reduction Reaction Activity Anode Catalysts (Section 5)
- Task 3: Scale-up and Real-Life Testing (Section 6)

The Specific Tasks will be explained in detail in the following sections of this report. All organizations have roles in tasks 1 and 2. Task 3 was primarily 3M's responsibility in cooperation with AFCC Company.

1.4.1. Milestones, go/no-go, quantitative criteria, and project schedule

Until new DOE targets for this topic were established, the milestones were based on the discussion and the broad goals defined in the project planning phase. We proposed two milestones and a go/no-go decision. The timing schedule is presented in Figure 1.8.

- Milestone #1, end of 4th quarter, Year 1: Cell performance in electrolytic mode (Cell Reversal; CR) of 1 mA/cm^2 at 1.4 V, and 10 mA/cm^2 at 1.5 V with total additional PGM of 2 µg/cm^2.
- Milestone #2, end of 4th quarter, Year 2: Cell performance in CR of 1 mA/cm^2 at 1.35 V, and at current density of 100 mA/cm^2 at 1.5 V with total additional PGM of 1.5 µg/cm^2. ORR current at the anode reduced by a factor of 2. Demonstrated ORR and HOR performance with integrated catalyst.
- Go/no-go decision, end of the 4th quarter, year 3. The decision was based on whether an integrated catalyst system has been developed that meets all the DOE performance metrics for durability, performance and PGM loading as demonstrated by 50 cm^2 FC testing and/or by the following quantitative criteria: Cell performance in CR: 1 mA/cm^2 at 1.35 V, and 1 A/cm^2 at 1.5 V with total additional PGM of 1 µg/cm^2. ORR current at the anode reduced by a factor of 10.

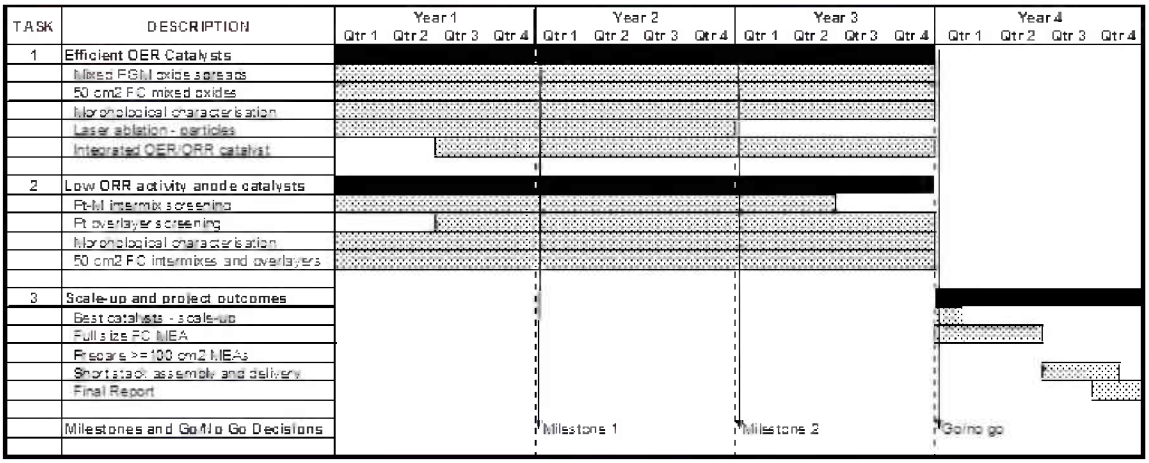


Figure 1.8. *Gantt chart summarizing proposed project timing.*

1.4.2. Project organization and team management and communication

Overall, the project organization was 3M's responsibility with essential inputs from all the subcontractors and the collaborators. The *technical organization* of the project took full advantage of the practices of many multi-organizational projects coordinated by 3M. The underlying principle for any 3M cooperative efforts is that all the participants act as one team with the same common goal. This practice started in the proposal and continued throughout the realization phase of the project, including the writing of this report.

The involvement of the **Partners/Collaborators** had a major impact on the project. Their specific roles are listed below:

- **AFCC -** (Automotive Fuel Cell Cooperation) Company, Burnaby, BC, Canada
  - Independent evaluation, Short-stack testing, Ex-situ/in-situ characterization, Integration, Fundamental understanding (Collaborator and Subcontractor)
- **Dalhousie University** (Subcontractor)
  - High-throughput catalyst synthesis and basic characterization
- **Oak Ridge National Lab** (Subcontractor)
  - STEM Characterization
- **Argonne National Lab** (Collaborator and Subcontractor)
  - Stability Testing, XAFS, Selective ORR Inhibitor

A list of all *individual participants*, including the names of the DOE management team and advisors who actively contributed in guiding this project follows:

Radoslav T. Atanasoski (Principal Investigator),
E-mail: rtatanasoski@mmm.com
Dennis F. van der Vliet, Gregory M. Haugen, Jimmy Wong, Theresa M. Watschke, Andy Armstrong, George D. Vernstrom, Susan M. Hendricks, Amy E. Hester Ljiljana L. Atanasoska,
Energy Components Program, 3M Company, St. Paul, Minnesota

Timothy C. Crowtz, Jessie E. Harlow, Robbie J. Sanderson, David A. Stevens, Jeff R. Dahn
Dalhousie University, Halifax, Nova Scotia, Canada

David A. Cullen, Karren L. More, Shawn Reeves
Oak Ridge National Laboratory, Oak Ridge, TN

Deborah J. Myers, A. Jeremy Kropf, Vojislav R. Stamenkovic, Nenad M. Markovic
Argonne National Laboratory, LeMont, IL

Hao Zhang, Sumit Kundu, Wendy Lee
AFCC (Automotive Fuel Cell Cooperation) Company, Burnaby, BC, Canada

DOE Technology Development Managers: Kathi Epping Martin and Jacob Spendelow
DOE Project Officer: David Peterson
Technical Advisors: Thomas Benjamin and John P. Kopasz, ANL.

2. Task 1: Efficient Oxygen Evolution Reaction Catalysts

2.1. Initial assessment of OER activity of individual elements on Pt/NSTF

All potentials in this report are recorded versus the standard hydrogen electrode (SHE), unless otherwise noted. Cell voltage when operating on 100% hydrogen is close enough to SHE (<5mV difference) to assume equality. Potentials versus 1% H_2 can be approximately converted to SHE scale by adding 50 mV.

At the time of the start of this program, the number of start-up and shut-down cycles for an automotive fuel cell was estimated to be over 30,000,while the number of these events when the cathode electrochemical potential exceeds 1.23 V was being assessed. In a cooperative effort with the DOE FC management team, the *technical targets for the first year* of the project were defined as follows:

Develop a cathode catalyst that can withstand currents of

- 1 mA/cm^2 at potential of <1.45 V and
- 10 mA/cm^2 at potential of <1.50 V with added OER catalyst of < 2 μg/cm^2 of PGM.

The major *accomplishments* of the initial assessment were:

- Produced OER catalysts with 2 μg/cm^2 PGM that achieved the first year milestone for OER activity of 1 mA/cm^2 at 1.45 V.
- Catalysts containing Ir only exhibit activity above the milestone of 10 mA/cm^2 at 1.5V, with the 2 μg/cm^2 additional PGM.
- Developed integrated OER/ ORR catalysts with only 2 μg/cm^2 (Ru + Ir) showing no loss of ORR activity relative to the baseline ORR catalyst.
- Canvassed the space around the components (Ru, Ir, Ti) of the model OER durable catalyst in the real PEM fuel cell environment.
- Established that Ru is the most active OER catalyst, Ir is the most stable and that combinations of Ru + Ir retain some of the properties of the two.
- Attained mass activity for OER of 4 A/mg for Ru at 1.45 V and 3.9 A/mg for Ir at 1.55 V
- Modified the anode catalyst to inhibit ORR while preserving the same activity towards hydrogen oxidation reaction (HOR).

The most significant results that illustrate the above accomplishments and which have been governing the future development of this program will be presented in this report. Some specific details of the experimental procedures can be found in our publications [28 - 30].

The OER catalysts prepared were based around the model catalyst containing ruthenium, iridium, and titanium as presented in previous section. As discussed in the introduction as well as in our previous publications, the NSTF fabrication process of physical vapor deposition via sputtering in vacuum allowed for a wide range of materials in variety of compositions to be synthesized [1 - 3].

To our knowledge, the most comprehensive study to date of the behavior of Ru, Ir and Ti in the real PEM fuel cell environment was completed during the first year of this project. In addition to testing samples with only 2 μg/cm^2 added PGM, as required by the year one milestone, we have produced and tested samples with up to 10 μg/cm^2 added PGM to enhance the impact of the presence of ruthenium and iridium on the cathode ORR catalysts. The OER activity was assessed by quasi-steady state measurements where polarization curves for oxygen evolution were recorded at 2 mV/s. Three consecutive potential sweeps in a cyclic voltammetry (CV) mode, going first in the positive direction, were performed up to each of the voltages set for the year one milestones, 1.45 V and 1.5 V, as well as 1.55 V, 1.6 V and 1.65 V. The first sweep allowed us to assess the intrinsic OER activity while the second and the third sweep provided insights into the stability of the OER catalysts. The impact of the added OER catalyst on ORR activity was assessed through standard fuel cell performance testing before and after the OER test.

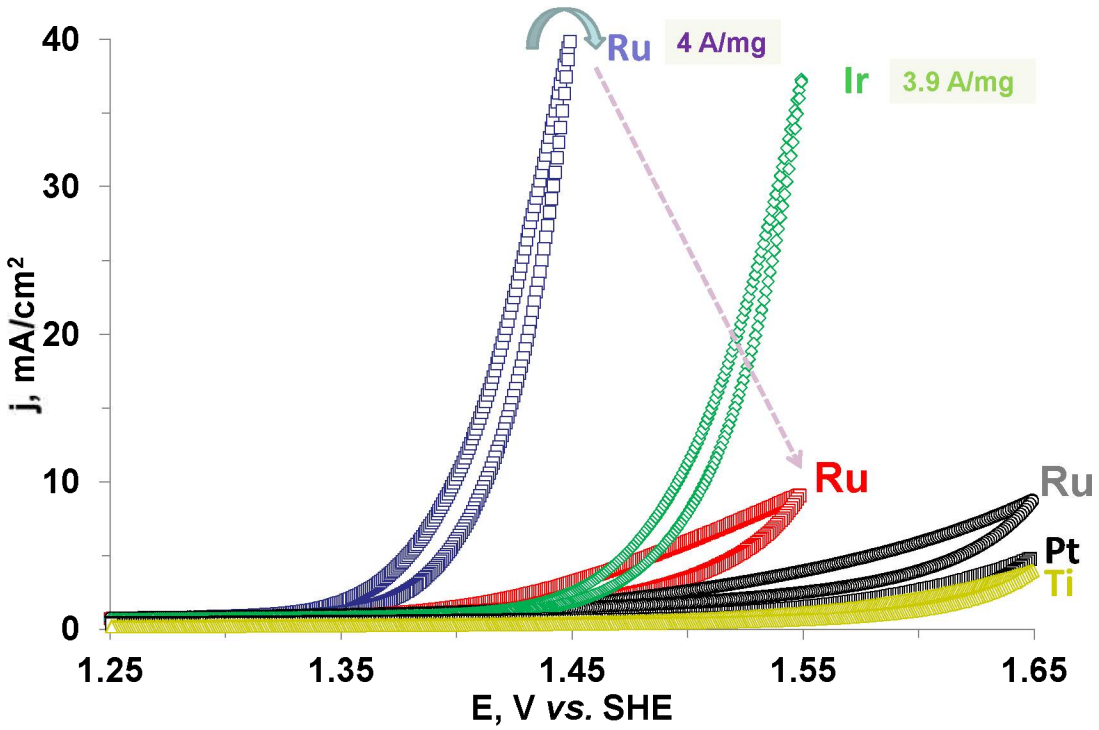


Figure 2.1. Polarization curves for oxygen evolution on 10 μg/cm^2 Ru, Ir and Ti sputter-deposited on Pt-NSTF; the OER curve of the bare Pt-NSTF substrate is also included. Three consecutive sweeps were performed for Ru at each upper limit potential of 1.45 V, 1.55 V, and 1.65 V, but only the first scan of each set is presented. The mass activity for OER of 4 A/mg for Ru at 1.45 V and 3.9 A/mg for Ir at 1.55 V

is indicated in the figure. All polarization curves recorded at 2 mV/s in a 50 cm^2 MEA under nitrogen/1% hydrogen, 70 °C, fully saturated. Potential has been converted to SHE.

In Figure 2.1, an overview of the most important findings during the initial evaluation is presented. Up to the first voltage limit of 1.45 V, only the added Ru produced a substantial current of 39 mA/cm^2. This value is almost a factor of 20 higher than the current on Ir at the same potential. Furthermore, the onset of OER, defined as 1 mA/cm^2 current density after the subtraction of the background current, on Ru occurs at 1.37 V, while on Ir it occurs at 1.45 V. The OER on unmodified platinum as well as on Ti covered Pt does not start until ~ 1.6 V.

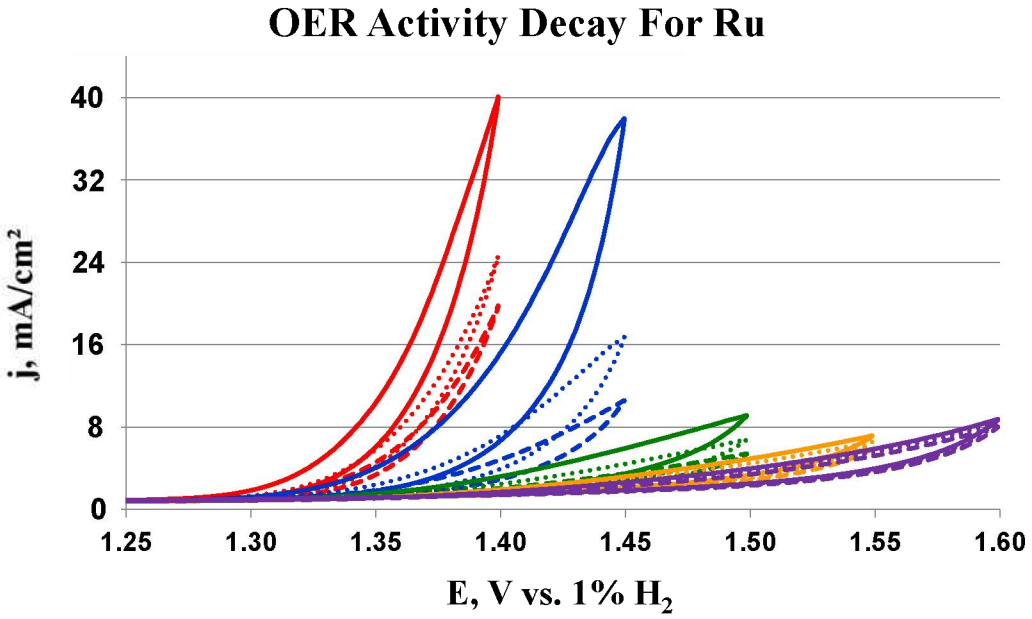


Figure 2.2. Polarization curves for 10 µg/cm^2 Ru in the potential range from 1.45 – 1.65 V. Three consecutive polarizations curves at each upper end potential. All polarization curves recorded at 2 mV/s in 50 cm^2 MEA under nitrogen/1% hydrogen, 70 °C, fully saturated.

While the OER activity of Ru is the highest, it is not stable as indicated by the polarization curve up to 1.55 V (the red curve in Figure 2.1, recorded subsequently to 3 scans to 1.45 V). This is in contrast to the behavior of Ir for which the polarization scans were overlapping (not presented). Because the stability of the added OER catalyst is of utmost importance, we have followed the kinetics of Ru instability in more detail by comparing the current of the repeated scans to 1.45 V (Figure 2.2). Following the first scan, the current drops by ~40% in the second scan and then by 52 % in the third scan. This drop in the activity is even more pronounced when the upper limit increases to 1.5 V. The peak current between the first and the second sweep drops by 57% and in the third by 75%. This is also visible by the hysteresis in the first scan, which is the largest of all the potential scans to any potential limit. This hysteresis is explained in more detail below. After the exposure to 1.5 V, the OER activity is more stable but remains very low, only a factor of three

better than platinum. As large as the Ru loss is, the stability of Ru on Pt–NSTF is appreciably better in comparison with published data on Ru in non-NSTF settings. This will be discussed after some complementary experimental evidence is presented.

As indicated already, integration of the OER catalysts with the existing cathode catalyst (Pt-NSTF in this study), was examined via 50 cm^2 MEAs (Figure 2.3). Within the reproducibility of the fuel cell testing, the integrated catalysts fall in two groups:

- No impact – no loss of ORR activity: Ir with 2 and 10 $\mu g/cm^2$ and Ru with 2 $\mu g/cm^2$.
- Negative impact – significant loss of ORR activity: high Ru content (10 $\mu g/cm^2$) before OER testing and any added Ti.

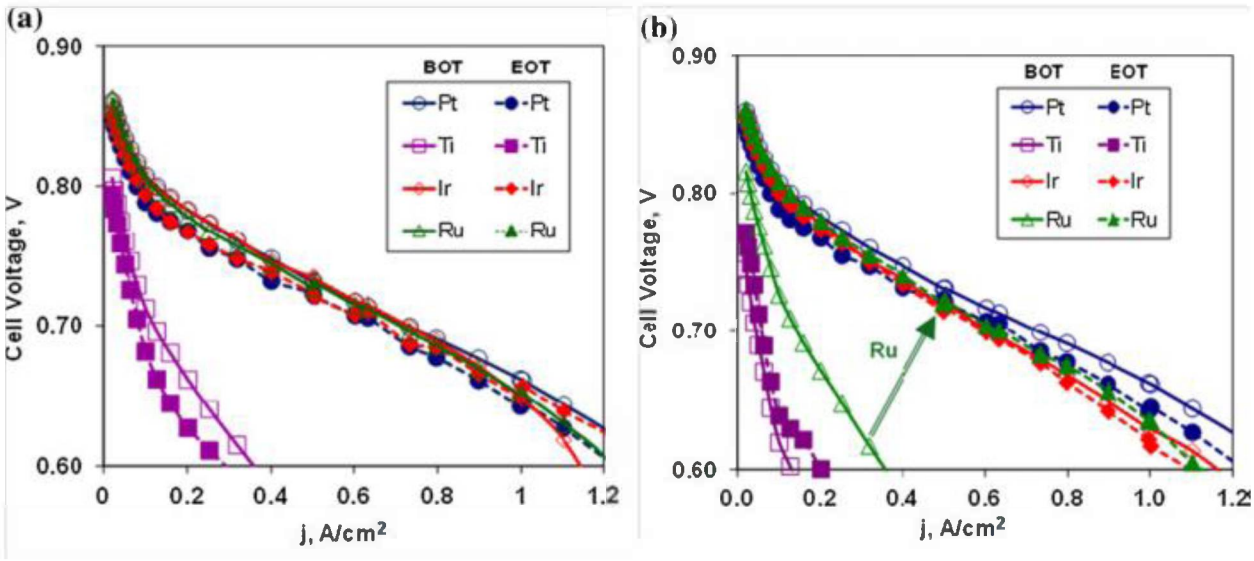


Figure 2.3. Fuel cell polarization curves before (BOT) and after (EOT) OER testing for MEAs with 0.25 mg/cm² Pt-NSTF overcoated with (a) 2 µg/cm² and (b) 10 µg/cm² of Ti, Ir and Ru. Bare Pt-NSTF presented for comparison. Test conditions: Galvanodynamic scans at 80 °C, H_2/air, constant stoich 2.0/2.5, 68 °C/68 °C Dew point, 50/50 kPa

Loss of Ru during OER testing allowed the 10 $\mu g/cm^2$ Ru cells to move from the negative impact group to the no impact group after OER testing. ORR activities measured at 0.9 V according to the DOE protocol follow the same pattern as the fuel cell polarization curves (Figure 2.4).

The behavior of catalysts with only 2 $\mu g/cm^2$ additional PGM followed the same pattern as End-of-test (EOT) samples with 10 $\mu g/cm^2$ additional PGM. At the year one milestone potentials, both Ir and Ru catalysts are above the milestone OER activity of 1 mA/cm^2 at 1.45 V. However, at 1.5 V only catalysts containing Ir exhibit activity above the milestone of 10 mA/cm^2 for 2 $\mu g/cm^2$ additional PGM (data not shown).

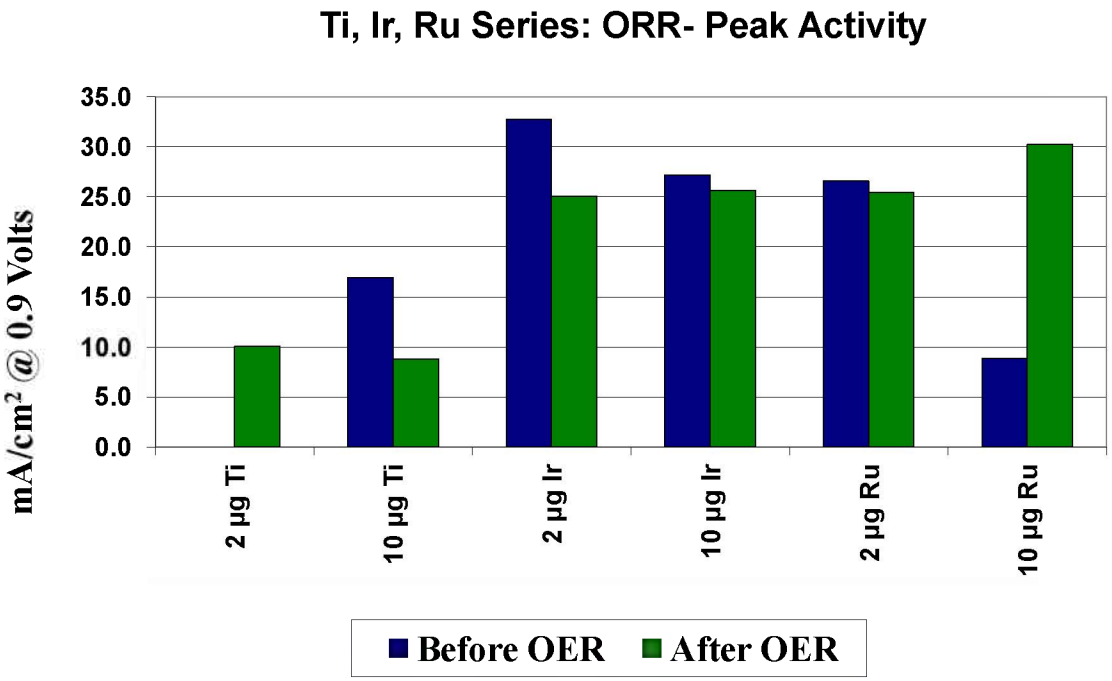


Figure 2.4. ORR activities measured at 0.9 V according to the DOE protocol before and after the OER test (exposure to 1.65 V); Loadings indicated on the graph.

The impact of the exposure to high potentials on Ru stability can also be followed via CVs recorded after each set of three polarization curves in the voltage range between hydrogen evolution and the onset of the OER. This provides insight in the changes of the overcoated Ru catalyst (Figure 2.5). The CV of the "as received" sample is defined by the pseudo-capacitive properties of Ru, which overshadow the underlying Pt-NSTF substrate in the H_{upd}, the double layer, and the Pt oxidation region. Following the three polarization scans to 1.45 V, the CV begins to resemble that of pure Pt, especially in the double layer region. The CV becomes almost Pt-like after the increase of the polarization limit to 1.5 V: well pronounced H_{upd} peaks, narrow double layer and clear Pt-oxide formation/reduction. Thus it is clear that loss of Ru from the Pt ORR catalyst causes the loss of OER activity. Further increase of the polarization limit up to the final upper voltage of 1.65 V had no noticeable effect on the CVs. In contrast, the cyclic voltammograms for Ir on Pt-NSTF are practically unchanged even after the exposure to 1.65 V.

In order to further address the Ru dissolution we have considered the partial current for Ru dissolution and compared the values with published data. A widely accepted mechanism for Ru dissolution is via formation of Ru^{8+} [11]. Hence, a complete dissolution of the 10 µg/cm^2 Ru would require a charge of 76.4 mC/cm^2. This charge is only ~ 2.3% of the total charge during the first three scans to 1.45 V (the charge of the third scan in the negative going potential was not included in the calculation; see Figure 2.2). Therefore, we can conclude that the current during the polarization scans is mainly due to OER. The dissolution of Ru continues at a faster rate during the next 3 scans to 1.5 V. The current densities reached at 1.5 V are 37, 15.6, and 9.2 mA/cm^2. In

addition to the large relative losses in activity for consecutive sweeps, the hysteresis between the positive vs. the negative going potential sweeps is much larger for scans to 1.5 V than for the sweeps up to 1.45 V, indicating again a rapid dissolution rate of Ru at this more positive voltage.

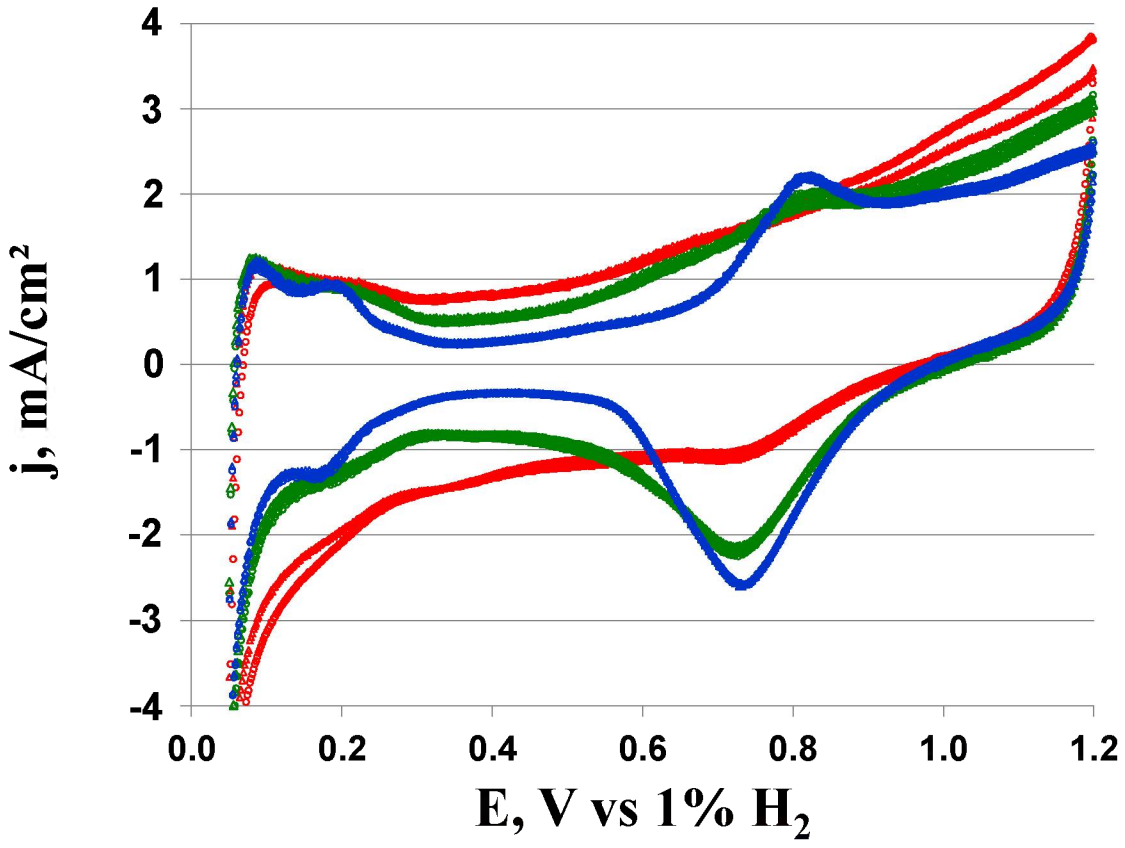


Figure 2.5. Cyclic voltammograms for Pt/NSTF with 10 μg/cm² Ru at beginning of test (red curves) and after exposure to 1.45 V (green curve) and to 1.5 V (blue curve). CVs scan rate at 100 mV/s. Test conditions: 50 cm² MEA under nitrogen/1% hydrogen, 70 °C, fully saturated.

At 1.5 V, a direct comparison of the Ru stability with published data is possible. While some OER activity is still detected on the potential scans upon the increase of the voltage limit to 1.55 V (see Ru curve in Figure 2.2), for simplicity we will assume that all the Ru has been dissolved completely by the third scan at 1.5 V. The total charge during the 6 polarization scans, three to 1.45 V and three to 1.5 V, integrated from 1.3 V to the upper potential limit, was ~ 8000 mC/cm². Therefore, the charge needed to dissolve all of the 10 μg/cm² Ru -- 76.4 mC/cm² -- is only ~ 1% of the total charge during the potential sweeps. In other words, the average dissolution rate of Ru accounts for only 1% of the average current during the six scans, which brings the average Ru dissolution current to 0.13 mA/cm². This dissolution rate of Ru on Pt-NSTF of 1% is extremely low when compared with the dissolution rate reported by Kötz and Stucki of 31% and 57% [15]. The latter was measured on a sputter-deposited 200 nm-thick film of Ru in the same voltage range

in sulfuric acid. A Ru corrosion rate of 10%, at constant current in a similar voltage range, has been reported elsewhere [see refs. 2,8,9 in 33].

The onset potential of Ru dissolution can also be a measure of the Ru stability. A rough estimate of this value for Ru on Pt-NSTF can be inferred by comparing the negative going potential scan with the subsequent positive going scan. As presented in Figure 2.6 (left) the two overlap up to 1.40 – 1.42 V, after which the current during the positive going scan starts to fall behind.

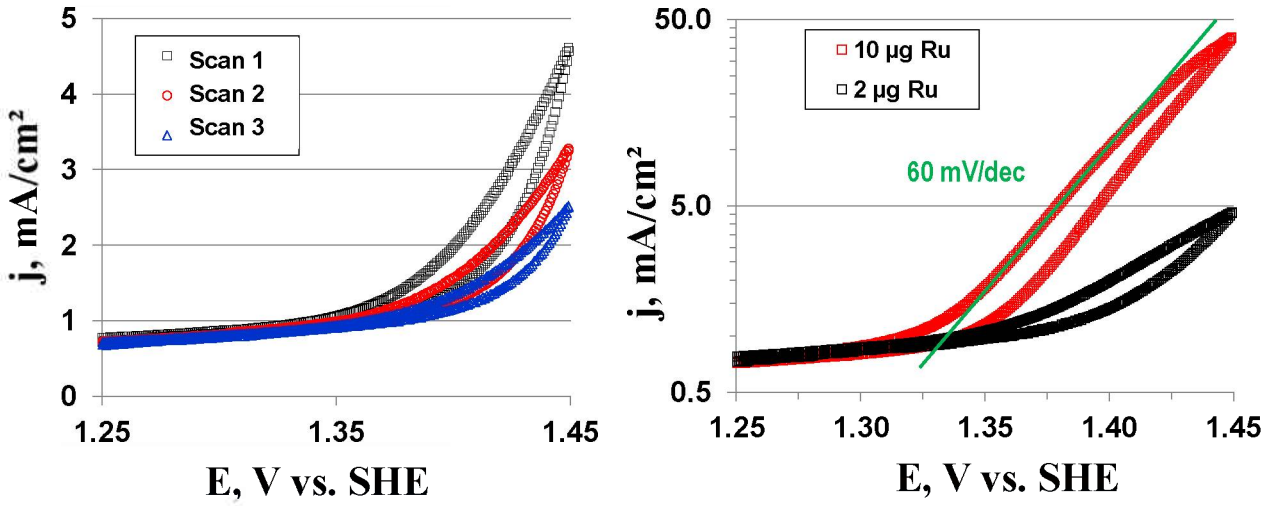


Figure 2.6. (left) Initial polarization curves for 2 µg/cm² Ru on Pt/NSTF. Three consecutive polarizations curves presented. (right) The first polarization scans for 2 µg/cm² (black) and 10 µg/cm² (red) Ru on Pt/NSTF; Note the exponential scale for the current density. Potential scan rate 2 mV/s; 50 cm² MEA under nitrogen/1% hydrogen, 70 °C, fully saturated.

The other indicator of Ru stability is the Tafel region on the positive going scans (Figure 2.6 right). The Tafel relationship holds for only a narrow potential range between ~1.35 -- 1.39 V, suggesting the Ru remains reasonably stable up to 1.39 V, a value close to the already estimated stability limit of 1.40 – 1.42 V. Kötz and Stucki were able to detect products of Ru dissolution only at potentials higher than 1.45 V. Thus, our estimate of the onset potential of Ru dissolution in an MEA environment is slightly lower. In spite of this, the stability of Ru on Pt-NSTF is much higher, as implied by our dissolution rate, than that reported by Kötz and Stucki [15].

2.2. OER activity of binary Ir – Ru Catalyst on Pt/NSTF

As pointed out in the introduction, the activity for OER is a necessary property of the modification to existing anode or cathode FC catalysts. However, the high OER activity, such as exhibited by the added Ru on Pt, must be able to withstand numerous high positive potential excursions during the lifetime of a FC stack in automotive applications. Besides the stabilization effect, the addition of Ir as a pathway to achieve this goal has exhibited some interesting properties.

Based on the evaluation of the single component OER catalysts with regard to the negative impact of Ti on the fuel cell performance, further effort in the project focused on the binary composition of Ir and Ru. The ratio of Ru:Ir was varied from 3:1 to 1:3 w/w (85–38 Ru at%), while keeping the total OER added PGM loading at 2 μg/cm^2, the level defined by the milestone for year one. In addition, the same catalysts were deposited in the presence of oxygen. While all catalysts achieved the milestone OER activity at 1.45 V, only some did at 1.5 V. Samples prepared with oxygen during the deposition process behaved identical to those deposited in inert atmosphere. As such the binary Ru–Ir catalyst has been chosen for future studies aimed at achieving different morphologies.

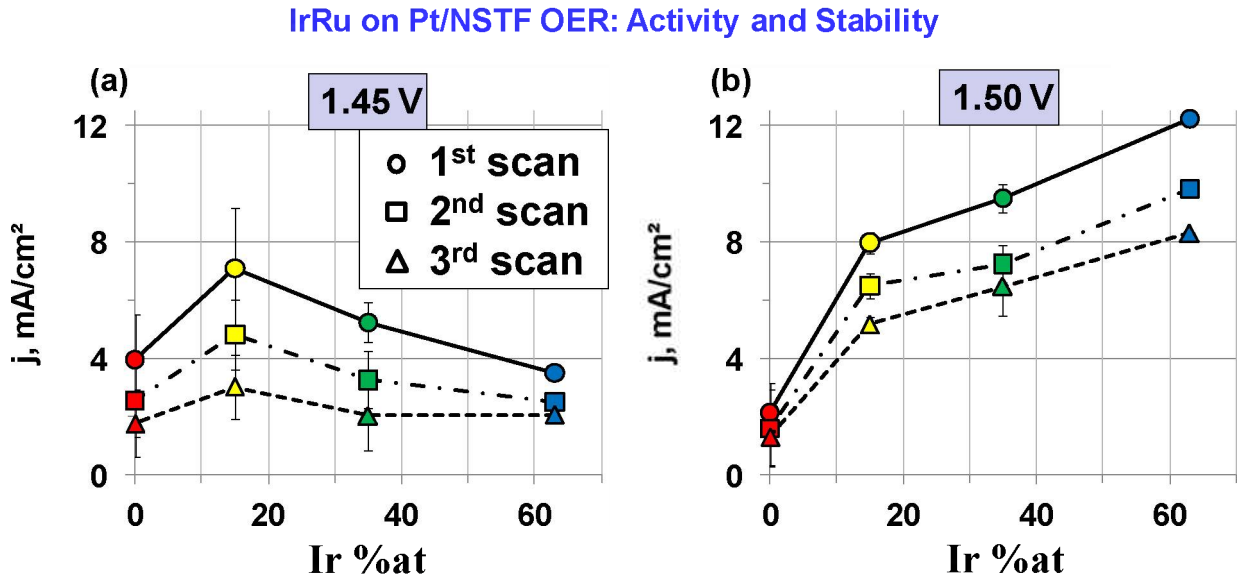


Figure 2.7. OER currents at the end of the three consecutive potential scans to 1.45 V (a) and 1.5 V (b) of sputter-deposited Ir on Ru with total amount of the two elements at 2 μg/cm^2.

The stabilization effect by sputter-deposited Ir on Ru is presented in Figure 2.7. First, it is interesting to observe that the OER activity during the first potential sweep to 1.45 V was lower than that for pure Ru only when ¾ (1.5 μg/cm^2) of the Ru was substituted by Ir. At ½ and ¼ Ru substituted by Ir, the OER activity was expressly higher than for pure Ru. While this observation may be explained by greater Ru retention by the time the electrode reaches 1.45 V, it is plausible that a synergistic effect exists between Ru and Ir. From a utilitarian point of view, by the third excursion to 1.45 V, the catalyst with the highest Ir content retains the most activity, ~ 57 %, while the others, including pure Ru, retain only 39 – 45%. The maintaining of the OER activity of the high content Ir catalysts becomes more obvious when the upper voltage limit is increased by 0.05 V to 1.5 V. At 1.5 V, the OER activity behaves as expected, namely the highest sustained OER activity was present on the catalyst with the highest Ir loading (75%). The relative OER activity retention is also the highest at 68% from cycle #1 to cycle #3. At 1.5 V, one has to consider

that Ir has a better OER activity on its own, which makes it difficult to speculate on the contribution of the retained Ru catalyst towards the total OER current.

Besides the more stable behavior of the binary Ir – Ru catalysts, it is of interest to compare the activity with the published data elsewhere. Kötz and Stucki studied the OER activity and stability of 200 nm thick Ru-Ir metallic alloys sputter-deposited on glass [31]. In sulfuric acid, they found that 14% at. Ir already had produced a substantial stabilization effect on Ru which is similar to our data for 15% at. Ir (Figure 2.7). Based on XPS measurements before and after the electrochemical testing, they concluded that the stabilization is due to the formation of a protective oxide layer with increased Ir content. However, unlike our findings, they saw a steady decrease in the OER current with an increase of Ir content. In addition, our Ru-Ir catalyst, estimated to be only 2 nm thick, has at least an order of magnitude higher OER activity. This obviously points to differences in the structure and the morphology between the two films which could be due to the preparation procedures as well as the NSTF substrates.

We can also compare our measurements on Pt-NSTF-supported RuIr with the work of Fuentes *et al.*, who are using metallic RuIr deposited on anatase TiO_2 as a support [32]. Tested in acid aqueous environment, they reported a mass activity of 100 A/g RuIr. As presented in Figure 2.6, our 2 $\mu g/cm^2$ RuIr at the same potential of 1.5 V has a mass activity of between 5600 – 6200 A/g.

Qualitatively, the behavior of our RuIr is also in agreement with the behavior of thermally-produced mixed RuO_2 and IrO_2 tested in aqueous systems (Matos-Costa *et al.* [33]). The range of the Ru:Ir ratios for the best activity (70% at. Ru reported by Matos *et al.*) and the best stability (50-90% at. Ir) is very similar. However, the oxides of Matos *et al.* exhibit huge differences in inherent activity when compared with our metal catalysts. At 1 mA/cm^2, a current density where Ru is presumed to be stable and the ohmic drop corrections are negligible, the electrode potential range of all the compositions containing Ru (excluding pure IrO_2) in Matos *et al.* are within 1.42 V and 1.47 V. At the same current density, our samples are in the range of 1.38 – 1.40 V. What makes this difference significant is the fact that the Matos-Costa *et al.* samples are 2 μm thick, with a loading of ~2 mg/cm^2, which is a factor of 1,000 more than ours. If evenly distributed over the real surface area of the Pt – NSTF substrate, a Ru + Ir loading of 2 $\mu g/cm^2$ would result in a layer thickness of less than 2 nm.

The "thickness" consideration can shed some light on the enhanced catalytic effect of the mixed samples with 1.5 and 1.0 $\mu g/cm^2$ of Ru compared to the sample with pure Ru at 2 $\mu g/cm^2$. Matos *et al.* ascribed the enhanced activity of the mixed Ru + Ir samples to "a combination of catalytic and roughness effect". In the case of our samples, the catalyst is so thin that we cannot speak of any kind of layer and consequently we can disregard the roughness factor as a contributor to the enhanced activity. This leaves the enhanced inherent activity as the predominant reason for the increased activity.

2.2.1. Fundamentals of OER of Ru and IrRu on NSTF and on Pt/NSTF

In order to better understand the fundamentals of the OER activity of individual metals, we studied in more detail the activity and the stability of ruthenium deposited *directly* on NSTF. Ruthenium is the most interesting because of its strong chemical interaction with perylene, which up to this study was thought to be practically inert. For this purpose, 1, 2, 5, 10, and 20 μg/cm^2 Ru was deposited on NSTF. The systematic XPS and STEM characterization of the Ru/NSTF interface was done on all the samples and the results will be reported in Section 7.

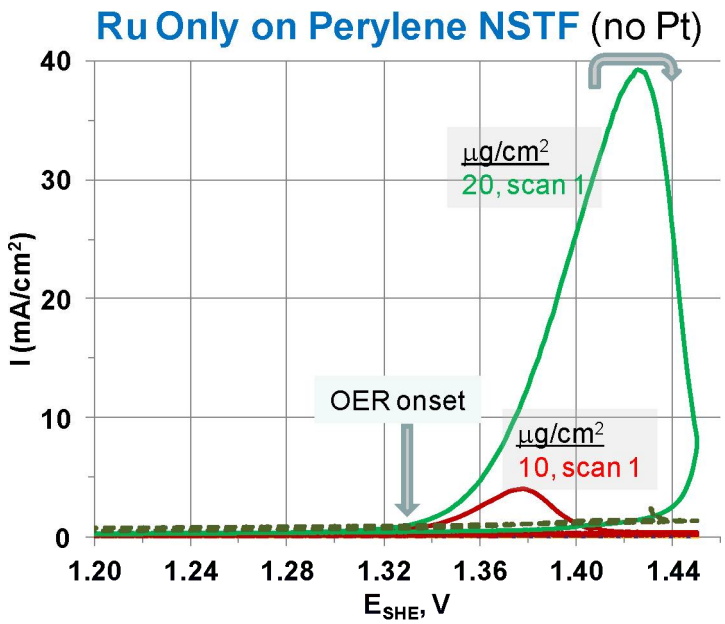


Figure 2.8. Initial polarization curves of 10, and 20 μg/cm^2 Ru deposited directly on perylene whiskers (NSTF). Two consecutive polarizations curves presented. Black dashed line: the second polarization scans for 20 μg/cm^2 Ru; the second scan for 10 μg/cm^2 Ru (dotted line) has current densities close to zero and cannot easily be distinguished. Potential scan rate: 2 mV/s; 50-cm^2 MEA under nitrogen/1% hydrogen, 70 °C, fully saturated.

The electrochemical activity was assessed by quasi steady state scans to 1.45 V. The initial two cyclic voltammograms scans of 10 and 20 μg/cm^2 samples are presented in Figure 2.8. The polarization scans of the lower Ru loadings did not produce any distinguishable current above the background. On the other hand, the OER onsets of 1.34 V for 10 μg/cm^2 and 1.33 V for 20 μg/cm^2 Ru samples were among the lowest of all the catalyst varieties evaluated in this project. However, both samples show an inflection point during the positive-going scan. This is a clear indication of Ru dissolution. The Ru dissolution rate increases with the potential and the remaining Ru is eventually not sufficient to sustain the OER kinetics observed before the inflection point. The comparison between the 10 μg/cm^2 and 20 μg/cm^2 Ru loadings shows that the lower loading loses activity disproportionally faster. This could be an indication that not all of deposited Ru is OER

active. Actually, the XPS analysis has shown that for the 10 μg/cm^2 Ru, the portion of Ru that has reacted with the perylene is close to 70% leaving 3 μg/cm^2 of unreacted Ru. For the 20 μg/cm^2 Ru, the reacted portion is 60%, leaving 8 μg/cm^2 of unreacted Ru. The ratio of 8 to 3 is close to the ratio of the current densities at 1.38 V, where 10 μg/cm^2 Ru has its maximum. The portions of unreacted Ru for the lower loadings of 5, 2 and 1 μg/cm^2 are 1.3, 0.3 and 0.06 μg/cm^2, respectively. Under the assumption that the unreacted Ru is provides the active sites for the OER, the extremely low loadings of the unreacted Ru could explain why the 5, 2 and 1 μg/cm^2 total Ru samples had no measurable OER current. Additional insight is offered by comparison of the morphology of the Ru deposits (see STEM images in section 7).

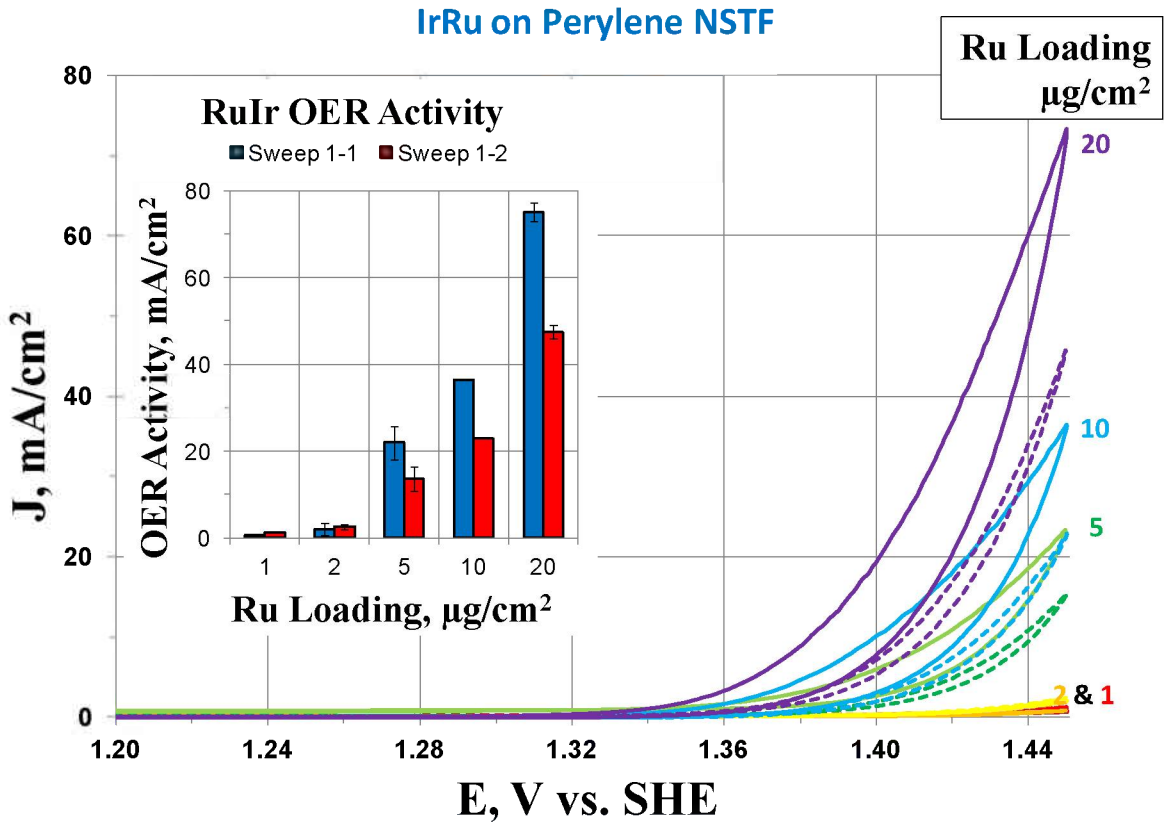


Figure 2.9. Initial polarization curves of 5 μg/cm^2 Ir added on top of 1 - 20 μg/cm^2 Ru deposited directly on perylene whiskers (NSTF). Ru loading indicated in the right margin of the graph. Two consecutive polarizations curves are presented; 1st scan is the solid line, 2nd scan is the dashed line of the same color. Inset: OER activity at 1.45 V for the first two potential scans. All other details as in Figure 2.8

The next step to examine was the effect of adding iridium on the Ru deposited directly on the perylene NSTF (Figure 2.9). 5 μg/cm^2 Ir was placed *on top* of each Ru deposition on perylene from the same series as described in the previous paragraphs. The impact of the presence of Ir is dramatic. In comparison with the curves in Figure 2.8, there are no inflection points as an obvious indication of the dissolution of Ru. Actually, the polarization curves resemble those presented in

Figure 2.1, where either Ru or Ir was deposited on top of Pt/NSTF. The detailed XPS study showed that the addition of Ir actually increased the amount of metallic or 'unreacted' Ru (see section 7).

It appears that for the 5, 10 and 20 μg/cm^2 of Ru, the OER activity loss is the same, around 35%. However, for the lowest Ru loadings, 1 and 2 μg/cm^2 of Ru, there is a measurably higher OER activity at the second sweep, even though the currents are relatively small. This phenomenon of activating the catalyst during the initial phase of testing is not uncommon for Ru and Ir. Another observation is that the loss of OER activity from sweep 1 to sweep 2 is almost the same as found for the equal amount of Ru deposited on Pt/NSTF (see Figure 2.1).

The last step in this systematic study was to introduce the third necessary anode component – platinum. In order to the emphasize the fundamental effects of the presence of platinum, the two Pt loadings in this study were at the low end: 5 and 10 μg/cm^2 Pt. Platinum was deposited directly on the perylene NSTF, followed by 20 μg/cm^2 Ru and (when present) 5 μg/cm^2 Ir on top, as the outer layer. The OER activities for the first two scans are presented in Table 2.1. The choice of the potential at which the activities were measured was 1.39 V, where the scan for pure Ru had the inflection point. This was done with the assumption that by this point no significant Ru dissolution occurs and the catalyst is relatively stable. As a result, the original loading of 20 μg/cm^2 Ru would be still present on all the samples during the first positive going scan.

As expected from the previous two figures, Ru has the best activity and the worst stability. The addition of Ir retains most of Ru activity and provides some stability.

It is also interesting that when Ru is deposited on platinum, its behavior is only slightly modified in respect to Ru deposited directly on NSTF. Actually, it appears that 10 μg/cm^2 Pt modifies the Ru behavior more than 5 μg/cm^2 Pt; for 10 μg/cm^2 Pt, the Ru activity is lower while the durability higher.

The deposition of iridium on top of the ruthenium and platinum produced another set of interesting results. On the one hand, the OER activity at 1.39 V dropped for both 5 μg/cm^2 Pt (60%) and 10 μg/cm^2 Pt (54%), but on the other hand, the durability of these catalysts was superior. In respect to the 1st scan, they lost only 13% (2.8 mA/cm^2) for 5 μg/cm^2 Pt and 11% (3.8 mA/cm^2) for 10 μg/cm^2 Pt in the 2nd scan. While current densities are lower than for the Ru covered with Ir, it is reasonable to assume that in subsequent scans, the activity retention on IrRuPt catalyst would be higher. This would result in the highest current densities of all the samples tested in this series of catalysts.

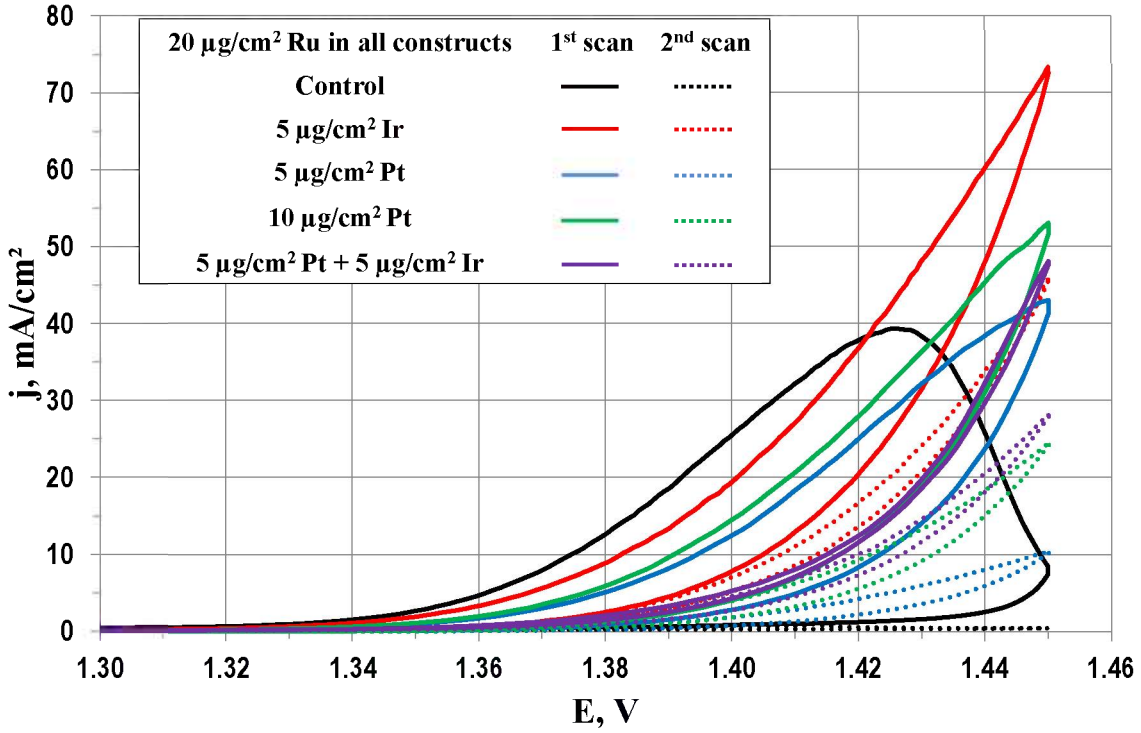


Figure 2.10. Initial polarization curves of 5 and 10 µg/cm² Pt added on top of Perylene NSTF, followed by 20 µg/cm² Ru and 5 µg/cm² Ir. For comparison, the data for 20 µg/cm² Ru deposited directly on perylene whiskers (black curves) and 20 µg/cm² Ru with 5 µg/cm2 Ir (red curves) are included. Two consecutive polarizations curves presented; 1st scan (solid line) and 2nd scan (dotted line of the same color). All other details as in Figure 2.8

	i@ 1.39 V mA/cm² (1st scan)	i@ 1.39 V mA/cm² (2nd scan)	Δi loss (1st – 2nd)mA/cm²	Δi loss (1st – 2nd) %
Ru	18.6	0.6	18.0	97
Ru + Ir	13.4	4.2	9.2	68
5 µg/cm² Pt + Ru	8.0	1.2	6.8	86
10 µg/cm² Pt + Ru	9.4	2.4	7.0	75
5 µg/cm² Pt+Ru+Ir	3.2	2.8	0.4	13
10 µg/cm² Pt+Ru+Ir	4.3	3.8	0.5	11

Table 2.1. OER activity at 1.39 V for the first two potential scans for Figure 2.10 and the absolute and relative changes between the two scans.

Recently, the ANL electrocatalysis group studied the OER on well-defined surfaces of Ru, Ir and their modifications [34, 35]. One of the goals of their study was to establish *the fundamental relationships between the activity and the stability of the OER.* They found that, similarly to what we have presented here, there is a tradeoff between the two: the most active metals are the least stable. In their RRDE measurements, they have found that the onset of Ru and Ir dissolution is accompanied by the onset of the OER. The partial current corresponding to Ru and Ir dissolution relative to the total anodic current measured on the disk electrodes is only 10% for Ru and 1% for Ir. Our own catalyst with 20 $\mu g/cm^2$ Ru on NSTF (Figure 2.8) shows an average Ru dissolution rate of only 1.5%. We have not intentionally measured the dissolution rate of Ir, although it is clear from its ability to withstand high current densities for many hours (see Section 4), that the dissolution rate has to be much less than 1%. Further comparison between our work and ANLs shows much higher the OER activities on the NSTF based catalysts. Ru/NSTF reaches current density of 5 mA/cm^2 at 1.36 V (Figure 2.8), while the polycrystalline Pt at ANL is at 1.48 V. This is at least two orders of magnitude higher activity for the Ru/NSTF catalyst. Likewise, at 5 mA/cm^2 Ir on Pt/NSTF is at 1.47 V (Figure 2.1) while in the ANLs study is at 1.68 V. Even with the higher Tafel slope for OER on Ir than Ru, this is again more than two orders of magnitude higher OER activity for Ir on NSTF. While there are differences in the surface structures of the two types of material, which are beyond of the scope of this project, this comparison provides yet another justification that the OER catalysts supported on NSTF have inherent activities that are attractive for real life application.

2.2.2. RDE evaluation of OER of Ru and IrRu on NSTF (Dalhousie U.)

While valuable on their own, the effort at Dalhousie University complemented the results obtained in MEAs in more than one way. Since the catalyst was deposited on NSTF substrate grown on graphite disks, the only difference between the data in the RDE and the MEAs was the electrolyte: PEM vs. aqueous environment. The other important feature of the RDE evaluation was that the disks were available for XPS analysis at different stages of the evaluation process.

Typical results of the RDE evaluation of the IrRu catalyst are presented in Figure 2.11. This figure also illustrates the basic SU/SD steps of the test protocol, which is very similar but not identical to the 3M protocol for MEAs. Due to instrumental restrictions, Dalhousie used a constant charge approach implemented galvanostatically at 1 mA/cm^2 until 10 mC/cm^2 was delivered. The start-up/shut-down test sequence was repeated 1000 times to assess durability, with the Pt surface area estimated at every 200 pulses.

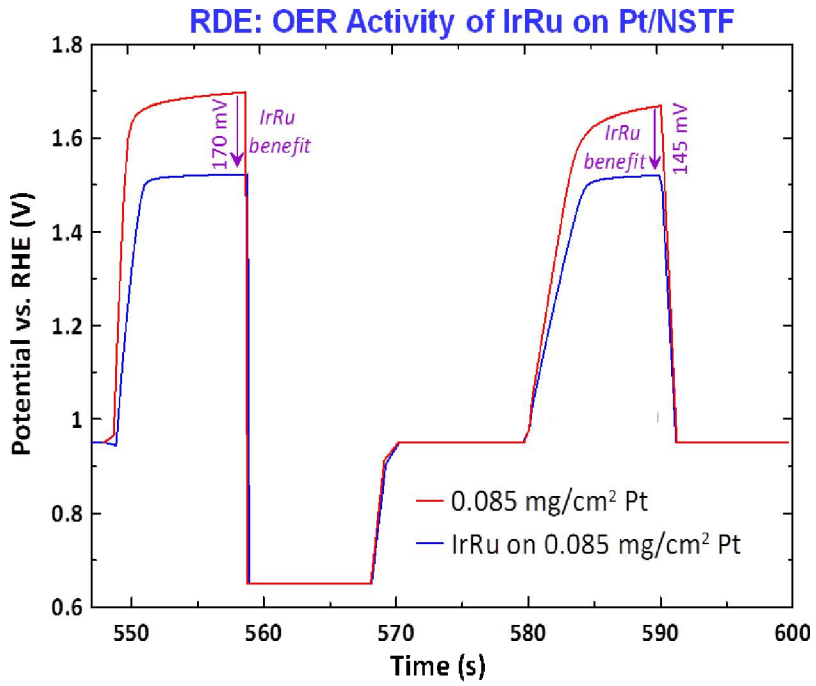


Figure 2.11. Electrode potential during the basic step of the RDE test protocol. Electrode potential held at 650 mV for 10 s before and after the current pulse simulating startup; started and ended at 950 mV to simulate the shutdown sequence. Catalysts: 0.085 mg/cm^2 Pt deposited on NSTF on GC disks (red), 0.006 mg/cm^2 $Ir_{0.94}Ru_{0.06}$ deposited on the Pt (blue). 900 rpm, 0.1 M $HClO_4$, room temperature.

Two observations can be made from Figure 2.11. First of all, when the electrode is held at 650 mV (shutdown), the potential at the end of the pulses is lower than when this step is absent. Secondly, the shapes of the polarization curves are different, with a higher capacitive charge contribution as the Pt surface is reduced, which delays the start of the OER. The other observation is that, as expected, $Ir_{0.94}Ru_{0.06}$ lowers the potential seen by the electrode under the same constant current test conditions by 170 mV for the startup and 145 mV for the shutdown.

SU/SD behavior of platinum with wide range of *intermixes* and *overlayers* of Ir or Ru are presented in Figures Figure 2.12 and Figure 2.13.

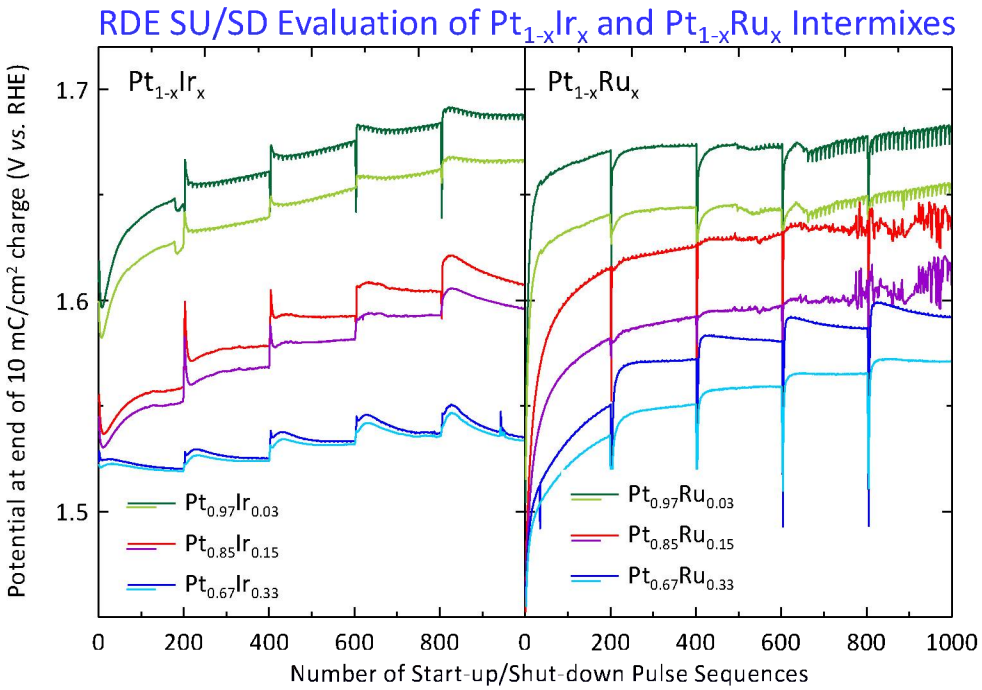


Figure 2.12. Electrode potentials of the end of the SU (upper lines for a given catalyst composition) and SD step (lower lines) for *intermixes* of $Pt_{1-x}Ir_x$ (left) and $Pt_{1-x}Ru_x$ (right). Pt loading constant at 0.085 mg/cm^2. Test conditions as in Figure 2.11

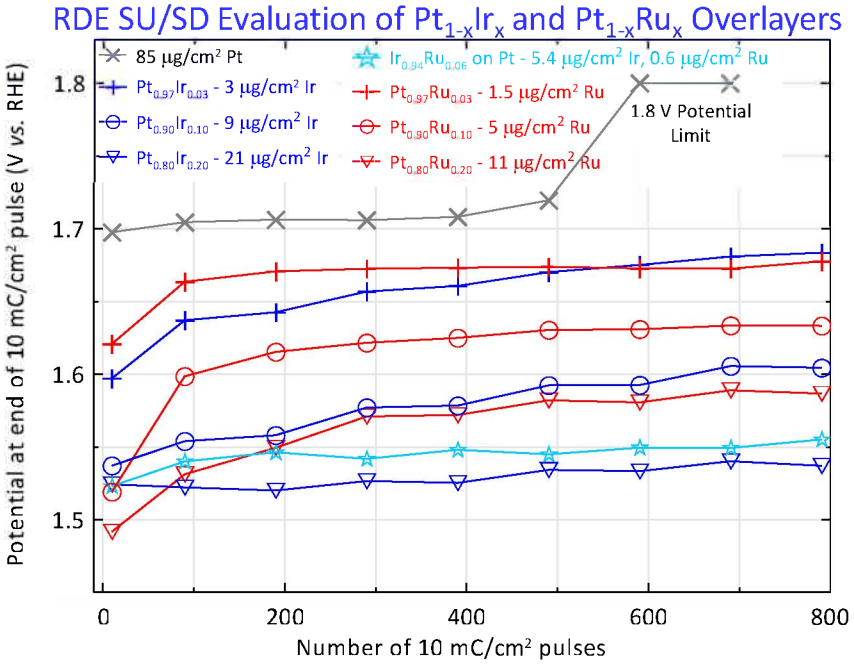


Figure 2.13. Electrode potentials of the end of the SU/SD step for *overlayers* of $Pt_{1-x}Ir_x$ (blue) and $Pt_{1-x}Ru_x$; (red); Pt and Pt with $Ir_{0.94}Ru_{0.06}$ for comparison; Test conditions as in Figure 2.11

In general, $Pt_{1-x}Ir_x$ has an approximately 50 mV higher initial potential than $Pt_{1-x}Ru_x$. However, $Pt_{1-x}Ir_x$ is more stable than $Pt_{1-x}Ru_x$ (Figure 2.12). Worth noting is also the fact that the stability of the smallest amount of Ru in this testing is better than with the testing in MEA environment. As we can see in the next figure (Figure 2.13), this same catalyst composition shows the same stability as when Ru is added as an overlayer. From a practical point of view, the most interesting finding is that 6 μg $Ir_{0.94}Ru_{0.06}$ on: 0.085 mg/cm^2 Pt/NSTF is as effective and stable as 21 μg Ir intermixed. From a fundamental point of view, the RDE experiments allowed for a systematic tracking of the compositional and the chemical changes that the catalyst with OER undergoes. For this purpose, the testing of individual disks (Figure 2.14) was stopped at certain predetermined potentials for XPS analysis, the detailed scans of which are shown in Figure 2.15.

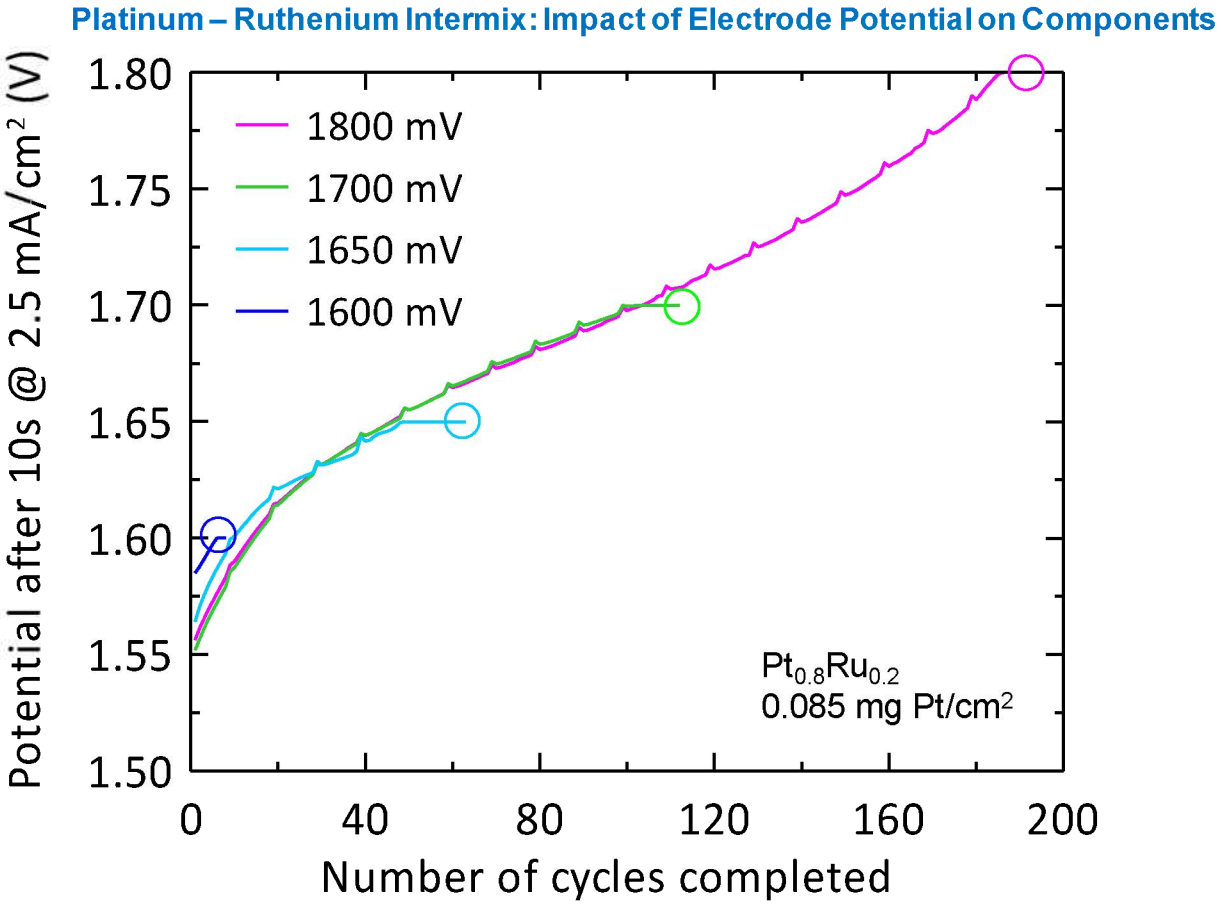


Figure 2.14. Accelerated SU/SD steps at 2.5 mA/cm^2 of $Pt_{0.8}Ru_{0.2}$, Pt loading 0.085 mg/cm^2. Circles denote points at when disks were removed from further testing.

The continual increase of the electrode potential during the RDE testing (Figure 2.14) can clearly be associated with the loss of Ru. However, more dramatic changes are taking place on platinum. As indicated by Pt 4f $_{5/2}$ and Pt 4f $_{7/2}$ peaks (Figure 2.15), once the Pt NSTF reaches 1.7 V,

platinum loses metallic character becomes heavily oxidized. In addition to the fact that this information is of big fundamental and practical interest, to our knowledge no prior proof of this type has been reported before. During this project it was found that the 1.7 - 1.8 V potential range coincides with the stability limit established during the MEAs testing.

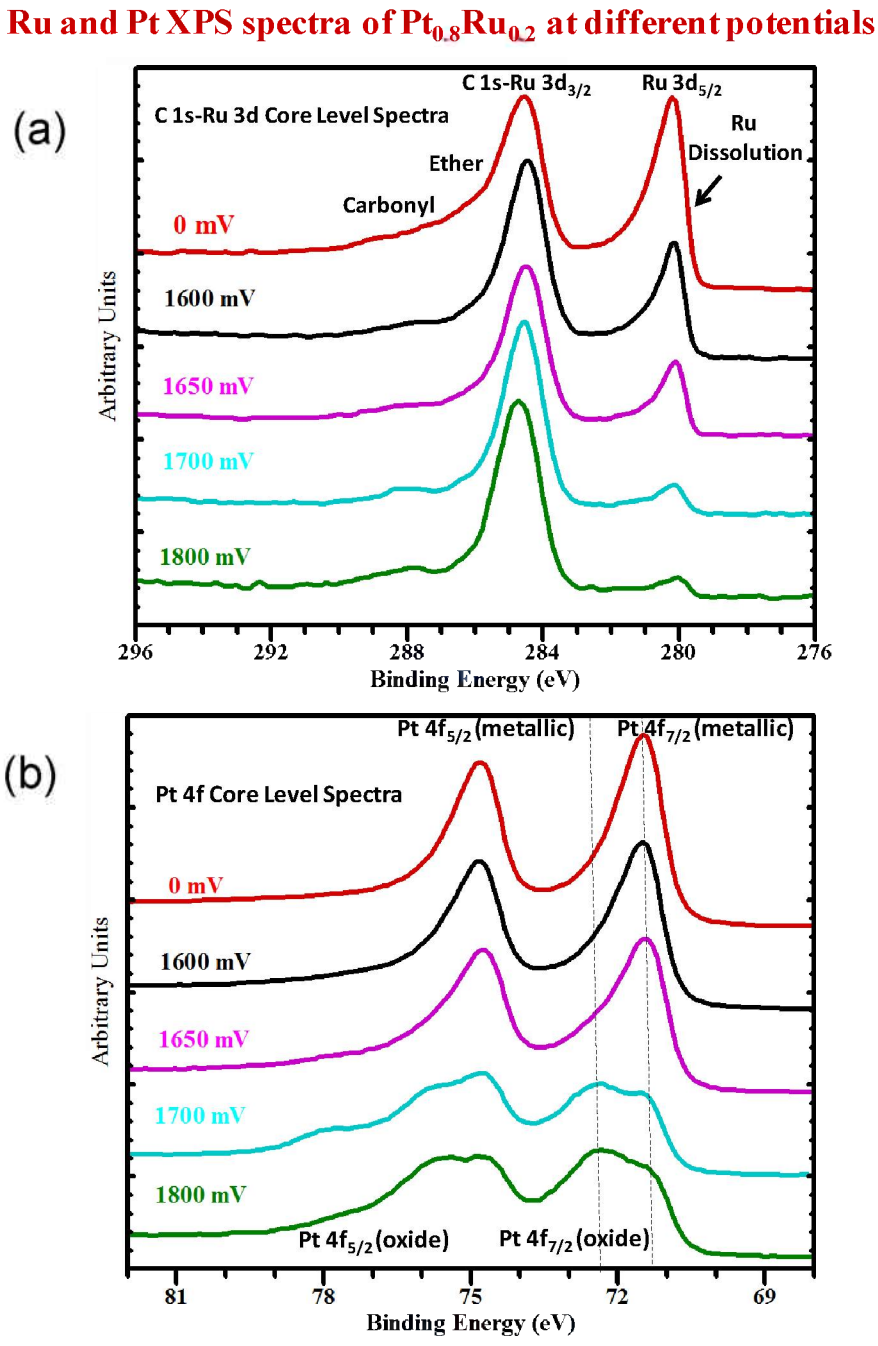


Figure 2.15. Ruthenium (a) and platinum (b) XPS core level spectra at different electrode potentials for $Pt_{0.8}Ru_{0.2}$ intermix. Test description in Figure 2.14

3. Task 1: Start up/ Shutdown

Having established the inherent activities of the OER catalyst, future catalyst evaluation protocols have focused on more realistic startup–shutdown test conditions, including cell reversal. In this section the focus will be on the SU/SD with the added OER catalyst on the cathode side.

In agreement with DOE, the technical targets have been initially defined as follows: For SU/SD, develop a cathode catalyst that can withstand 5,000 excursions at potentials < 1.45 V, at currents > 1 mA/cm^2 during a time of < 5 sec with added OER catalyst of no more than 2 μg/cm^2 of PGM.

During 2011 the project milestone was redefined in order to comply with the new 2015 DOE PGM total loading target of 0.125 mg/cm^2. Under the new, durability oriented, more realistic testing procedure that had to be developed, the following milestone were set:
- 5,000 startup cycles under the existing protocol with 0.095 mg/cm^2 total PGM on the cathode, with Pt ECSA loss of <12%.

3. 1. Accomplishments

- Generic electrochemical tests for SU/SD and Cell reversal were developed and implemented.
- 10,000 startup/shutdown cycles were achieved with addition of only 2 μg/cm^2 PGM.
- 5,000 startup cycles under the existing protocol with 0.095 mg/cm^2 total PGM on the cathode, with Pt ECSA loss of <12%.

3. 2. Test Protocol

The first subtask during the second year of the project was the development of a generic electrochemical test mimicking the real SU/SD events. The principle of the test was based on:

- The amount of air present in the anode compartment during the startup of the fuel cell stack
- The equivalent amount of charge required for a substantial portion of the oxygen fraction in the air to be reduced
- Requirement that the voltage does not go over 1.45 V (Project milestone)
- Requirement that the OER current does not fall below 1 mA/cm^2 (Project milestone)
- Constraint that the time for the required charge to be delivered is < 10 seconds
- The catalyst should withstand 10,000 of high voltage excursions (pulses/cycles)

As in most SU/SD durability tests, triangular-wave potential cycles were used with an upper voltage limit, in this case 1.6 V. However, since the OER catalyst prevents the fuel cell from reaching this upper voltage limit, it is necessary to introduce a *charge limit*. The charge limit corresponds to the complete consumption of the residual oxygen in the anode compartment,

marking the end of the SU/SD event. Thus, an effective OER catalyst will reach the charge limit by supplying the needed protons while maintaining the cell well below the voltage limit.

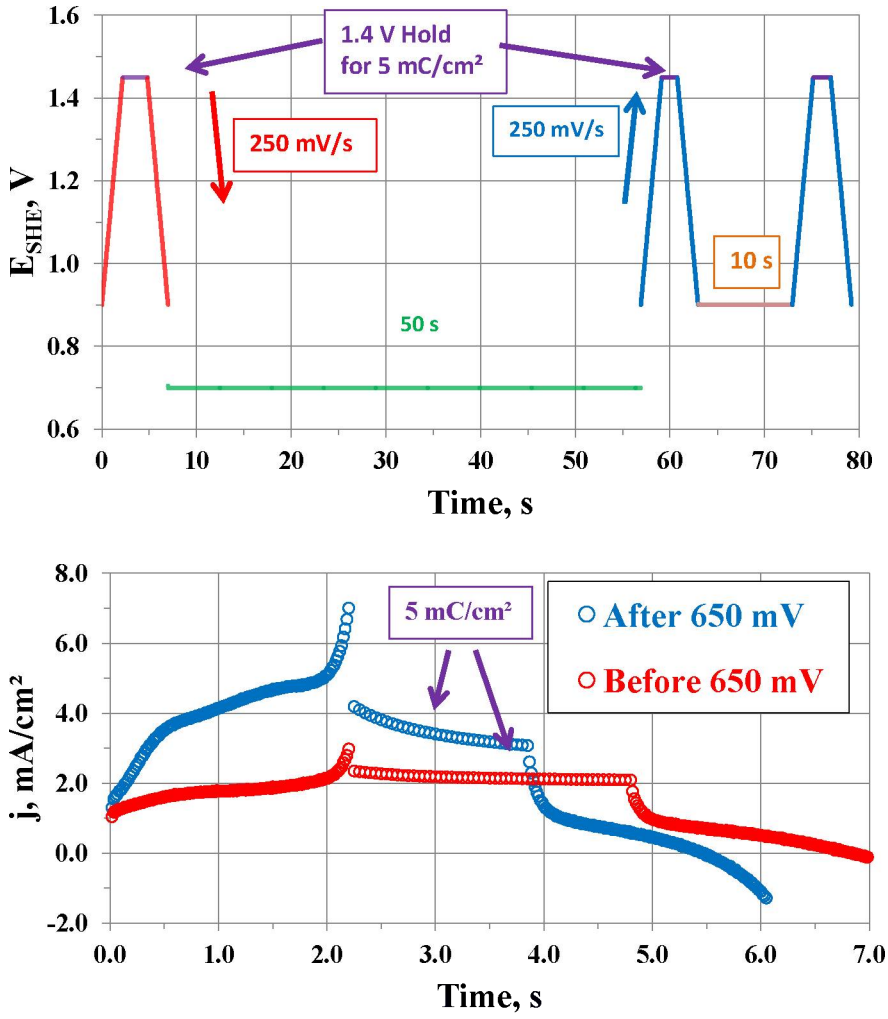


Figure 3.1. Schematic presentation of the electrochemical test protocol (upper) along with the actual cell response (lower). Step description: 250 mV/s potential sweep up; 1.45 V HOLD to 5 mC/cm^2; 250 mV/s potential sweep down; 10 s at 900 mV; 700 mV (in lower panel noted as 650 mV vs. 1% H_2) every 50 cycles/pulses; ECSA every 1,000 cycles. 50-cm^2 MEA under nitrogen/1% hydrogen, 70 °C, fully saturated.

In order to further mimic the real FC operating conditions, after every 50 pulses to 1.45 V versus SHE (which is equal to 1.4V vs. 1% H_2, the typical reference used in these tests to minimize crossover), the catalyst was periodically exposed to ~ 0.7 V vs. SHE (0.65V vs. 1% H_2). Further, in order to mimic the incoming hydrogen front during the startup, a potential ramp of 250 mV/s from the OCV voltage, 0.9 V, was imposed. Schematic presentation of the test protocol along with the actual cell response is presented in Figure 3.1. There is a difference in the current response

depending on whether the potential ramp is imposed immediately after the cell has been exposed to 0.7 V, or later on during the consecutive cycles (Figure 3.1B). This is due to the oxidation current going towards formation of the PtOx on freshly reduced catalyst. The OER, however, starts at ~ 1.3V regardless of the state of the platinum. Actually, by the time the potential reaches the OER onset potential, platinum is already covered with an oxide film which renders it OER inactive.

As is illustrated in Figure 3.1, the (mostly reversible) current responses during the potential sweep up depend dramatically on the OER catalyst oxidation state. Typical results illustrating the behavior of the OER catalyst and the final outcome of the testing after 10,000 startup equivalent cycles are presented in Figure 3.2 Figure 3.3. In Figure 3.2 (left), typical current responses from 0.9 V to 1.45 V are presented for Pt-NSTF, with and without10 μg/cm^2 of IrRu. The two upper curves were recorded during the first cycle after the catalyst was held at 0.7 V, while the two lower were recorded at cycle 50. In both cases the current traces run almost identical to each other until the potential reaches ~ 1.35 V, at which point the current for the catalyst with the added IrRu takes off due to the onset of oxygen evolution. The higher current before the OER onset potential in the cycle 1 curves is due to the oxidation of platinum. Immediately prior to the potential ramp the NSTF was held at 0.7 V, which means the Pt was in its metallic state. During subsequent cycles, the potential does not drop below 0.9 V, which means that the Pt oxide does not get reduced and consequently the current on the following upward potential ramps to 1.35 V is practically zero.

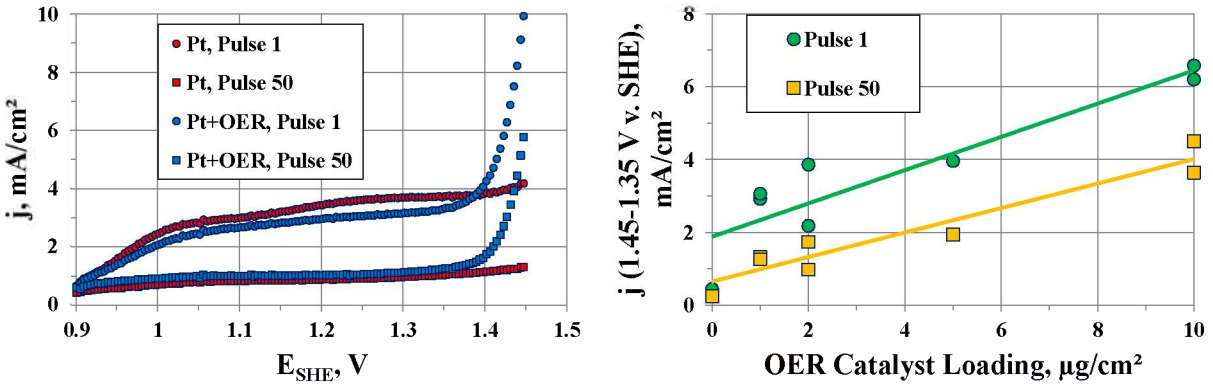


Figure 3.2. Characteristic graphs during the evaluation of OER catalyst in MEA by electrochemical test mimicking the SU/SD. Left: Current responses from 0.9 V to 1.45 V vs. SHE for 10 μg/cm^2 of IrRu on Pt-NSTF and for the Pt-NSTF substrate; 250 mV/s. Two upper curves: the first cycle after the catalyst was held at 0.7 V; two lower curves: at cycle 50.Right: OER peak current dependence on the IrRu loading at pulse #1 (circle) and pulse 50 (square).

The difference in current density between the onset of the OER at 1.35 V and at the peak voltage of 1.45 V is a good measure of the activity of the OER catalyst. In Figure 3.2b the dependence of this current difference on the amount of the IrRu catalyst is presented for the two characteristic cycles, namely the one immediately after (reduced surface) and the other just before (oxidized surface) the catalyst is held at 0.7 V. A linear relationship is observed in both cases.

However, this linearity has a slope of only 1/3, in other words, adding 3 μg/cm^2 catalyst only results in an increase of 1 mA/cm^2 of activity, which in combination with the observed activity of about 1-3 mA/cm^2 at 1 μg/cm^2 loading suggests that only 1/9 (pulse 1) to 1/3 (pulse 50) of the deposited IrRu contributes to the electrochemical surface area.

Since the OER activity is defined in the milestones, this issue will be addressed in more detail. In Figure 3.3, the changes in the current at 1.45 V for the characteristic cycles throughout the 10,000 cycles are presented. The first observation is that the activity of the OER catalysts steadily decays. The second is that the OER currents form three distinctive "bands". The upper band (in green) contains only ten points (four shown in the figure); the first point of each of the 10 scans immediately following the evaluation of the surface area. During these measurements the electrode potential is close to 0 V and, therefore, the electrode surface is fully reduced, *i.e.* regenerated. The middle band (red) contains the partially regenerated surfaces, after the voltage is dropped to 0.7 V (see the example in Figure 3.2b). There are 20 of these points per 1000 cycles. The third band (blue) represents the currents recorded on the most oxidized catalyst surface, *i.e.* at 50th pulse from 0.95 V (immediately before the voltage is dropped to 0.7 V). On average, the OER catalyst itself lost 30% of its original activity. However, at the end of any given pulse during every cycle the current is *always higher than the milestone requirements of 1 mA/cm^2*: 2.8 mA/cm^2 or 0.14 A per the 50 cm^2 MEA at pulse 10,000.

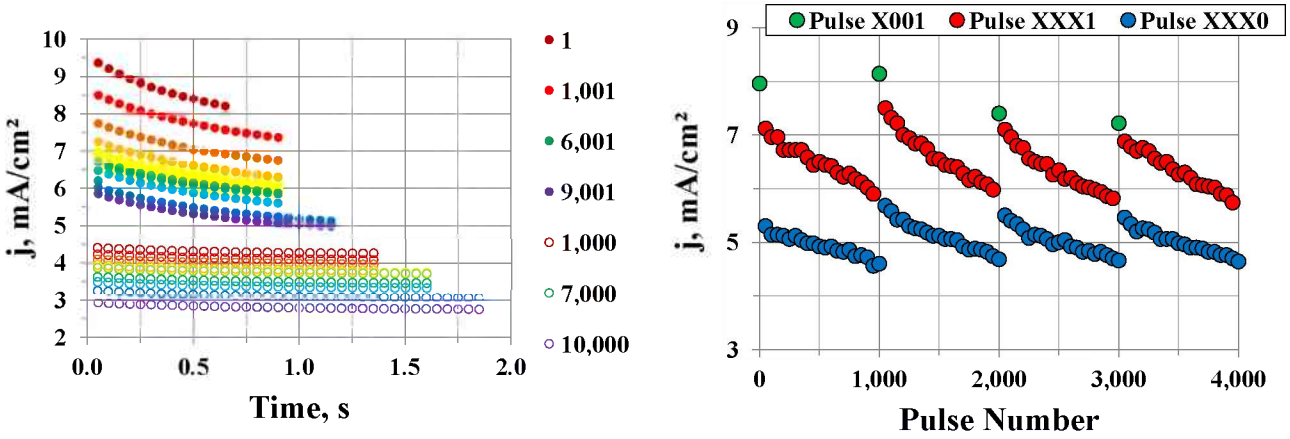


Figure 3.3. Left: Currents at cell voltage 1.4 V (1.45 V vs. SHE) for the characteristic cycles during the 1.4 V HOLD until 5 mC/cm^2 charge is reached) throughout the 10,000 cycles; Note: current decay results in longer time. Right: Initial currents for every 50th cycle for the first 4,000 presented cycles: Green: pulse# 1, 1001, …., 3001; Red: pulses ending at xx51; Blue: pulses ending xx50 or xx00 (see description in the text)

Finally, the effectiveness of the OER catalyst to slow down Pt dissolution is demonstrated in Figure 3.4, which illustrates the changes in Pt surface area, measured at every 1000 cycles for six different MEAs; two with 2 μg/cm^2 and four with 10 μg/cm^2 of IrRu. On average, the rate of the surface area Pt loss was at only 2% per 1000 cycles, which is acceptable for the lifetime of

automotive stacks. One obvious reason for the Pt retention is the ability of the OER catalyst to keep the voltage down.

However, an additional effect, applicable in an MEA environment only, was recently offered as a possible explanation of the suppressed carbon corrosion in the presence of IrO_2 [36]. Namely, during the oxidation of water, the local environment around the catalytic sites gets deprived of water molecules. Since water is a reactant in the corrosion process, water deprivation will have a positive effect in the corrosion retardation. Water certainly plays a role in the dissolution of platinum and this could be an additional benefit of the presence of the OER catalyst. Nonetheless, as we will see in the section on cell reversal, high positive potentials are the main cause for the degradation of Pt.

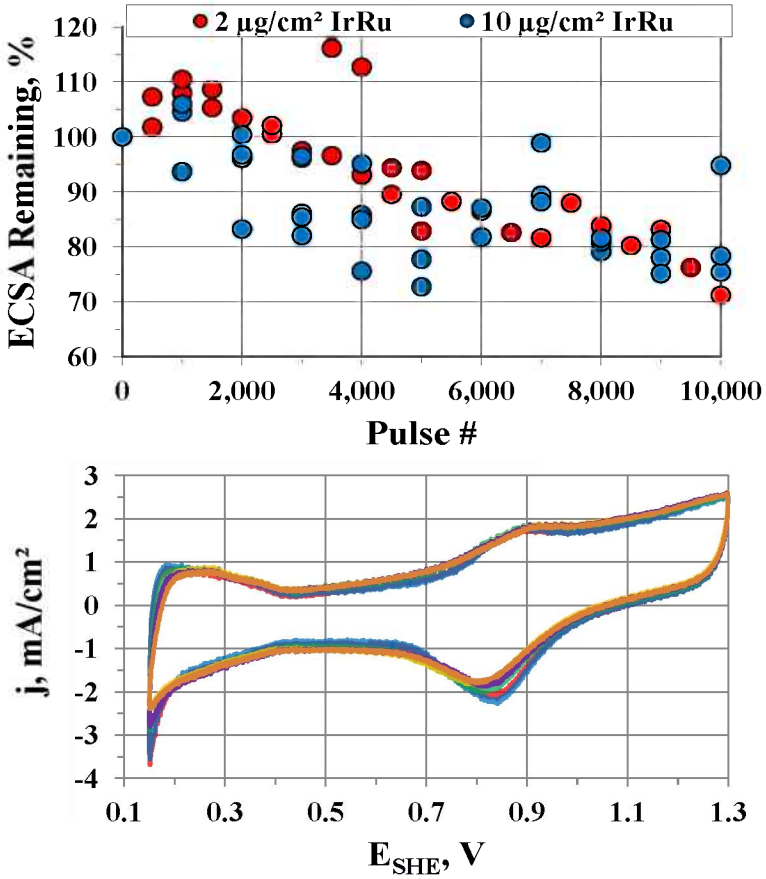


Figure 3.4. Pt ECSA changes during SU/SD test during 10,000 cycles. Pt surface area measured at every 1000 cycles for six MEAs; two with 2 μg/cm² (red dots) and four with 10 μg/cm² (blue dots) of IrRu on 0.25 mg Pt/NSTF. Test conditions identical to those in Figure 3.1. Bottom: CVs at different stages of the test protocol show no significant changes on Pt.

3. 3. Go/No go Requirements

As pointed out, during 2011 the project milestones were redefined with the new 2015 DOE PGM total loading target (0.125 mg/cm^2) and with a new, durability oriented, more realistic testing procedure that had to be developed:

- 5,000 startup cycles under the new protocol with 0.095 mg/cm^2 total PGM on the cathode with Pt ECSA loss of <10%.

This work was performed with an OER catalyst consisting of 90% Ir and 10% Ru at., heretofore referred to as IrRu. The IrRu loading was varied between 1 - 10 μg/cm^2 in order to evaluate the effect of loading on activity and durability. Ru followed by Ir over-layers was deposited on 0.085 mg/cm^2 Pt-NSTF substrate by a DC-magnetron sputtering process with ultra high purity Ar as the sputtering gas. Four different IrRu catalyst over-layers were formed using mass loadings of 1, 2, 5 and 10 μg/cm^2 geometric area.

All electrochemical testing was done in 50 cm^2 FC assemblies. The MEA was prepared by laminating the catalyst-coated NSTF onto a 50 μm membrane (3M PEM 825 equivalent weight) [9]. The OER catalyst evaluation was done under nitrogen with diluted hydrogen on the anode, at 70 °C, fully saturated. The impact of the added OER catalyst on ORR activity was assessed through standard fuel cell performance testing before and after the SU/SD test (80°C, H_2/air, constant stoich 2.0/2.5, 68°C/68°C Dew point, 50/50 kPa).

Upon recommendation of the Tech team and the Durability working group, the electrochemical equivalent of the gas switching SU/SD test consisted of the following steps:

- Starting potential at 0.95 V mimicking the presence of air on the anode;
- 100 mV/s potential ramp representing the H_2 front;
- Ramp reversal back to 0.95 V when 5 mC/cm^2 are accumulated, emulating the equivalent amount of O_2 to be reacted away, in order for the H_2/H^+ electrode potential to be established, or;
- Ramp reversal back to 0.95 V when 1.65 V (the upper potential limit) is reached;
- Every 10 cycles/pulses potential drop to 700 mV for 50 seconds, mimicking the cell voltage during normal operation;
- Electrochemical Surface Area (ECSA) evaluation every 1,000 cycles.

In Figure 3.5 a schematic of the test protocol is presented, while the results of this study are summarized in Figure 3.6 and Figure 3.7. The comparison between the Pt/NSTF substrate without and with OER catalyst is shown in Figure 3.6. In the upper panels, the voltage cycles and the current responses of unmodified Pt/NSTF and Pt/NSTF with 2 μg/cm^2 of IrRu are shown. The voltage ramp was reversed at 1.65 V unless a sufficient charge to react away all of the remaining oxygen in the cathode compartment was achieved. Due to software limitations, the voltage reversal took place at 20 mA/cm^2; a value high enough to accumulate more than the required 5 mC/cm^2 during

the scan. As expected, bare platinum was not able to produce the required current and, therefore, always reached the 1.65 V test limit. On the other hand, only 2μg/cm^2 of IrRu was needed to reach the OER current of 20 mA/cm^2 at 1.53 V. The logical consequence of the lower voltage should be a reduction in Pt dissolution. In the middle panel, the current responses for characteristic cycles of the test procedure are presented: the cycle before the potential is lowered to 0.7 V (cycle *n*10) and the two cycles following the 0.7 V step (cycles *nn*1 and *nn*2). First of all, the figure illustrates the effectiveness of the IrRu catalyst. In comparison with Pt, IrRu produces a much higher OER current at lower voltage. Secondly, it demonstrates how the drop to 0.7 V regenerates the current response on the following voltage sweep for both Pt and IrRu. On Pt, this is due to the oxide formation on the reduced surface of Pt after being exposed to 0.7 V, while in the case of IrRu, it is mostly due to the regeneration of the OER catalyst itself. This is further confirmed by the next cycle, *nn*2, where the peak current on Pt is much lower while the current on the IrRu catalyst is only slightly smaller.

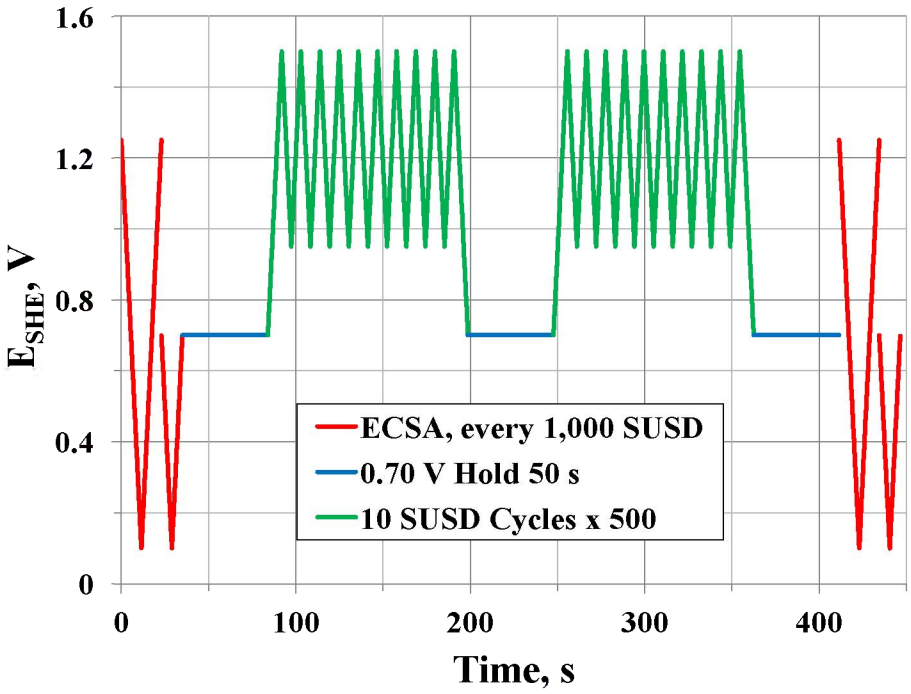


Figure 3.5. Schematic of the modified SU/SD test protocol; Approximate Potential variations during the test protocol are presented.

The lower panel in Figure 3.6 presents the change in the OER activity during the 5,000 SU/SD cycles monitored by the peak voltage at the end of the positive going sweep from 0.95 V until the current surpasses 20 mA/cm^2, or until the upper voltage limit of 1.65 V is reached. As previously mentioned, unmodified Pt always reaches the upper voltage limit of 1.65 V. The activity of the three samples with 1, 2, and 10 μg/cm^2 of IrRu follows the anticipated trend, with the 10 μg/cm^2 of IrRu having the lowest peak voltage. During the first 2,000 cycles, there is very little variation in the behavior of the three IrRu loadings, indicating that no measurable change/dissolution in the

OER catalysts take place. However, with further cycling the differences between the three samples become noticeable, indicating clearly the superior OER activity retention of the highest loaded IrRu sample.

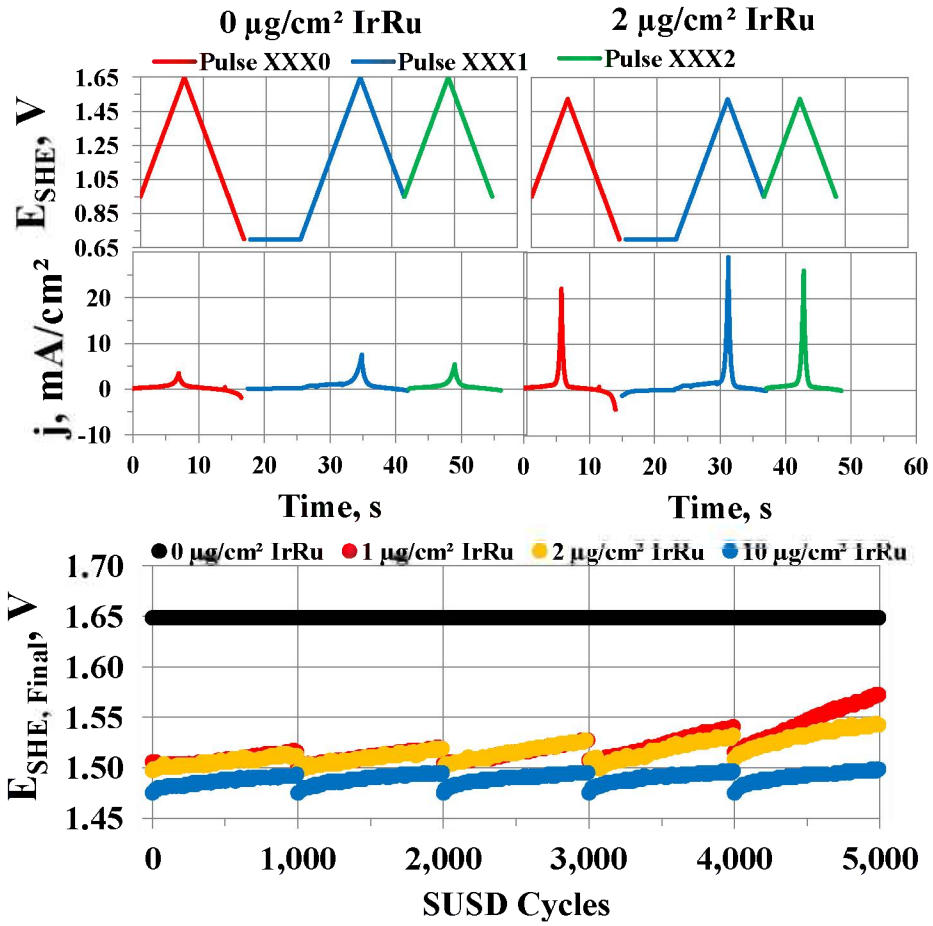


Figure 3.6. Comparison between the Pt/NSTF substrate and OER added catalyst loading under 2012 SU/SD test protocol (see text); 0.085 mg_{Pt}/cm^2; OER catalyst loading 1 – 10 $\mu g_{IrRu}/cm^2$. 50 cm^2 MEA under nitrogen/1% hydrogen, 70 °C, fully saturated. (upper) Voltage response for characteristic cycles for Pt/NSTF and 2µg/cm^2 of IrRu on Pt/NSTF. Voltage allowed to reach 1.65 V unless current attained 20 mA/cm^2. (middle) Current responses for the cycles in the upper panel. (lower) End voltage at the positive-going potential sweep when the current reached 20 mA/cm^2 during the 5,000 SU/SD cycles.

In Figure 3.7, the surface area changes during the SU/SD testing is presented along with the impact of the presence of the IrRu on the FC performance. A large number of MEAs (45) were tested in order to compensate for the inevitable glitches which occur during these very long procedures. The upper panel presents the Pt surface area changes before and after the 5,000 cycles measured via H_{upd} (ECSA). The loss of Pt ECSA is clearly correlated to the OER catalyst loading, since the Pt is exposed to lower cell voltages with higher IrRu loading. The bottom panel follows the relative changes of Pt ECSA during the 5,000 SU/SD cycles. Here, again, the difference between bare Pt/NSTF and IrRu-modified samples is quite obvious. This panel highlights an

important achievement, as the samples with 2 and 5 μg/cm^2 of IrRu are both within the range of DOE targets, namely a total PGM loading of less than 90 μg/cm^2 and Pt ECSA loss of less than 10% over 5,000 cycles.

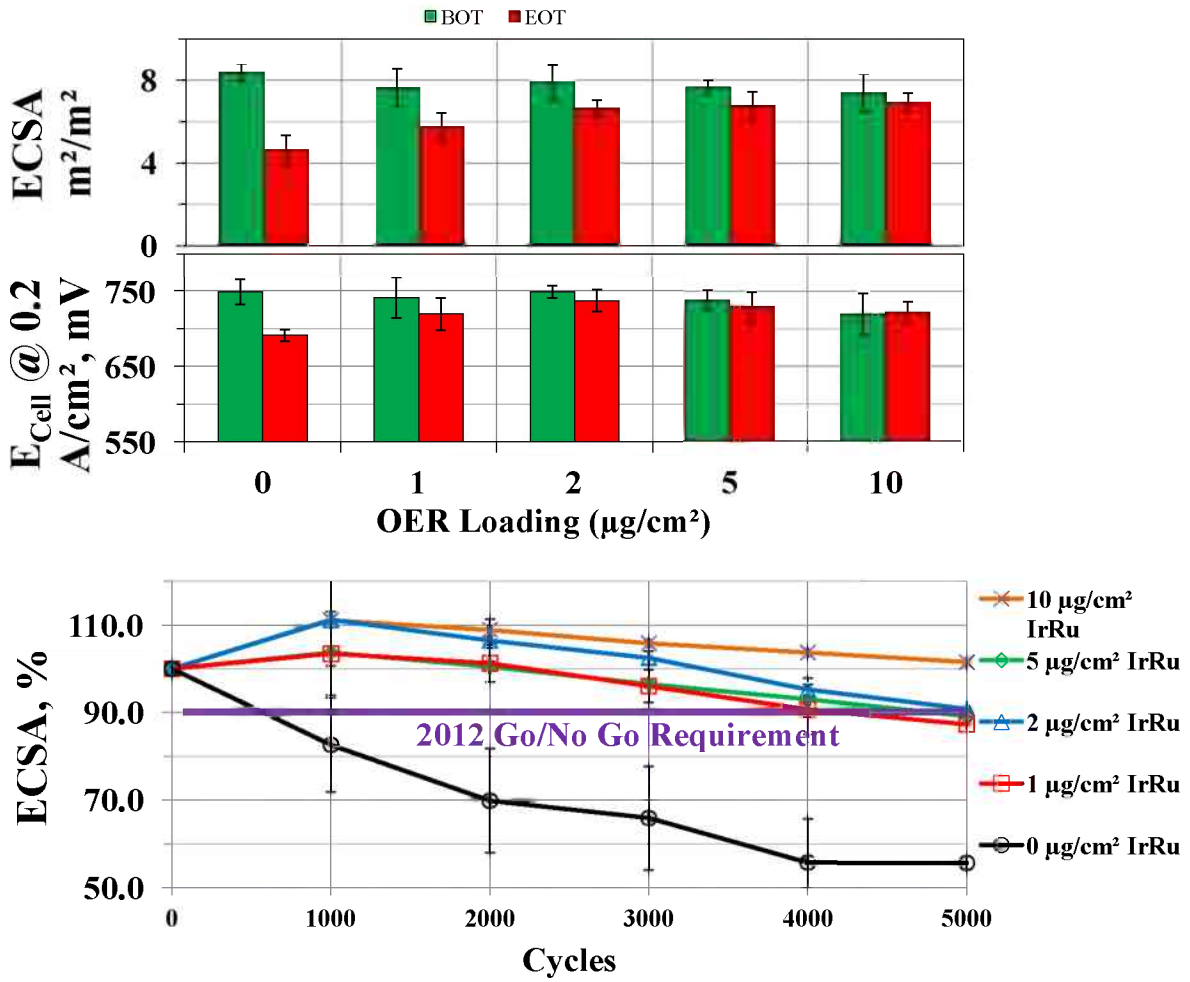


Figure 3.7. (upper) Surface area and (middle) FC performance changes before (BOT) and after (EOT) the 5,000 SU/SD ; Between 5 and 10 MEAs were tested at each loading; (bottom) Surface area evolution during the SU/SD test. Samples and testing methods are identical to those in Figure 3.6.

In order to examine the impact of the added IrRu catalyst on the ORR, the FC performance evaluation is presented in the middle panel of Figure 3.7. Based on Pt ECSA retention and a comparison of the FC performance before and after the SU/SD test, the samples with 2 μg/cm^2 of IrRu provided the optimal overall functioning.

In Figure 3.8, the changes in the OER activity before and after 5,000 SU/SD cycles for different IrRu loadings is presented. As in section 2, the OER activity was measured via polarization curves at slow sweep rate of 2 mV/s. As is obvious from the graphs, the OER activity is maintained better with higher OER catalyst loading. For 5 μg/cm^2 and 10 μg/cm^2 the changes

are within the variation for these long tests; while for 2 μg/cm^2, the decrease in the OER activity is measurable but still maintained at a sufficient level to provide adequate protection to the platinum substrate (see Figure 3.7).

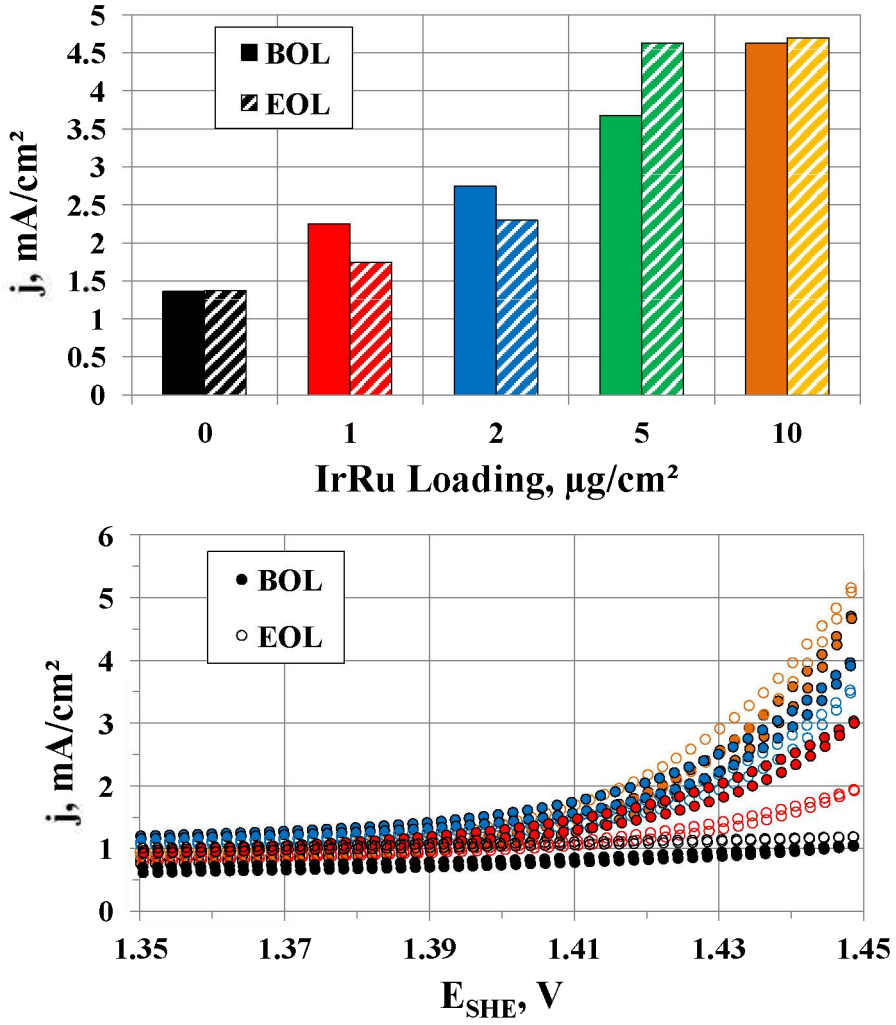


Figure 3.8. Bottom: OER Polarization Curves before and after 5,000 SU/SD Cycles for different IrRu loadings. Top: Current density at 1.44V. Pt loading: 85 mg/cm^2; Scan Rate 2 mV/s. Potentials versus 1% H_2. In excess of 45MEAs were tested.

One of the potential issues during the real life test is the frequency with which the cell experiences high potentials and the magnitude of both the upper limit during startup and the lower limit during normal operation, which is illustrated in Figure 3.9. The first observation from the left panel in this figure is that the differences in ECSA values when scanned to the three different upper limit potentials between 1.42 – 1.5 V are all within experimental error. Some 2 μg/cm² IrRu and all 5 and 10 μg/cm² IrRu loadings pass the 5,000 SU/SD cycles with only < 10% ECSA loss.

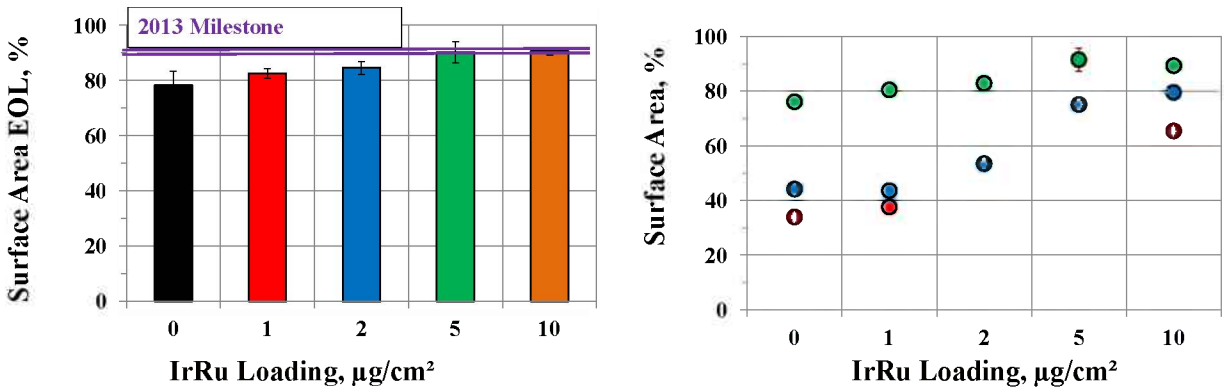


Figure 3.9. Platinum surface area retention after 5,000 SU/SD cycles under the modified 2012 SU/SD test protocol; different IrRu loadings on 0.085 mg/cm² Pt-NSTF substrate. (left) Average of tests to upper voltage limits of 1.42 V, 1.45V and 1.5 V; frequency to lower 0.65 V voltage limit: every 10th time; number of replicates per catalyst indicated on the bars. (right) Green and blue: upper voltage limit 1.45 V; Red: upper voltage limit 1.6 V; Frequency to lower limit of 0.65 V: Green – every 10th cycle, blue – every cycle, red- every cycle.

The main message from Figure 3.9 (right) is that the main impact on the Pt ECSA values is due to the frequency with which the scans are going to the lower voltage limit of 0.7 V. Samples which experience excursions to 700 mV at every cycle (line with blue symbols) show a much larger surface area loss than in the tests where this excursion takes place at every 10th cycle (line with green symbols). The increase of the upper voltage limit by 150 mV to 1.65 V (line with red symbols) enhances the loss of platinum even further, but the effect is less dramatic than the one produced by the frequency of the excursions to 0.7 V. While the frequency effect is perhaps larger than anticipated, it can be understood by the fact that by going to 0.7 V, platinum gets almost completely reduced. It is a well-established fact that Pt dissolution is enhanced by the consecutive formation and the reductions of its surface oxides.

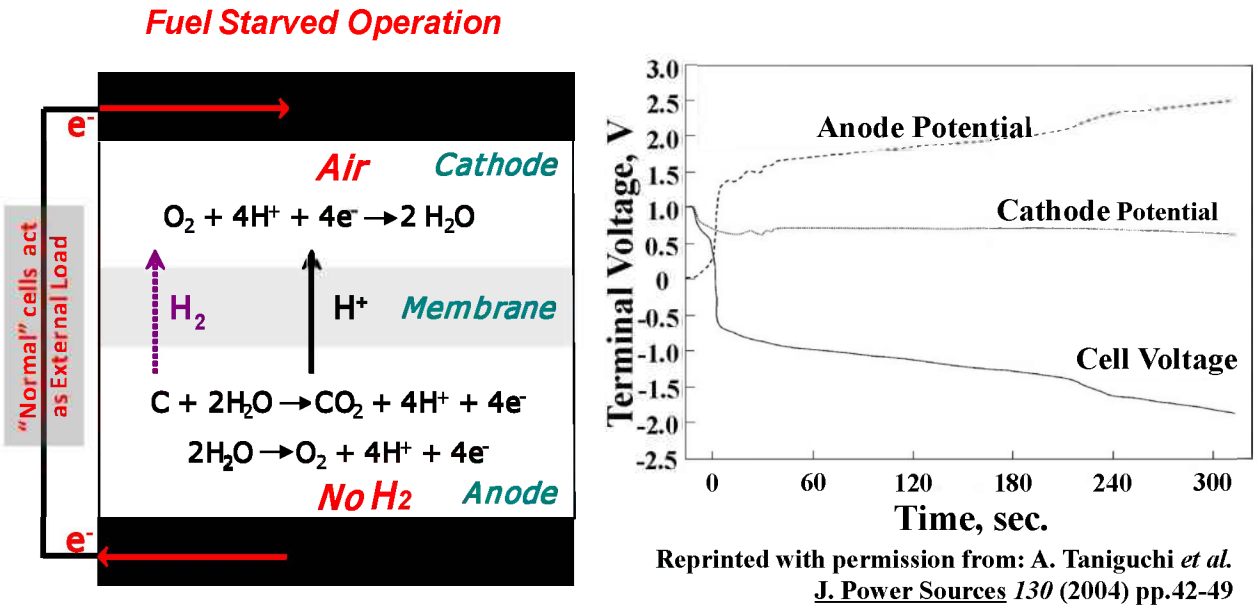
By the end of the 5,000 cycles, the OER activity of the MEAs with 1 µg/cm² IrRu have fallen into the range of Pt samples. However, the samples with 10 µg/cm² have more than enough OER catalyst to still protect Pt. The question of fundamental importance that remains to be answered is why Pt, when exposed to the same potential regime, dissolves at a lower rate when the OER catalyst is present on its surface.

In conclusion, we have developed an efficient IrRu OER catalyst for controlling cathode potentials that has been successfully tested under a protocol developed to mimic SU/SD conditions. Under the constraint of maintaining the cell voltage below 1.65 V, 5,000 start-up/shutdown cycles were achieved with only 0.087 mg/cm^2 PGM on the cathode: 0.085 mg/cm^2 Pt + 0.002 mg/cm^2 IrRu. The added OER catalyst satisfactorily maintained platinum stability and performance at the cathode. The Pt dissolution rate was maintained below 10%, and the end cell voltage after 5000 cycles remained below 1.55V.

4. Task 1: Cell Reversal

The 2011 milestone target for cell reversal was to develop an anode catalyst that can withstand 200 pulses of -200 mA/cm^2, while maintaining a cell voltage of less than 2 V.

As we pointed out in the introduction, cell reversal requires the OER to proceed at much higher current densities and therefore, as illustrated in Figure 4.1, at much higher anode potentials – up to 2.5 V in 5 minutes:



Reprinted with permission from: A. Taniguchi *et al.* J. Power Sources *130* (2004) pp.42-49

Figure 4.1. The processes taking place during the complete fuel starvation (left) and the electrodes' potential changes yielding to cell reversal voltage of the affected cell. Note that the cathode potential remains practically constant and that the necessary protons for the ORR to proceed are coming from the anode side; preferably from the oxidation of water, rather than carbon.

In addition to the OER proceeding at the anode during CR, the necessary Pt loading for adequate fuel cell performance is much lower relative to the cathode. Thus, as presented in Figure 4.2, the impact of Pt loading, with and without the added IrRu catalyst, on the peak anode voltage was explored first. The most obvious observation drawn from Figure 4.2(left) is the large difference in the polarization between the bare Pt and the IrRu overcoated Pt. All the data points for bare Pt are above 1.6 V *vs.* 1% H_2 (1.65V *vs.* SHE); while, even for the highest current density, the IrRu samples are below that value. This difference in experienced potential is directly related to the stability of the Pt. Secondly, within the reproducibility of the tested MEAs, the Pt loading does not appear to have much of an impact on anode potential. Further, the Tafel slope for bare Pt is ~ 200 mV while for the IrRu-coated Pt it is ~100 mV, both in line with literature data and the data presented previously in section 2 for the behavior of Ru and Ir overlayers on Pt-NSTF. The impact of the current pulses on the Pt surface area is rather striking (Figure 4.2 right). After the 44

mA/cm^2, the surface area of Pt-NSTF is less than half of the original value, while the samples with overcoated IrRu hardly lost any Pt surface area even after 200 pulses at 200 mA/cm^2.

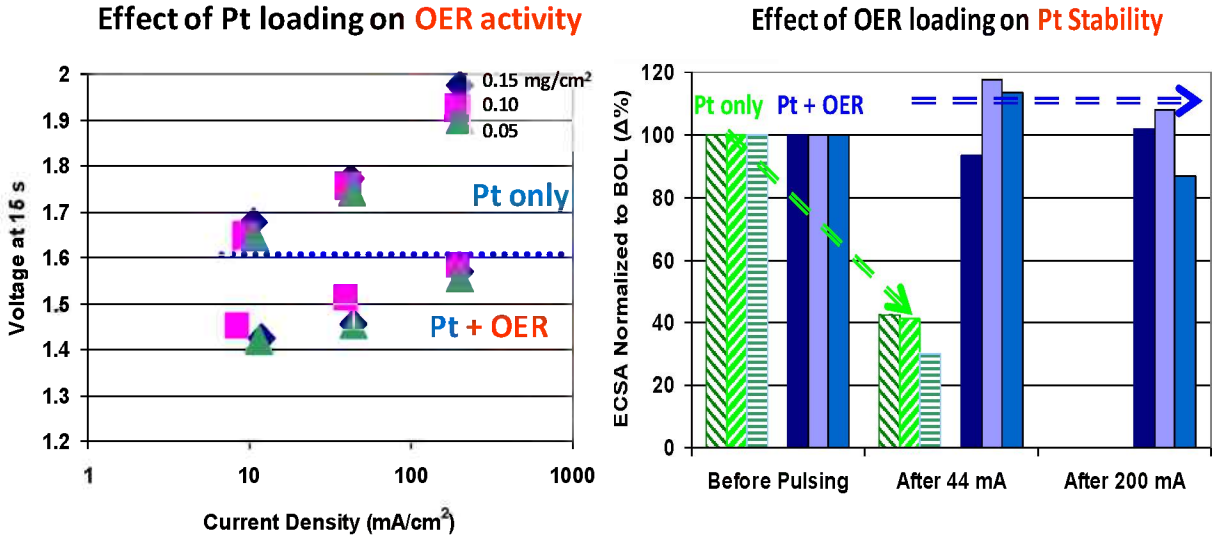


Figure 4.2. The impact of Pt loading on the OER polarization. (left) Above dotted line: Pt-NSTF substrate with 0.05, 0.10 and 0.15 mg/cm^2 Pt. Below dotted line: same Pt-NSTF substrates with 10 μg/cm^2 of Ir(90% at.)Ru(10% at.); Voltage (versus 1% H_2) recorded 15 s after constant current pulse from – 1 mA/cm^2 to 12, 44 and 200 mA/cm^2. (right) Relative electrochemical surface area changes of Pt with (solid bars in blue) and without (patterned bars in green) the OER catalyst before any current pulses, after 20 x 44 mA/cm^2, and after 200 x 200 mA/cm^2 (IrRu on Pt-NSTF only)

For the preliminary screening of the effectiveness of the added OER catalyst and for diagnostic purposes later in the program, a standard test procedure was devised (with some initial inputs from AFCC), which is presented in Figure 4.3.

Essentially, the test protocol is based on the fact that during cell reversal the anode is exposed to very positive voltages, 2 V and higher. Usually, such highly damaging conditions do not last for a very long period of time. Consequently, the core of our test consists of 200 pulses at 200 mA/cm^2, followed by 1 minute at a potential close to 0 V. As depicted in Figure 4.3, the potential is more positive with every consecutive 200 mA/cm^2 pulse. However, the presence of a good OER catalyst does keep the potentials below 1.7 V. The test protocol involved a systematic tracking of the impact of the high potentials on platinum by evaluating the ECSA after each of the characteristic stages of the OER testing.

- **Test protocol:**
- **1. MEA Conditioning**
- **2. ECSA**
- **3. 20 pulses* @ 12 mA/cm² ; 60 s**
- **4. 20 pulses @ 44 mA/cm² ; 30 s**
- **5. ECSA**
- **6 100 pulses @ 200 mA/cm²; 15 s**
- **2 V upper limit**
- **7. 10 min at close to 0 V**
- **8. 100 pulses @ 200 mA/cm²; 15 s**
- **2 V upper limit**
- **9. ECSA**
- ***) All pulses square wave followed**
- **by -1 mA/cm² for 1 min.**
- **FC conditions: 70/80/80 °C; 1000 sccm; A: N_2; C: H_2**

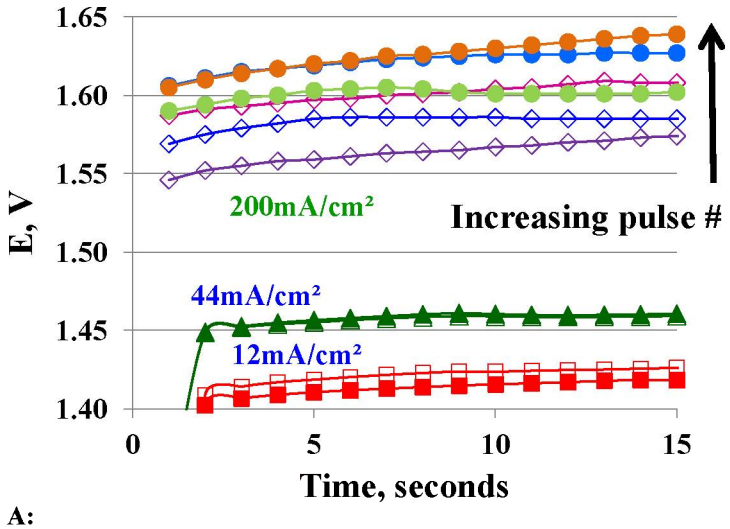


Figure 4.3. The cell reversal test procedure and typical voltage responses of the MEA, based on current pulses of 12, 44 and 200 mA/cm²

During the length of the project, this test protocol underwent slight modifications, mostly around the requirements for stricter upper voltage limits and the anode catalyst loadings; platinum as well as IrRu. New milestones were established for each year and for the Go/No go decision.

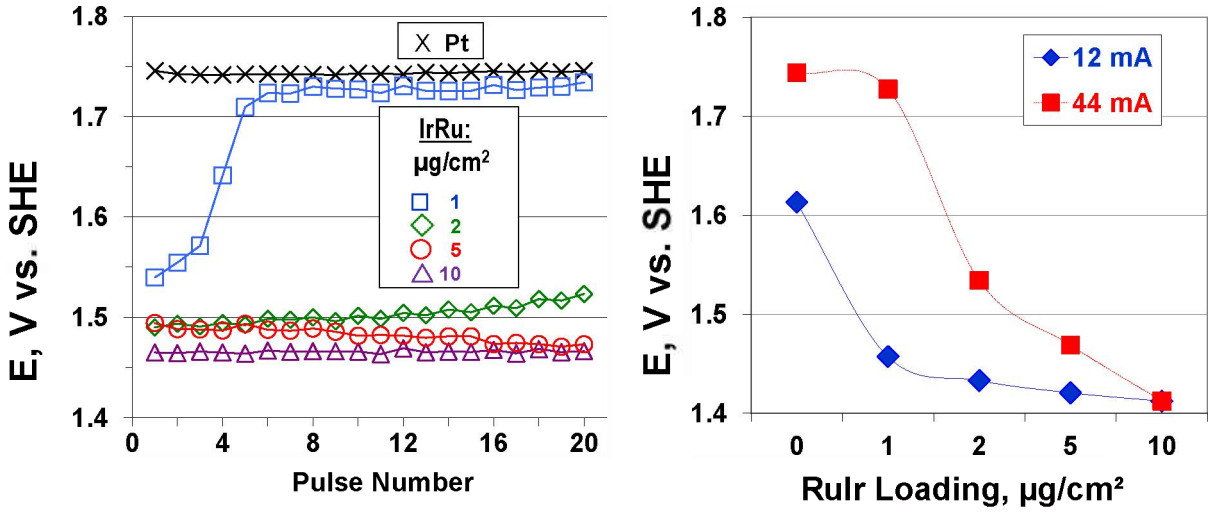


Figure 4.4. The impact of IrRu loading on the OER activity and the catalyst stability. Pt-NSTF loading 0.05 mg/cm²; IrRu loading 1 – 10 µg/cm². (a) End voltage after 30 seconds at 44 mA/cm²; two MEAs tested for each IrRu loading. The lines follow the IrRu loading, uncoated Pt-NSTF at the top, 10 µg/cm² at the bottom. (b) The end voltage at 20th current pulse at 12 mA/cm² (lower curve) and 44 mA/cm² (upper curve)

As is illustrated in Figure 4.3 (right panel), the potential region for the 12 and 44 mA/cm^2 is much lower than for the 200 mA/cm^2 and will be discussed in some details. In Figure 4.4, the impact of IrRu loading in this current range for different OER catalyst loadings (0 – 10 μg/cm^2) is presented. The purpose of the test is to determine the minimum amount of IrRu that will satisfy the cell reversal requirements. In addition, some important observations about the OER activity and the stability of IrRu at high current densities can also be made. For low current densities, the OER potential is higher at lower IrRu loadings, the highest being on uncoated Pt-NSTF. Even more relevant are the findings about the durability of the IrRu. At the smallest loading, 1 μg/cm^2, the potential rises rapidly with the repeating pulses and, at pulse #7, approaches the polarization of Pt. This can be interpreted as a clear indication of the dissolution of the catalyst. Even after dissolution occurs, the 1 μg/cm^2 IrRu samples still level off at a potential ~20 mV lower than pure Pt. In that aspect, the effect of the OER coating is similar to the effect of pure Ru on Pt-NSTF as pointed out in Figure 2.1. The summary of the loading effect is presented in Figure 4.4b, where, except for the highest IrRu loading of 10 μg/cm^2, all OER catalyst loadings showed some deterioration in the OER activity after testing, which was more pronounced with decreasing IrRu loading.

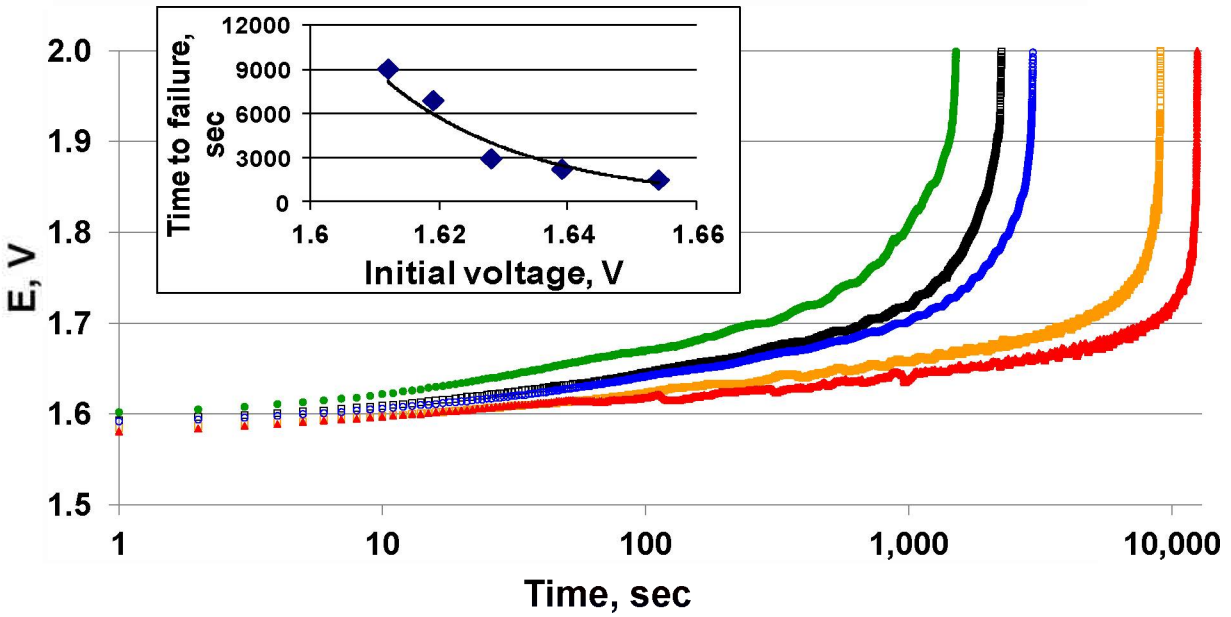


Figure 4.5. Time to failure (2 V) at constant current of 200 mA/cm^2 after the 200th 15 seconds pulse of the same current density. The curves represent five MEA replicates of nominally the same 10 μg/cm^2 of IrRu on 0.1 mg/cm^2 Pt. Inset: Time to failure as function of the initial voltage at beginning of test.

The requirement for practical transportation applications is that the OER catalysts endure 200 current pulses of 200 mA/cm^2, with a pulse duration of 15 seconds each, without reaching a cell voltage of 2 V. To mimic the normal FC operation, the potential between the 200 mA/cm^2 pulses

was brought down to 0 V for 1 minute. Practically all samples with 10 μg/cm^2 of IrRu fulfilled this requirement with the voltage at the end of the 200th pulse at ~1.65 V. However, in order to further pursue the limits of the durability of the IrRu, following the 200 pulses, a constant current of 200 mA/cm^2 was applied until the voltage reached 2 V. This endurance test, as will be shown later on, has also a practical value because some Original Equipment Manufacturers (OEMs; AFCC and others) require much longer tests for safety purposes, up to 10 hours at 0.2 A/cm^2. The results of this test are presented in Figure 4.5.

Five MEA replicates of nominally 10 μg/cm^2 of IrRu on 0.1 mg/cm^2 Pt were successfully tested under the protocol that included 200 current pulses of 200 mA/cm^2. The end voltage of the samples at the end of pulse number 200 was below 1.7 V. These voltages were essentially the starting points for the endurance test. As presented in Figure 4.5, the starting voltage of these replicates is within a narrow range of ~ 40 mV. Yet, as is presented in the inset, the time to reach 2 V varies by a factor of five; between 1800s and 9000s. The variations in the last phase, the end-of-life testing, exacerbates all the imperfections and variations in all the stages of the catalyst testing, from the catalyst fabrication, through the MEA assembly and through the FC test conditions. Note that the catalyst durability is inversely related to the starting voltage, an interesting observation that can serve as an additional criterion to predict the catalyst durability.

From both a practical and a fundamental point of view, a more interesting event occurs around the potential range between 1.7 - 1.75 V. It appears that this is the voltage limit of the IrRu catalysts, since beyond this voltage a rapid increase in cell voltage takes place. STEM studies were performed on the end-of-life MEAs for each loading, and indicated that little to no Ru or Ir remains on the whisker surfaces once the critical 2 V limit was reached. Thus, dissolution is the key deactivation mechanism. Some Ir was found with Pt in the membrane near the NSTF electrodes, while most was present within the MPL as small, pure metallic nanoparticles (discussed later in section 7).

4.1. Go/ No Go CR testing

- Target: 200 cycles of –200 mA/cm^2 for cell reversal with 0.045 mg/cm^2 total PGM on the anode with 1.8 V upper limit.

In electrochemical terms, the cell reversal test procedure remained the same. However, the total PGM loading target was decreased to 45 μg/cm^2. The upper voltage limit requirement (2 V for the 2011 fiscal year) was lowered by 0.2 V, to 1.8 V for the Go/No go decision. For this systematic study, 200 lineal feet of anode material was fabricated at the **3M** Menomonie pilot plant. A total of 23 MEAs were tested; at least 4 replicates per OER loading

In Figure 4.6, the number of 15 second-200 mA/cm^2 cycles that the catalyst can experience before it reaches the two voltage limits (2 V and 1.8 V) are presented for catalysts with 40 μg/cm^2 Pt/NSTF as a substrate, with 1 – 10 μg/cm^2 added IrRu. There is linear relationship between the

OER catalyst loading and the number of cycles to 'failure', *i.e.* until the voltage limit was reached. Only some of the 5 μg/cm^2 IrRu samples fulfilled the 2 V required and none achieved the Go/No go 1.8 V. Only the samples with 10 μg/cm^2 IrRu fulfilled the 200 pulse to 2 V (not presented) and to 1.8 V, but these have a higher than targeted PGM loading. Therefore, additional samples were made with the Go/No go target total PGM loading of 45 μg/cm^2: 37 μg/cm^2 Pt/NSTF and 8 μg/cm^2 IrRu. As presented in Figure 4.6, these samples reached the 200th 200 mA/cm^2 pulse without going over the limit of 1.8 V.

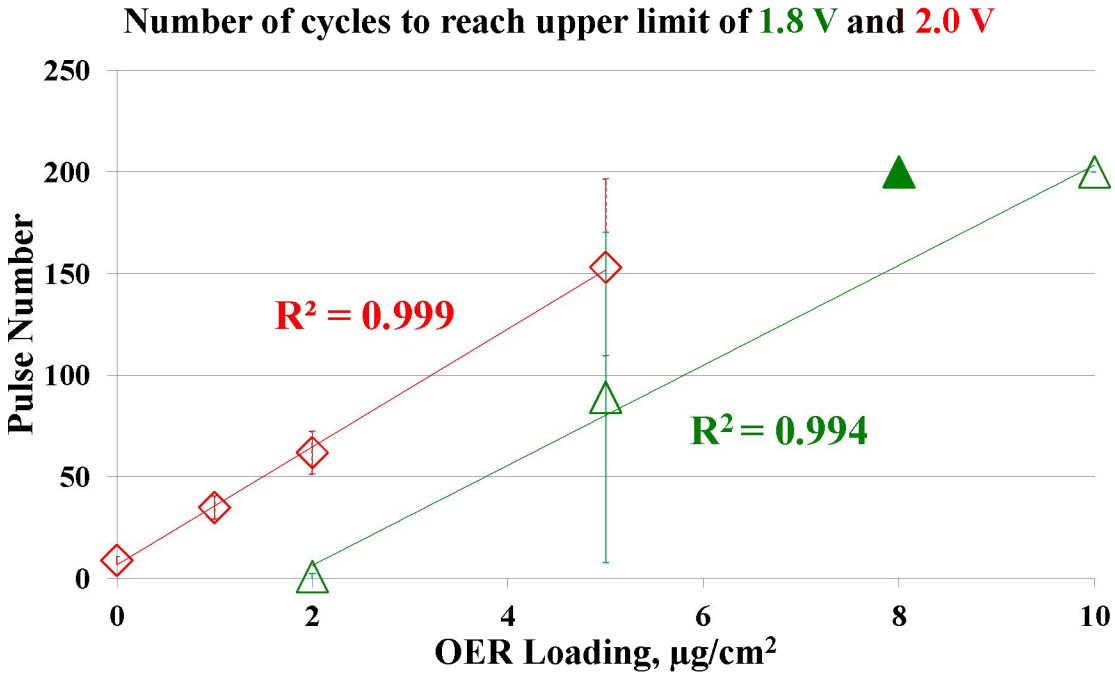


Figure 4.6. Cell reversal testing of OER catalyst with IrRu loading 1 – 10 μg/cm^2 on 40 μg/cm^2 Pt/NSTF. Number of cell reversal pulses of 200 mA/cm^2 up to the target voltage are presented. Solid triangle represents the sample with 8 μg/cm^2 IrRu on 37 μg/cm^2 Pt/NSTF. This sample is omitted from the trend line due to the altered Pt loading.

As a matter of fact, the voltage at the end of the test was more than 0.15 V lower than the Go/No go target. In the left panel of Figure 4.7, the evolution of the end voltages of all 200 pulses for three different combinations of Pt and IrRu loadings are presented. An interesting observation from this figure is that both the IrRu loading and the Pt loading influence durability and OER activity. This could be important in designing the future catalyst, where an obvious optimization between the amount of Pt, a necessary component for the HOR activity, and the added IrRu, the key to the cell reversal performance, has to be attained.

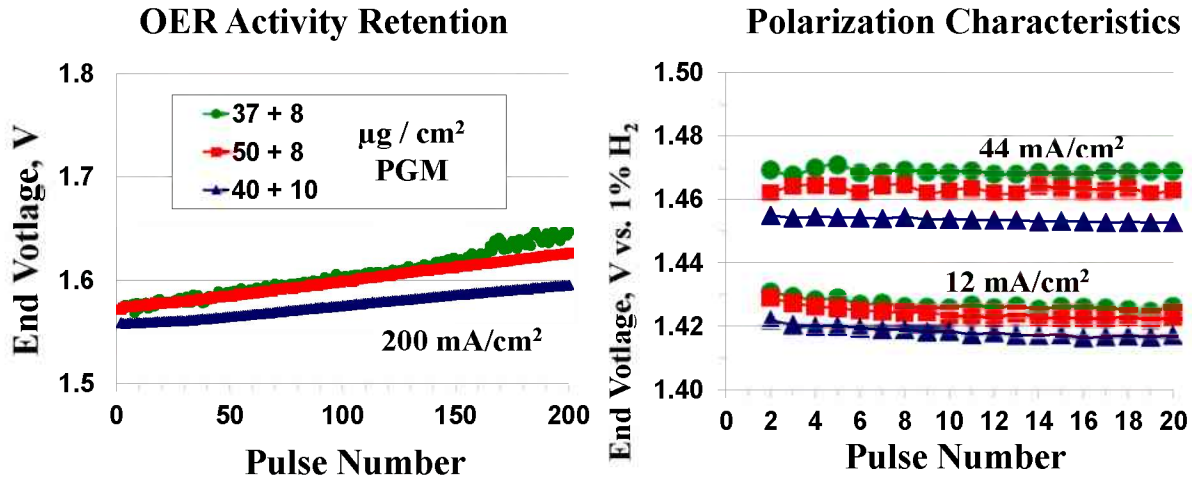


Figure 4.7. Cell reversal testing of OER catalyst with of low loading Pt and IrRu. (left) Cell voltage at the end of each of the 200 mA/cm² pulses for different Pt and IrRu loadings; (right) the polarization characteristics at low current densities expressed through the end voltages of the 12 and 44 mA/cm² pulses.

The main finding from the above data is that irrespective the platinum loading, the IrRu loading is determinant for the OER activity. The 10 µg/cm² IrRu anodes have a lower polarization than the samples with 8 µg/cm². It also appears that platinum loading enhances OER activity. As presented in Figure 4.8, this trend holds for the other important properties of this set of catalysts. The platinum surface area follows the Pt loading (Figure 4.8a). Note that in all cases the Pt surface area is higher after the initial pulsing at lower current densities. Furthermore, a higher loading of OER catalyst exhibits better durability and the small differences in initial voltage before the "HOLD" are translated in appreciable changes in stability (Figure 4.8b). Finally, the most important attribute for the proper functioning of the anode during the normal operation is that it is not negatively affected by the presence of the OER catalyst. The OER added catalyst did not interfere with the normal anode operation as is shown by the H-pump values in Figure 4.8c.

The 2013 year milestone had a lower total PGM target of 37 µg/cm² and a new voltage limit target at the end of pulse 200 of < 1.7V. In order to explore the limits of the lower Pt loading, two series of IrRu catalyst on Pt/NSTF were produced. The IrRu loading was varied between 6 – 12 µg/cm² on both 25 and 30 µg/cm² Pt/NSTF (300 ft lineal of catalysts were produced at the 3M Menomonie pilot plant). Besides fulfilling the project milestone requirement, the purpose of this test was to establish a range of Pt to IrRu ratios that will allow the OEMs a choice most suitable to their needs and loading constraints.

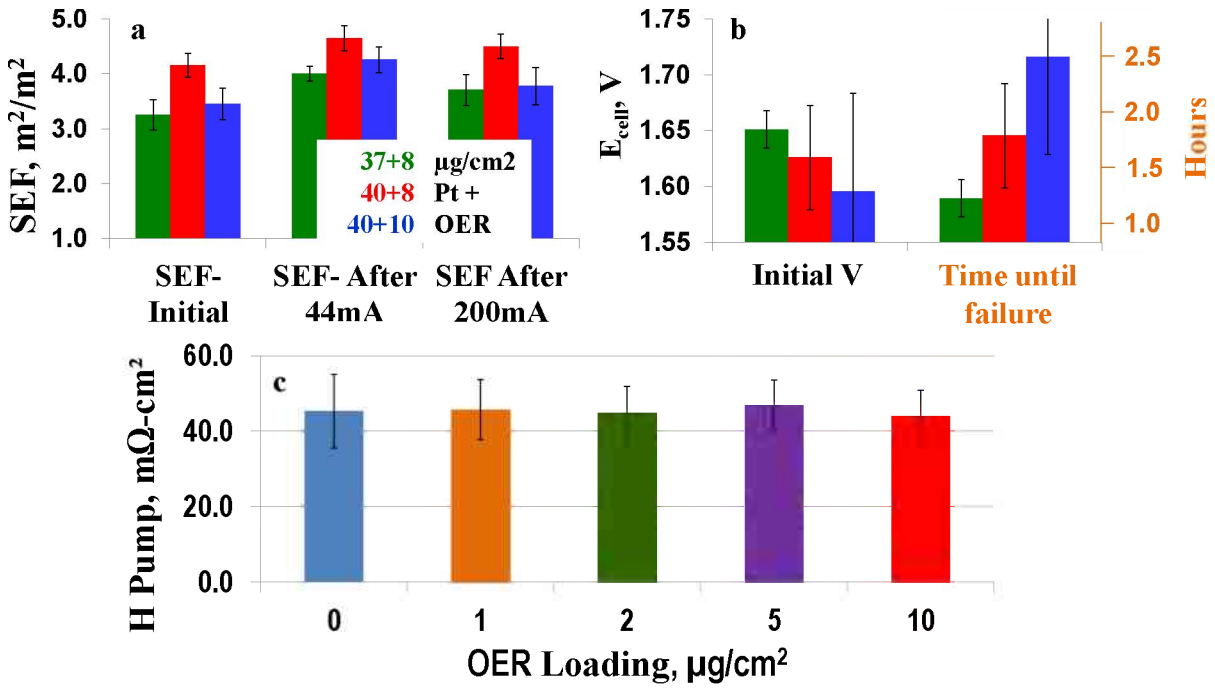


Figure 4.8. The key anode properties during and after the CR testing. (a) Evolution of the platinum surface area; (b) Initial voltage and the durability (hours until failure at 1.8 V) at a continuous 200 mA/cm² hold, after 200 pulses of 200-mA/cm²; (c) HOR polarization characteristics of the anode expressed through the H-pump values

As is obvious from Figure 4.9(a), both 25 and 30 µg/cm² Pt/NSTF series with > 8 µg/cm² RuIr fulfill 2013 milestone requirement, which means they have an end voltage lower than 1.7 V at the 200th 200 mA/cm² pulse, and ECSA loss at close to 10%. However, the series with the 25 µg/cm² Pt/NSTF has a significantly negative impact on the HOR activity; the H-pump value is a factor of four higher than the samples with 30 µg/cm² Pt/NSTF. For this reason, a special catalyst composition targeted at the 2013 requirement of total PGM loading of 37 µg/cm² was produced. The OER catalyst was kept at 8 µg/cm² while the Pt loading was at 29 µg/cm². The expectation was that the H-pump value will be drastically lower than for the 25 µg/cm² Pt. Indeed, within the standard deviations of the multiple samples tested, the H-pump values for the 29 µg/cm² Pt and the 30 µg/cm² Pt are practically the same.

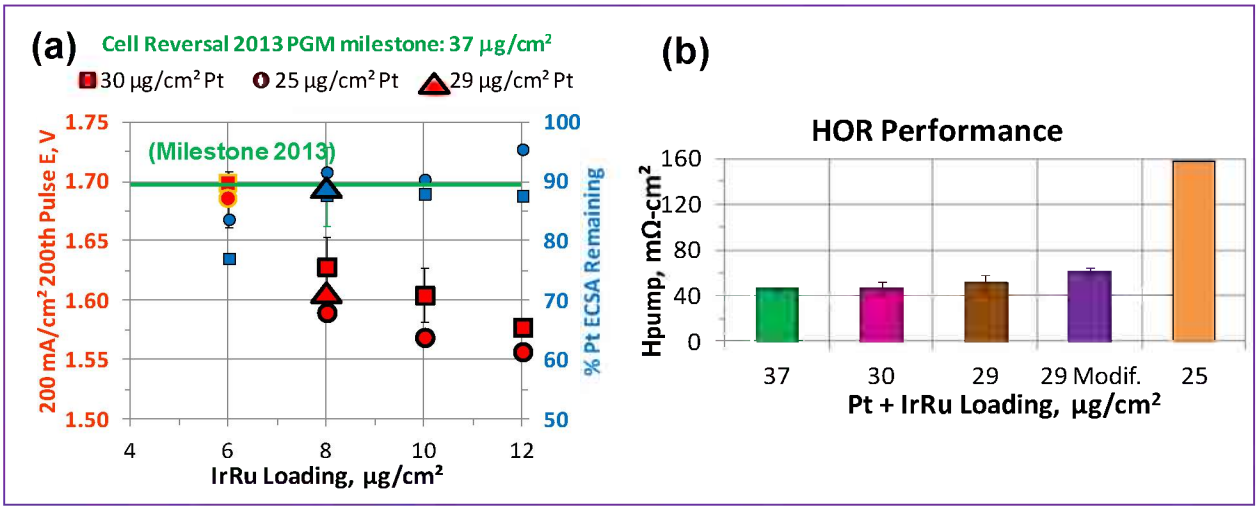


Figure 4.9. Cell reversal testing to establish the range of Pt and IrRu catalyst loadings fulfilling the 2013 milestone (a) The end voltage (red) and the platinum surface area (blue) of the last pulse (#200) of 200 mA/cm²; The triangle symbols are for 29 µg/cm² Pt/NSTF with 8 µg/cm² RuIr. (b) HOR polarization characteristics of the anode expressed through the H-pump values. Pt loading indicated on X – axes; all samples with 8 µg/cm² RuIr; 29 Modif. Sample is modified for ORR suppression (discussed under Task 2, section 5).

4.2. Independent and comparative evaluation.

The independent evaluation of cell reversal was mostly driven by inputs from AFCC corporation, based on their test protocols, performance targets and PGM loadings. Specifically, one of the AFCC main concerns was the extended durability of the OER-modified NSTF beyond the short duration pulses, which was referred to in the previous subsection as 'continuous' or 'hold'. At a current density of 0.2 A/cm^2, this OER-capable catalyst had to remain under the voltage limit of 2.2 V for at least 10 hours. The test was performed with the anode under nitrogen and the cathode under air. Since at 0.2 A/cm^2 the cathode potential is approximately 0.8 V, the cell voltage of 2.2 V in cell reversal mode the anode has to be lower than 3 V!

The first commercially oriented testing was done at the beginning of the second year of the program. The test consisted of the evaluation of a commercial OER catalyst under the test procedure described in the previous subsection (Figure 4.3), in comparison with the data with the OER modified Pt/NSTF catalyst. While the platinum loadings of both catalysts were the same, the OER component of the dispersed electrode had 2.5 times as much IrRu as the Pt/NSTF catalyst. Nonetheless, the durability and the activity of the IrRu modified Pt/NSTF is far superior than the commercial OER-admixed catalyst with dipersed Pt/C, as shown in Figure 4.10 and Table 4.1.

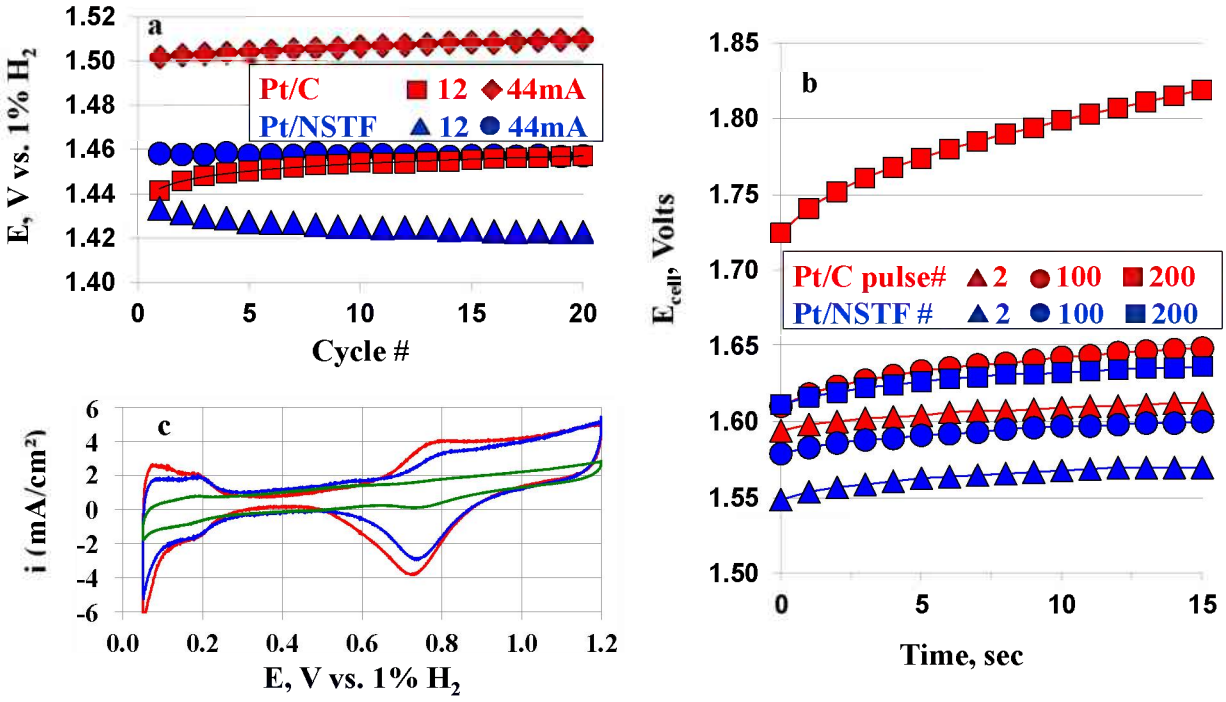


Figure 4.10. Cell reversal comparative test results of commercial OER-added-Pt/C catalyst (3M prepared) with OER modified Pt/NSTF. Same Pt loading; 2.5 times as much OER catalyst on the Pt/C. (a) End points during initial characterization at 12 mA/cm^2 and 44 mA/cm^2 (b) Three characteristic 200 mA/cm^2 pulses for each catalyst are presented (pulse number 2, 100 and 200); (c) CVs for OER admixed Pt/C catalyst as the beginning of test (red, largest H_{upd} and oxide features), after the initial characterization at low current densities (blue, intermediate H_{upd} and oxide features) and after pulse #200 (green, lowest H_{upd} and oxide features). Catalyst loadings: 25 μg/cm^2 of Ir + Ru catalyst, admixed with 0.05 mg/cm^2 Pt/C (graphitized, 100 m^2/g); 10 μg/cm^2 of OER catalyst on 0.05 mg/cm^2 Pt/NSTF

ECSA (cm_{Pt}^2/cm_{geo}^2):	Pt/C	Pt/NSTF
Before Pulsing	13.4	4.1
After 44 mA/cm²	9.2	4.5
After 200 mA/cm²	1.9	4.1
Time to failure at 200 mA/cm² hold:	69 s	4,800 s

Table 4.1. Numeric values for Pt ECSA at different stages of the procedure. Failure criterion: 2.2V.

From all the data of the comparative testing, it is obvious that in spite of the lower IrRu loading, the NSTF based catalyst is more active with the end voltage at pulse #200 substantially below 1.7 V. As we have discussed earlier (Figure 4.5), because of this activity, the Pt/NSTF surface area is practically unchanged during this testing and the OER activity only decayed by 70 mV. On the other hand, the carbon supported dispersed catalyst started losing Pt surface area even after the initial low current density pulses. The reason for this becomes obvious after inspecting the CV after the pulse #200, at which point the cell voltage was close to 1.9 V. The Pt H_{upd} peaks are much smaller while the double layer shows a slight widening. However, the shape of the double layer is such that it indicates the presence of the typical quinone/hydroquinone redox couple for oxidized carbon. In fact, the Pt/C ECSA lost 86% of its original value by the end of the pulsing test.

Most importantly is that the 3M lab findings were soon confirmed by AFCC (Figure 4.11). As stated by AFCC, OER Pt/NSTF outperforms Pt/C with OER. Actually, the OER Pt/NSTF was the first catalyst ever tested by AFCC to reach the 10 hours mark without reaching the voltage limit of 2.2 V. By the end of the test, the OER Pt/NSTF endured even 23 hours.

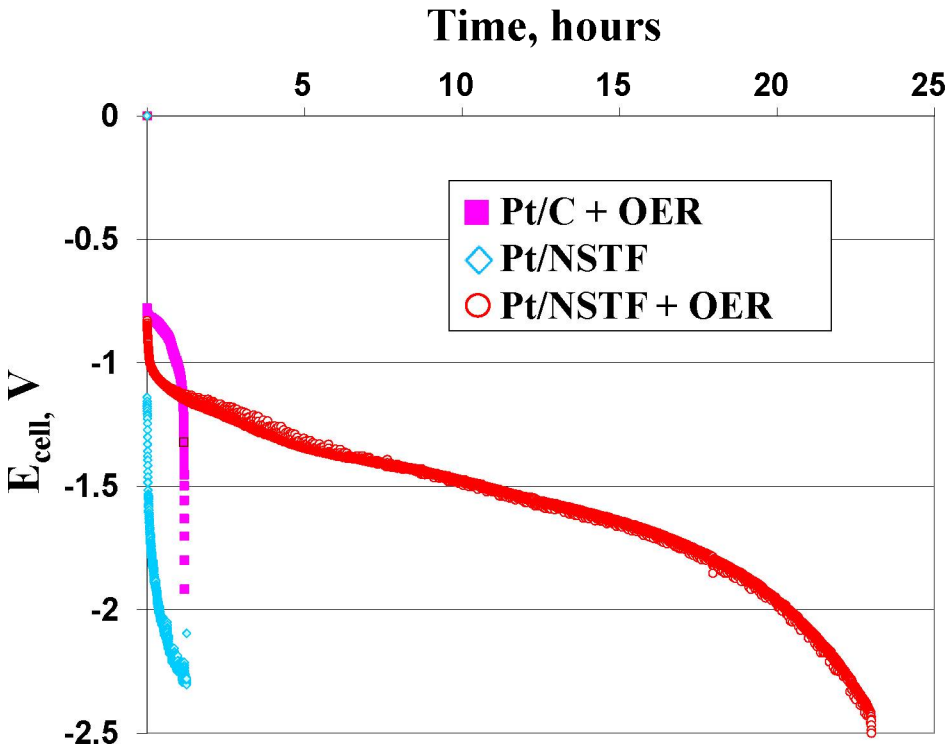


Figure 4.11. Cell reversal AFCC Evaluation of 3M OER Modified Anode; 0.06 mg/cm² total PGM/NSTF; 3M coated *commercial* 0.05 mg/cm² *Pt/C* with OER catalyst and 3M 0.05 mg/cm² Pt/NSTF anodes tested for comparison; Negative current (-0.2 A/cm²) imposed; Anode: Nitrogen; Cathode: Air; Figure provided by AFCC

According to AFCC, the extensive subscale evaluation of the OER Pt/NSTF anode in combination with a variety of MEAs components produced very good results:

– Over all tested cells, the NSTF anode consistently outperformed dispersed baselines with similar loadings
– In many cases the NSTF anode + OER exceeded reversal requirements.

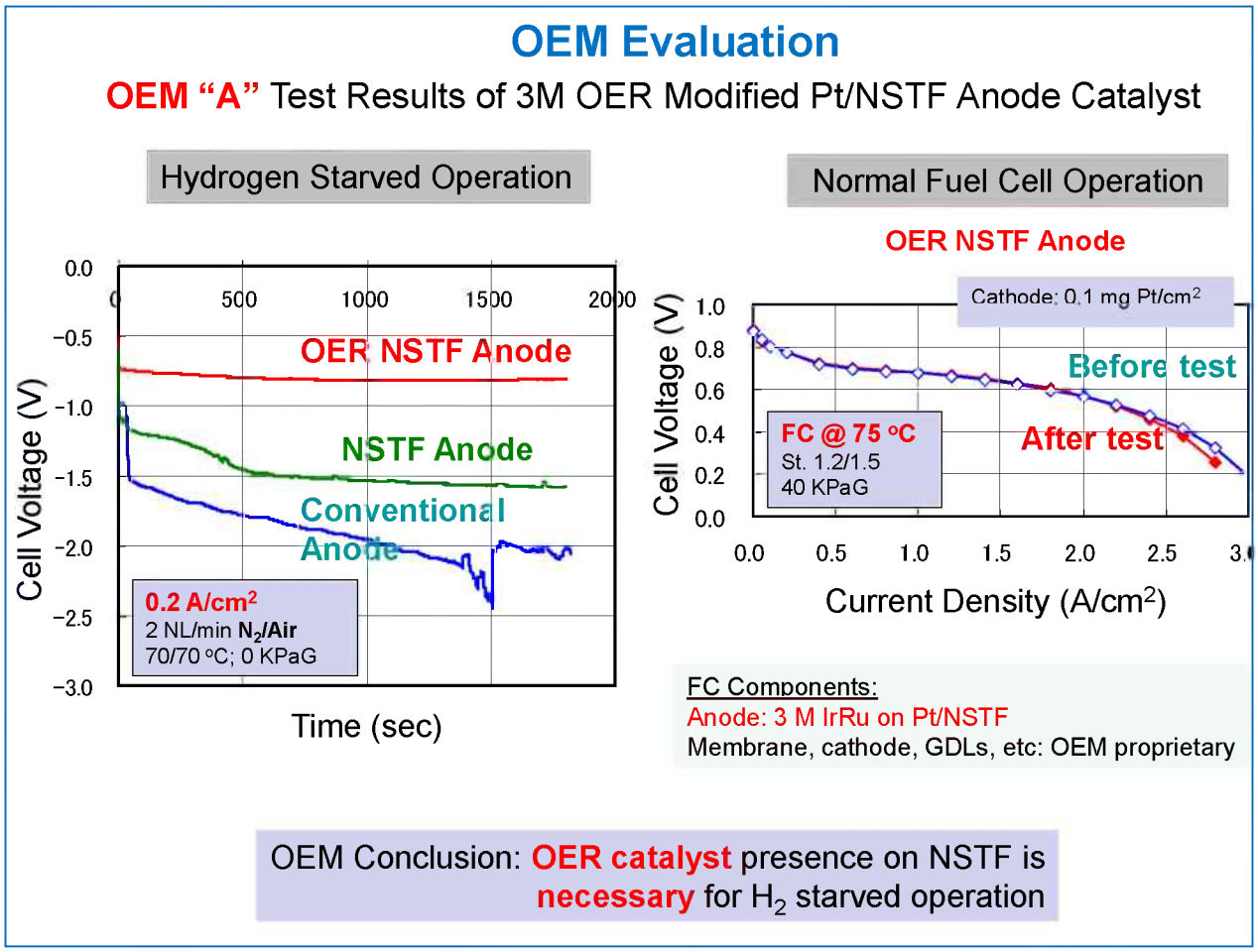


Figure 4.12. Cell reversal Evaluation of 3M OER Modified Anode by a major car OEM

During the third year of the project another major automotive OEM tested the OER-Pt/NSTF. Their findings are summarized in Figure 4.12, which was provided by the OEM, and read as follows: The OER catalyst presence on NSTF is necessary for H_2 starved operation. This is true not only in comparison with the conventional catalyst but also in comparison with the 3M NSTF catalyst without the OER modification.

In year 4 of the project, yet another major OEM tested the 3M OER modified NSTF catalyst and reported that in their 3.5 hour long test, the performance of the catalyst was in agreement with the publically presented data by 3M.

5. Task 2: Oxygen Reduction Suppression on Anode

Technical targets:

- Go/No go: Factor of 10 in the kinetic region
- 2013: Factor of 100 in the kinetic region

This task is based on the notion that HOR as a facile reaction can proceed with practically unchanged rate when a Pt catalyst gets passivated by additives such as tantalum [26]. On the other hand, the rate of the ORR, a more demanding reaction, decreases much more rapidly [27].

In order to efficiently screen a large number of modifications, both with and without additive with potential inhibitive effect for the ORR, we used a rapid screening methodology that was developed and further adapted for the use in this project at Dalhousie University. Series of carbon disks for RDE testing served as the support material for the synthesis of the catalysts. The graphite disks (Poco Graphite grade AXF-5Q) are 5 mm in diameter, polished to a 5 μm finish and then pyrolitically coated to seal open porosity. Similar material is often used for flow field plates in fuel cells. Subsequently, the disks had 3M's NSTF coated on one face. The whisker coating enhances the surface area of the sputter-deposited film by about an order of magnitude. Sets of five or nine of these whisker-coated disks were included in each sputtering run, evenly spaced across the binary library [37]. The films sputtered on the various substrates were used to characterize the film structure, mass and composition as a function of position across the film. The results obtained were then compared to the location of each of the disks used for RDE to determine the composition, structure and mass of the sample being tested. Catalyst loadings as a function of position were determined from pre-weighed Al disks, commonly expressed in mg of catalyst per cm^2 of geometrical surface area. The elemental composition of the film as a function of position was determined with wavelength dispersive spectroscopy (WDS) using a JEOL JXA-8200 Superprobe. The crystallographic structure of the films deposited on the whisker support and on a Si wafer was assessed with a Bruker D8 discover X-ray system equipped with an *x-y-z* translation stage.

A comprehensive protocol consisting of a series of automatic RDE tests was developed to assess several aspects of catalytic activity in a single experiment. The protocol consisted of several sets of tests including a series of low potential step-wise scans while purging H_2 to test HOR activity and establish a reference potential, a set of Ar/O_2 CVs to test ORR performance and sets of high potential pulses to test OER activity and durability during starved operation. Software was written to control Pine RRDE test stations (potentiostat and rotator) and to automate the switching of gas flow. This allows the test station to be set up to run a 24 hour protocol with little to no user input needed while the data is being collected. A total of 5 complete, computer controlled test stations available devoted to this project, allowed rapid processing of the multiple RDE disks produced from one sputtering run.

The system, the catalyst synthesis and the testing protocol was first executed with the Pt-Hf binary system, of which more experimental details can be found [67]. While this is an interesting

system for other aspects of this project, the stability of hafnium was such that it did not fit the requirements as an ORR inhibitor.

During the initial period, the series of $Pt_{1-x}(Ta_2O_5)_x$ coatings on NSTF whiskers grown on glassy carbon disks for HOR and ORR showed the best results. As expected, the presence of significant amounts of Ta_2O_5 decreases the ORR by an order of magnitude while the exchange current densities for HOR decrease by only a small amount (Figure 5.1).

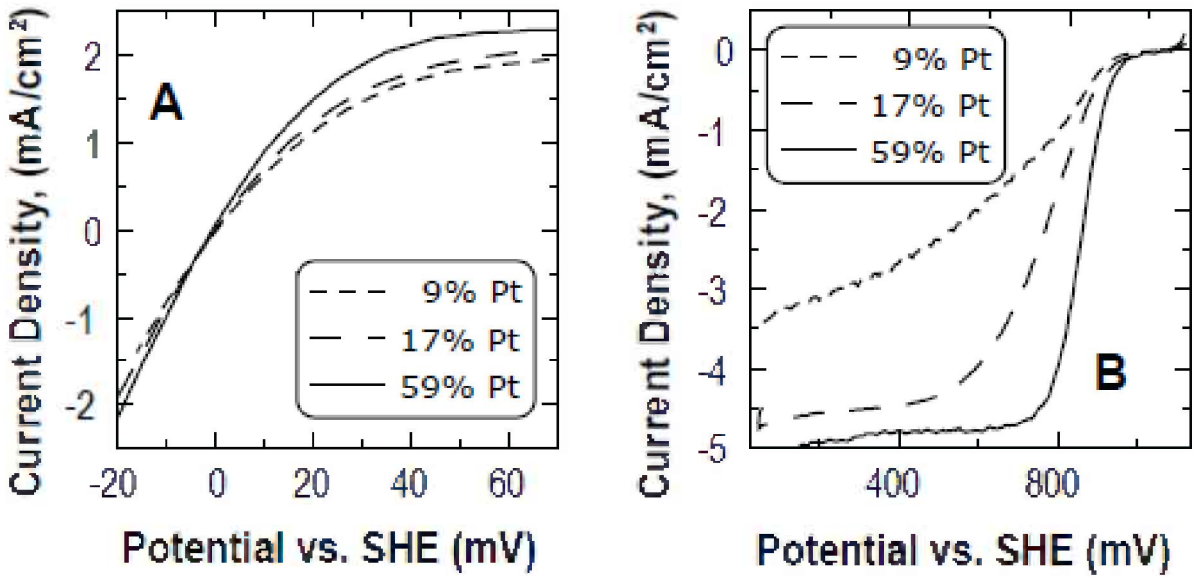


Figure 5.1. Hydrogen polarization curves on rotating disk electrode (RDE: (A) and oxygen polarization curves (B) on a series of $Pt_{1-x}(Ta_2O_5)_x$ catalysts deposited on NSTF-coated carbon disks. RDE at 900 rpm in 0.1 M $HClO_4$ saturated with hydrogen or oxygen at room temperature; Pt loading 0.15 mg/cm^2. (Dalhousie University data).

A variety of libraries produced with inorganic and organic materials added to Pt/NSTF were tested in the later periods of the project; the most successful ones will be reported later on.

5.1. Selective catalysts for the hydrogen oxidation and oxygen reduction reactions

The research group of Drs. Nenad Markovic and Vojislav Stamenkovic at Argonne National Laboratory (ANL) found that an organic compound, when adsorbed on platinum, showed an exceptional selectivity of interest for the goals of Task 2 of this project. In 2010 they have published a paper entitled "Selective catalysts for the hydrogen oxidation and oxygen reduction reactions by patterning of platinum with calix[4]arene molecules" where they showed that the HOR proceeded uninhibited with calix[4]arene molecules adsorbed on Pt single crystal while the

ORR was completely suppressed. The next step was to check if this compound was able to produce the same effect on a real catalyst. The Pt/NSTF presented itself as an ideal substrate for this experiment. During the collaborative effort in this project, the desired outcome was reproduced on Pt/NSTF (Figure 5.2) and subsequently the calix[4]arene was synthesized at 3M in quantities that overcome the scarcity of this custom made material and sufficient for the next set of experiments.

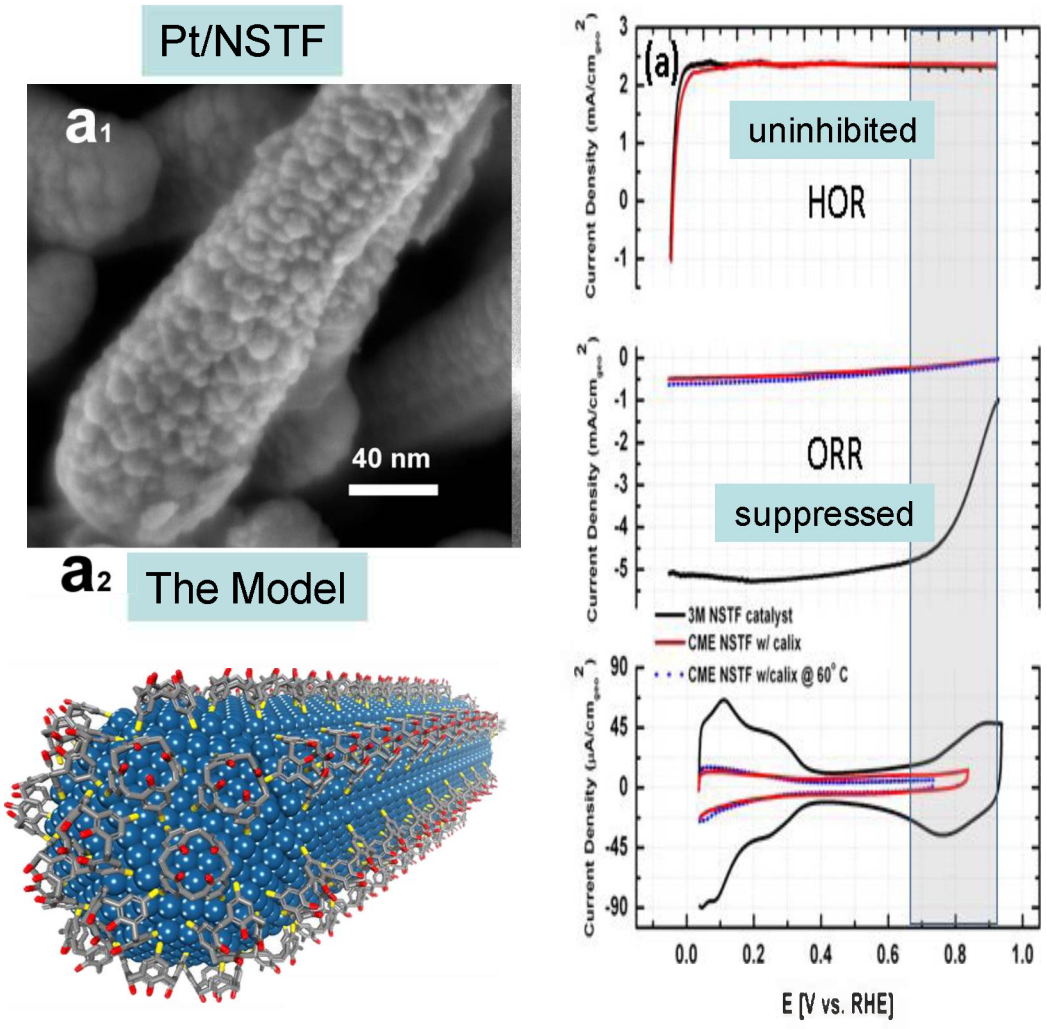


Figure 5.2. RDE evaluation of selectivity of Pt/NSTF with adsorbed calix[4]arene. (a) Uninhibited HOR (top); Suppressed OER (middle); Cyclic voltammograms of Pt/NSTF - outer curve, with calix[4]arene at room temperature – red curve, and at 60 °C – blue curve; (a_1) High resolution TEM of a single Pt/NSTF whisker; (a_2) the model of adsorbed calix[4]arene on the platinum sites of Pt/NSTF. Figure provided by ANL.

The first conclusion from the figure is that selectivity towards the HOR that was found on single crystals was completely transferred to the practical fuel cell catalyst. The fundamental explanation for this effect is best illustrated on the cyclic voltammograms by the complete blockage of the Pt H_{upd} sites by the calix[4]arene molecules (Figure 5.2). Important information

from practical application is the finding that at 60 °C the cyclic voltammogram is the same as at room temperature, the implication of which is that the adsorption of calix[4]arene is strong in the temperature range of interest for fuel cell operation.

The procedure for the synthesis of the calix[4]arene are rather lengthy and involves multiple steps appropriate for very small scale lab effort. After several attempts, the procedure at 3M was slightly simplified. The testing of the 3M produced compound was done at ANL.

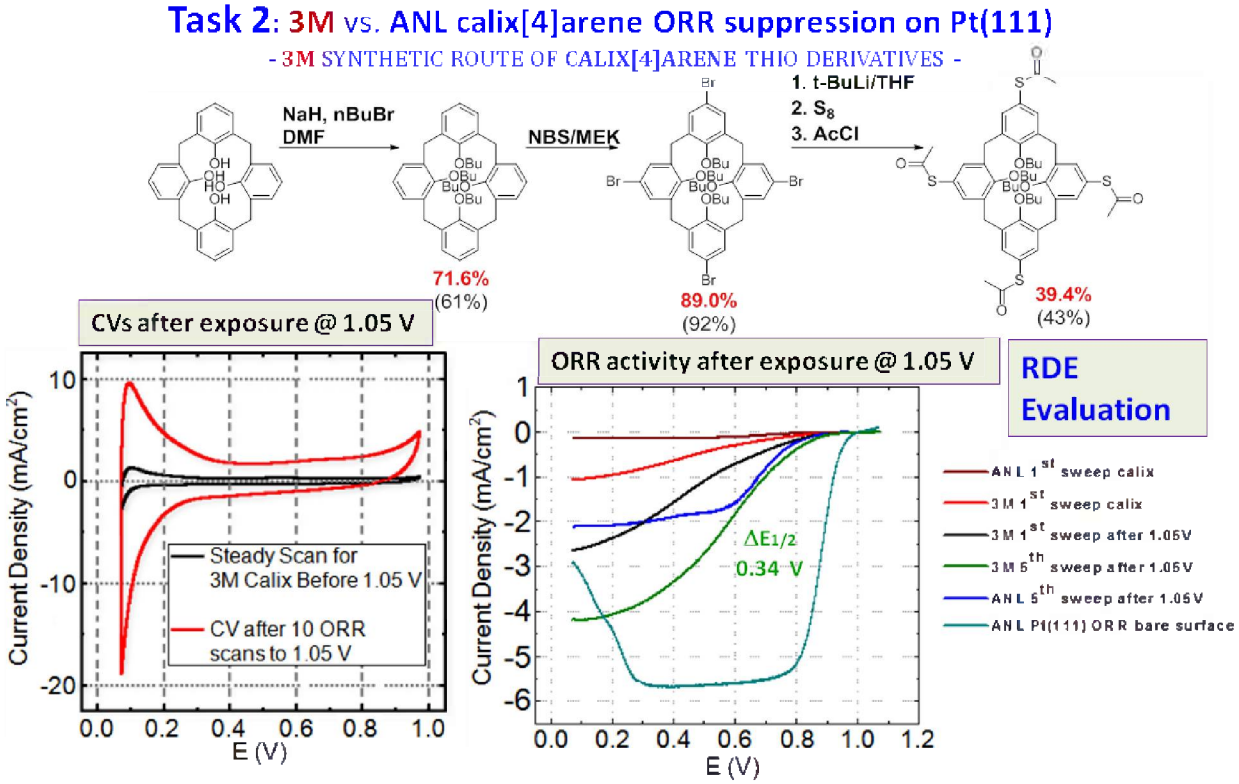


Figure 5.3. The 3M synthesis path of the calix[4]arene and RDE evaluation of its in comparison to ANL selectivity results as presented in Figure 5.2.

In the upper part of Figure 5.3 the 3M synthetic route and the yield of the intermediaries is presented. The numbers are similar to the ones reported by ANL. Nuclear Magnetic Resonance (NMR) was run after every step and the spectra showed that the intermediaries are of good purity. Besides to the upper potential limit of 0.95 V, the CVs were also run to a higher potential upper limit, to 1.05 V. The first cycle to 1.05 V is practically the same as the one run 0.95 V (the graph on the lower left). The tenth cycle is much broader but the characteristic Pt Hupd sites appear to be absent. This is all reflected on the ORR polarization curves (graph on the lower right). The first sweep with the 3M calix[4]arene shows higher activity for the ORR than the original ANL curve. However, the ORR current at 0.8 V, the value expected for the air part of the anode during the SU/SD, is close to zero. The first sweep after the exposure to 1.05 V departs to higher current densities, even though at 0.8 V the values are still close to zero. More substantial currents were

measured after the fifth exposure to 1.05 V, both for the ANL and for the 3M compound. While the sweeps follow each other down to 0.6 V, it appears that the ANL calix[4]arene is inhibiting the ORR more since its limiting current indicates a 2-elctron process. The limiting current for the 3M compound indicates a mixed 3- and 4-electron process. Finally, if we estimate the half-wave potential, the shift of 0.34 V in respect to pure platinum surface can be approximated as over three orders of magnitude of ORR inhibition.

Based on the lab results in aqueous environment, the calix[4]arene appeared to be almost ideal for this task. However, based on the organic nature of this compound a suspicion was raised by the DOE FC Tech Team about its stability at potential much higher than 1.05 V to which the anode is exposed during the cell reversal events. Considering the involvement and the resources required to synthesize quantities appropriate for MEA testing, the decision was made not to pursue this avenue any further.

5.2. Oxygen Reduction Suppression by IrRu on low Pt loading

As we have presented in Figure 2.3, the initial deposition of 10 μg/cm^2 of ruthenium on 0.25 mg/cm^2 Pt substantially slowed down the ORR kinetics. As the DOE PGM loading targets became more restrictive, the anode platinum loading was lowered to 29 μg/cm^2. Exploratory experiments were performed to validate if the loading could be lower yet. At such low platinum loading the ORR kinetics are significantly slower than at 0.25 mg/cm^2 loading. When covered with the OER catalyst one can expect it to become even more sluggish. To satisfy some of the OEMs durability targets for cell reversal, the anode requires a higher OER catalyst loading. Since the OER catalyst resides on top of Pt/NSTF, this yields a higher platinum surface coverage by IrRu.

In Figure 5.4, the progression of the ORR suppression over the first four years of the project is presented. For this purpose the fuel cell testing was done with reversed polarity, namely the anode was under air and the cathode under hydrogen. For comparative purposes, data are presented where the OER component of the anode was the same at 8 μg/cm^2 IrRu, while the platinum loading followed the milestone targets for cell reversal and was varied from 50 μg/cm^2 down to 25 μg/cm^2.

The suppression of the ORR in the kinetic region was measured at a current density of 0.2 A/cm^2. In Figure 5.5, the voltage difference between the baseline and the Pt/NSTF with the OER catalyst are presented. The sample with the Go/No go PGM loading of 0.045 mg/cm^2 total PGM (37 μg/cm^2 Pt and 8 μg/cm^2 IrRu) suppressed the ORR by 150 mV. Taking the usual 65 -70 mV/decade Tafel slope for ORR in MEAs, this suppression of 150 mV means that the ORR has been suppressed by two orders of magnitude.

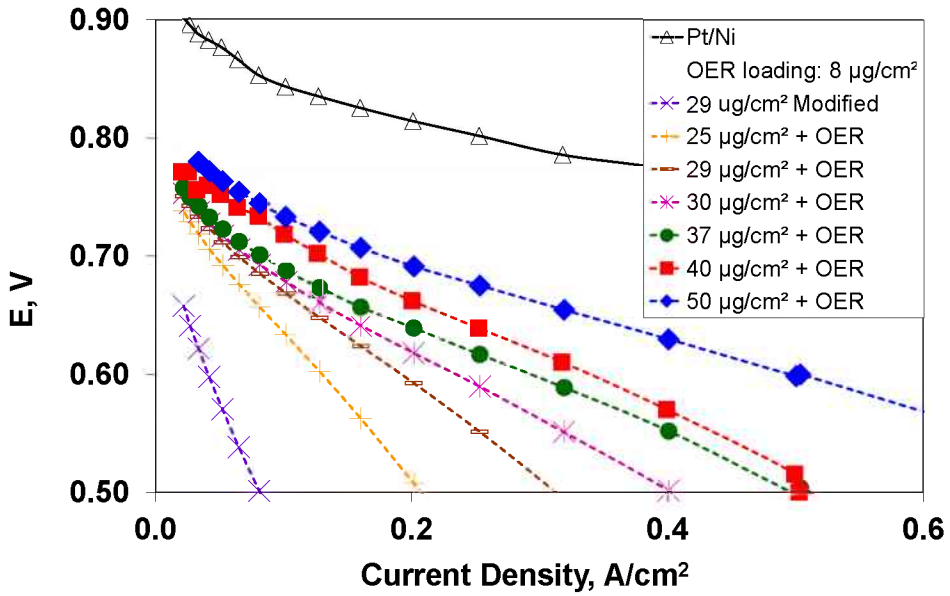


Figure 5.4. Fuel cell polarization curves of the 8 µg/cm² IrRu on Pt/NSTF anodes under air; 100% hydrogen on the opposite side (see text for details).

The MEA with the third year's PGM loading target of 29 µg/cm² Pt and 8 µg/cm² Ir Ru had a voltage decrease of 170 mV, or close to 2.5 orders of magnitude ORR suppression. In Figure 5.4, the MEA with an anode denoted '29 Modified', had the same Pt loading as the third year's target but was further modified with a component that very effectively suppresses the ORR. At 0.05 A/cm², the ORR kinetics in respect to the baseline is slower by approximately 5 orders of magnitude. This path was not pursued in detail and is presented here as an indication of the future opportunities in this area.

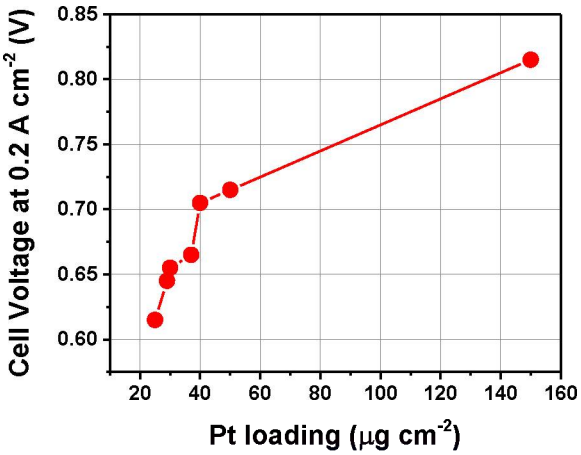


Figure 5.5. ORR suppression at 0.2 A/cm² as a function of Pt loading. OER loading in all cases 8 µg/cm²; except no OER catalyst was present on the baseline sample of 150 $\mu g_{Pt}/cm^2$.

5.3. *ORR Suppression with "Mixed" Anode Catalyst*

As suggested in the last paragraph of the previous subsection, a variety of mixed catalysts with nonmetallic components were evaluated for the ORR suppression. The synthesis of these materials was done at Dalhousie University because of the versatility of their sputtering system. In Figure 5.6, the effect of the mixed/added component to platinum is presented, with the ORR inhibition due to the low platinum loading is separated from the added component contribution by maintaining a constant Pt loading.

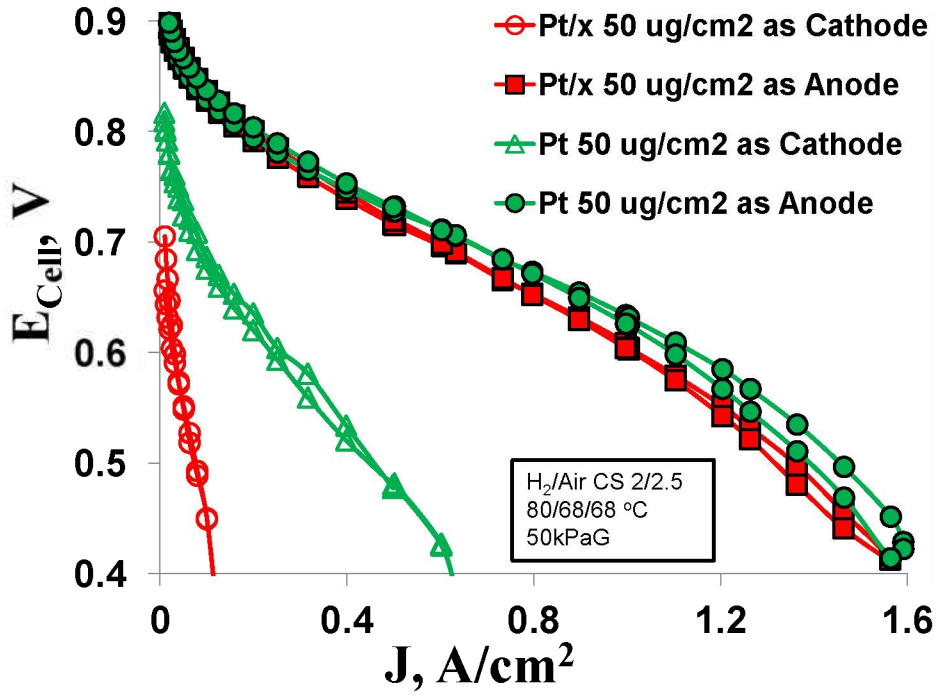


Figure 5.6. Fuel cell polarization curves of mixed Pt/NSTF (Pt"X") anode in normal configuration under hydrogen and under air (red curves); Pure Pt/NSTF presented for comparison (green curves). Counter electrodes in both cases 0.15 μg/cm² Pt/C.

As observed from this figure, when the MEAs are tested in the usual configuration (full symbols) with the low-loaded anodes under hydrogen and the 150 μg/cm² Pt cathodes under air, the polarization curves are essentially the same, especially in the kinetic region. The implication of this is that the added component in the anode catalyst has no adverse effect on the HOR. However, when the MEAs are tested in opposite configuration (open symbols) with air on the anode side, the polarization curves indicate a very strong ORR inhibition. The decrease of the platinum loading from 150 μg/cm² Pt to 50 μg/cm² Pt inhibits the ORR by 0.11 V in the kinetic region at approximately 50 mA/cm², a value similar to the one presented in Figure 5.5. The additive contributed an additional 0.26 V for a total of 0.36 V; in other words, five orders of magnitude of ORR inhibition in the kinetic region.

While the ORR suppression is a good attribute for the anode during SU/SD, there are many other properties needed for an anode catalyst to be accepted for real fuel cell operation. In this particular case, the additives affected other real life performance metrics in an unsatisfactory manner. In conclusion, having in mind the variety of available substances to be applied as additives and the variety of the catalyst constructs, this approach to solving the SU/SD problem via ORR inhibition might be worth paying attention to.

5.4. Independent evaluation

In parallel to the independent evaluation of cell reversal durability, AFCC corporation also studied the impact of the the IrRu modified Pt/NSTF anodes on SU/SD. Unlike our test protocol that was based on electrochemical equivalent pulses (see section 4), the AFCC test procedure had a real life feature: the inclusion of gas switches from air to hydrogen (Figure 5.7).

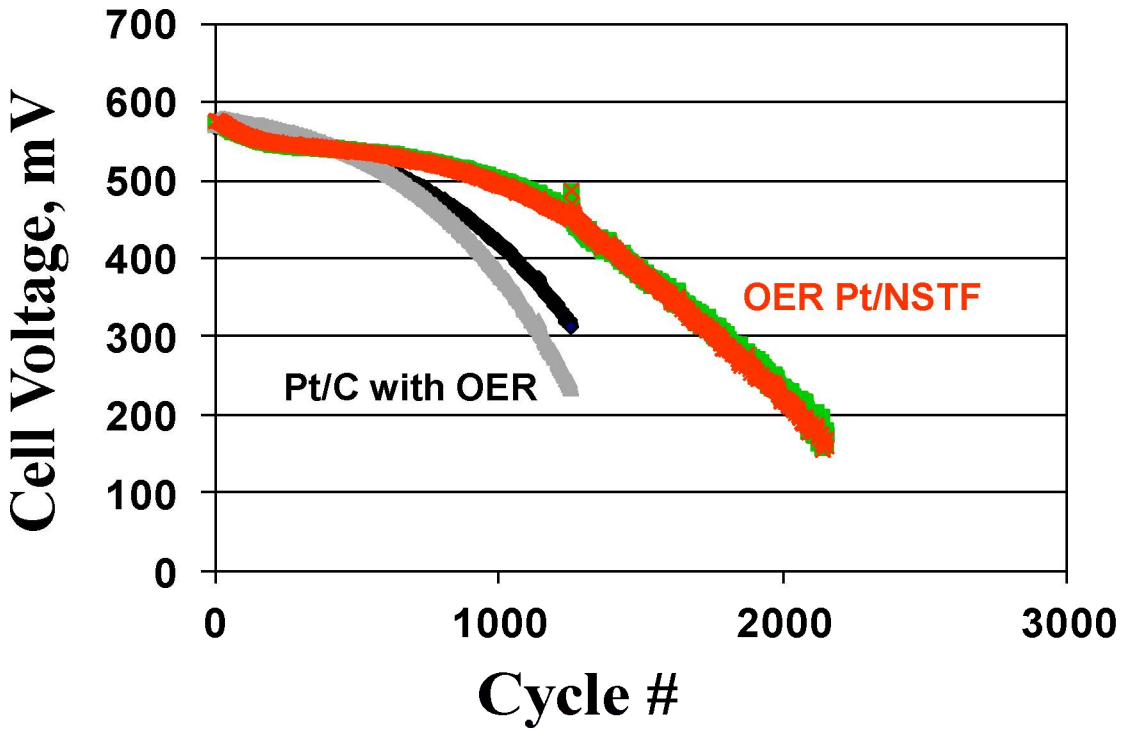


Figure 5.7. Fuel cell characteristic voltage during Gas switching SU/SD AFCC Evaluation of 3M OER Modified Anode; 0.06 mg/cm^2 total PGM/NSTF; Figure prepared by AFCC. Anode gasses switched between AIR and HYDROGEN.

As stated by AFCC, the OER Pt/NSTF outperforms Pt/C with OER in both tests. This test was the ultimate confirmation of the ORR suppression on the IrRu Pt/NSTF anode because that is directly reflected on the durability of the cathode, resulting in better preservation of the FC performance. Moreover, in later work, the gas switching served as a stability test for the IrRu modified Pt/NSTF (see section 8).

6. Task 3: OER Capable Anode Scale up

Technical targets for 2013 (defined in 2012):

- Scale up to full size cells;
- Independent evaluation

According to the DOE Request for Proposals 2008, the scale up phase comprises of two stages. The first one was from a lab/bench scale to 50-cm^2 MEAs, with the second stage to full size MEAs defined by the surface area > 300 cm^2. Since from the very start the basic testing in this project was conducted on 50-cm^2 MEAs, the scale up was to full size architecture. Due to the successful outcome on the subscale testing of the IrRu modified Pt/NSTF by AFCC, the actual scale up phase started during the second year rather than the fourth year of the project. The first results of these tests were reported publically at the AMR 2012. It is important to note that all of the scale up efforts in years 2 and 3 of the project were financially supported by 3M and AFCC. A relatively small part of this effort was charged to the project when in 2012 AFCC became a subcontractor. The results of the AFCC engagement as a subcontractor will be summarized at the second half of this section.

It is very important to state from the onset that the AFCC evaluation had a tremendous impact on the 'real life' directions that the project was undertaking during the three years of the AFCC involvement. AFCC played a role in the independent evaluation, short-stack testing, ex-situ/in-situ characterization, integration, and fundamental understanding.

All the scale up results and the statements in this report were produced by AFCC and are incorporated here as conveyed to 3M by AFCC. The first step in the scale up was the adaptation of the 3M Menomonie production facility to accommodate the large scale fabrication of the new catalysts in respect to the:

- New catalyst formulation
- Larger dimensions
- MEA integration.

Several lineal kilometers of OER modified Pt/NSTF catalyst were produced within the period of three years, from mid 2010 until 2013. The OER-Pt/NSTF was converted in hundreds of full size Catalyst Coated Membranes (CCMs). While the exact number of short stacks assembled and tested is AFCC proprietary information, it is reasonable to assume that several dozen short stacks were evaluated. Full scale testing included evaluation of key anode attributes:

- Performance
- Cell Reversal
- CO tolerance
- Hydrogen concentration sensitivity
- SU/SD durability
- Freeze start-up.

6.1. AFCC OER/NSTF Evaluation of the NSTF anode + OER concept

Major conclusions:

- Significant effort using both subscale and full scale testing has been done following AFCC's demanding technology development process using anodes tailored for AFCC requirements
- In 2011, over 10 short stacks and over 80 MEAs using OER-Pt/NSTF anode have been tested in full scale architecture
- Promising results demonstrating performance, CO tolerance, freeze tolerance, SU/SD benefits, and reversal tolerance
- Overall results: the OER modified NSTF anode is a promising MEA vehicle component.

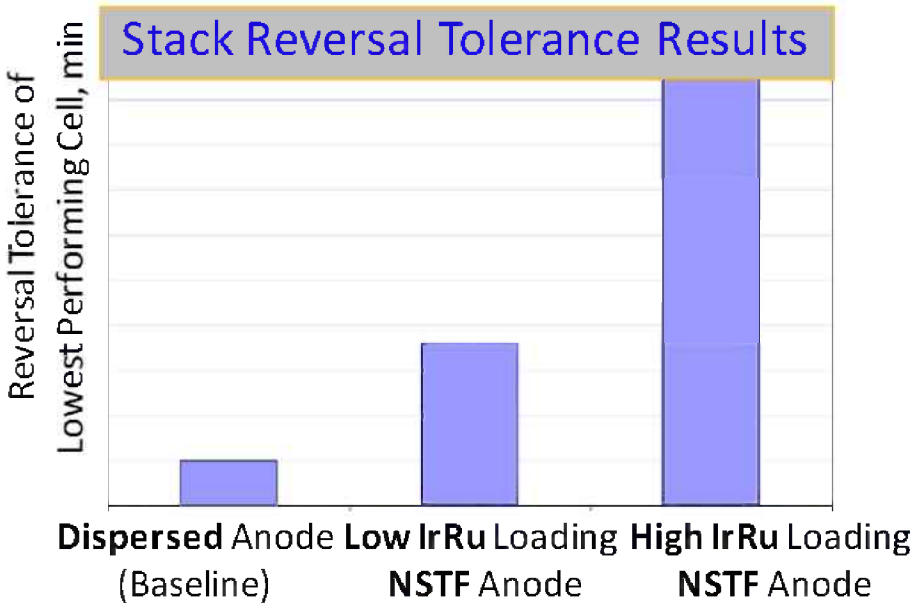


Figure 6.1. Stack Reversal Tolerance Comparison of OER-Pt/NSTF anode; full scale architecture; multiple stacks tested

In stacks, as in AFCC's subscale configuration (reported in section 4) the OER-Pt/NSTF anode consistently outperformed dispersed baselines with higher loadings. Despite lower tolerance than in subscale hardware, the NSTF anode concept still has a very good reversal tolerance for the given loadings (Figure 6.1). The overall result is that the OER modified NSTF anode is a promising MEA vehicle component.

The OER-Pt/NSTF anode has also a positive impact on SU/SD durability in a gas switching SU/SD accelerated stress test. The NSTF anode with OER catalyst is very *selective* as a result of which *inhibits ORR* as shown by the polarization results in Figure 6.2. This is similar to what the subscale testing showed (see Figure 5.6). The OER modified NSTF inhibition of ORR in the

kinetic region can be estimated to be approximately four orders of magnitude (Figure 6.2, right panel).

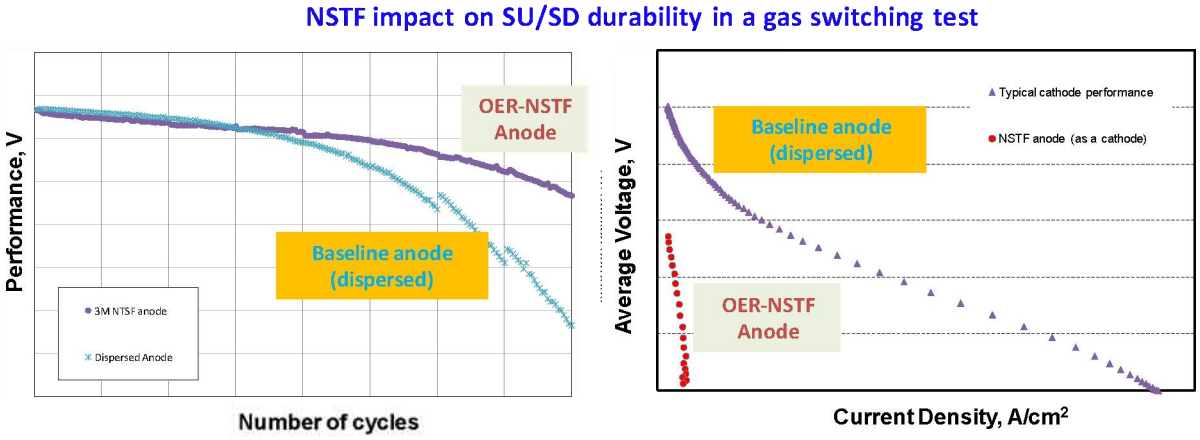


Figure 6.2. OER/NSTF SU/SD durability in a gas switching test in comparison with a typical dispersed anode; full architecture stack configuration; (left) Fuel cell performance retention during the SU/SD; (right) Polarization curves of the OER/NSTF tested as a cathode (under air) - lower curve and a comparative polarization curve for a typical dispersed anode – upper curve.

Some smaller (*secondary*) *effects* in comparison with the dispersed anode admixed with IrRu that

- Low Ru content leads to lower Ru crossover related degradation
- Some Ir may migrate to the cathode and have an OER cathode effect.

Based on extensive testing, AFCC listed the following *Future Challenges:*

- OER/NSTF performance *should have no negative impact* compared to a conventional dispersed anode
- *Stability* of the OER layer *under extended drive cycles* (2,000 hours) and after SU/SD testing
- Testing for *anode contaminants* (in addition to CO)

In conclusion, 3M and AFCC should be driving fundamental understanding of *engineering issues* related to *interfaces and compatibility* of OER/NSTF with other MEA components and anode layer designs.

6.1.1. Short stack evaluation within the AFCC subcontract

2013 Milestone: Evaluate three short tacks

The purpose of the subcontract with AFCC was twofold. First, the subcontract allowed 3M and AFCC to scale up and evaluate the low PGM loading OER modified anode. While these loadings are within the DOE targets, there might not be of immediate interest to the OEMs.

Secondly, all the components in the CCMs were produced by 3M and as such the results of the evaluation can be more freely reported. Most of the results reported hereto on are from the Final Report that AFCC submitted to 3M. The technical activities within the subcontract started in mid 2012 and lasted for approximately one year. The DOE funds covered a smaller portion of this evaluation.

The work under the subcontract was focused on anodes with better reversal tolerance, Cool/Wet performance, advanced anodes with improved start up/shut down durability benefits, as well as anodes with different OER contents including very low loaded anodes which meet DOE loading targets.

While 3M provided CCM components including the NSTF anode, for evaluation, AFCC leveraged its extensive testing background and knowledge of the interactions amongst components, when integrated into a full scale stack, and operating conditions under which they are exposed as the basis for testing the selected anodes. Specifically, AFCC provided performance testing of the anode under simulated system conditions ranging from Hot/Dry to Cool/Wet operation. For lasting anode function in a vehicle, reversal tolerance is necessary and was always measured throughout the scope of this project. Finally, further testing of the NSTF anodes' remarkable ability to mitigate start up/shut down degradation was also evaluated using AFCC's accelerated stress tests.

CCM Description	Anode Pt/OER	Membrane	Cathode
Dispersed anode	**EA50E.1 no OER**	**3M reinforced, 12 µm, 3.2 gsm, 725 EW**	**EA50E.4**
NSTF Anode	**NSTF 0.05 mg / cm^2 OER 0.15 mg / cm^2**	**3M reinforced, 12 µm, 3.2 gsm, 725 EW**	**EA50E.4**
NSTF low loading anode	**NSTF 0.29 mg / cm^2 OER 0.008 mg / cm^2**	**3M reinforced, 12 µm, 3.2 gsm, 725 EW**	**EA50E.4**
NSTF anode with short whisker length	**NSTF 0.02 mg / cm^2 OER 0.015 mg / cm^2**	**3M reinforced, 12 µm, 3.2 gsm, 725 EW**	**EA50E.4**
NSTF anode with modification for OER stability	**NSTF 0.02 mg / cm^2 OER 0.015 mg / cm^2**	**3M reinforced, 12 µm, 3.2 gsm, 725 EW**	**EA50E.4**

Table 6.1. Description on evaluated anode designs. EA50E.1 catalyst represents TEC10EA50E from TKK (Japan), with a Pt loading of 0.1 mg/cm^2.

As described in Table 6.1, five anode concepts were evaluated. All CCMs tested were 3M produced and used identical cathodes and membranes, with only the anode design changing. The purpose of the project is to evaluate the effect of different anode design on performance under

different operation conditions, on cell reversal tolerance and protection effect during startup and shut down (SU/SD). NSTF baseline is compared to the dispersed anode to evaluate the effect of NSTF, and other NSTF iterations are compared to the corresponding NSTF anode for evaluation. Description of the test performed is given below:

Performance evaluation was conducted on a 15-cell short stack at a full scale level using AFCC proprietary protocol. Polarization curves were obtained under four different operation conditions, namely normal operating condition (NOC), warm-up condition (WUP), dry condition and hot condition. H_2 concentration sensitivity was also evaluated for all concepts.

Extended reversal test to evaluate the tolerance of an anode concept to cell failure during fuel starvation. The test was conducted under fuel starvation at certain current density. The cell voltage was monitored until it reached certain criteria. Longer the time to reach the criteria, better the reversal tolerance.

Startup and shutdown. AFCC has a proprietary SU/SD protocol to mimic the vehicle operation and it is designed to evaluate the durability of the entire MEA, including cathode durability and anode selectivity, which provides protection on the cathode during SU/SD. Since all designs in this project have same cathode and membrane it is assumed that anode selectivity can explain differences in degradation rates.

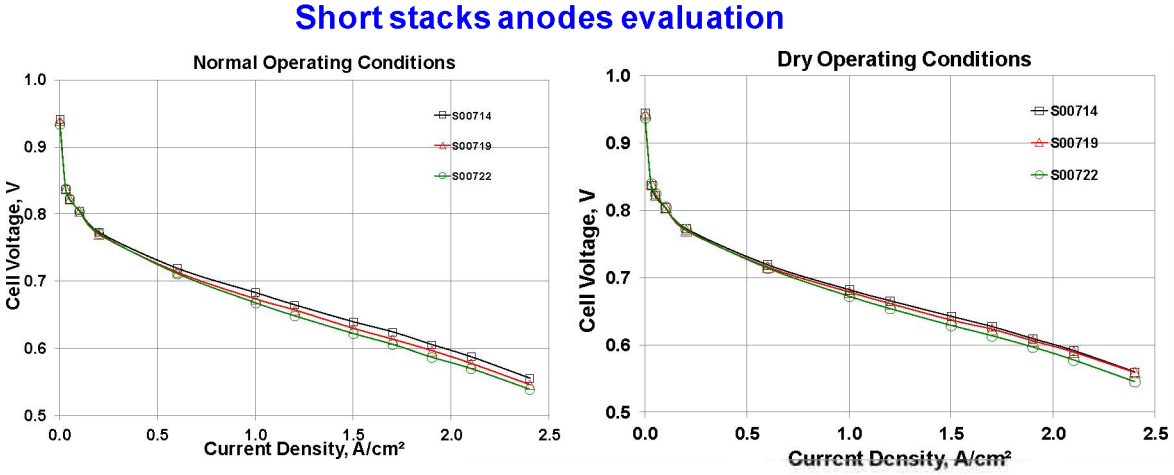


Figure 6.3. Stack Reversal Performance Comparison of OER-Pt/NSTF anodes under normal and dry conditions

Figure 6.3 shows the stack performance comparison between a dispersed anode and two different NSTF anodes. As obvious from the figure, there is not much difference between the three anodes under normal and dry conditions. The importance of this finding is that

- the NSTF as an anode performs as well as the dispersed Pt,
- the low loading Pt NSTF performs as well as the higher loading one.

There is a maximum difference of ~30 mV at 1.2 A/cm^2 between dispersed anode and NSTF anode under warm up condition. At higher current densities the performance is comparable. Overall, the NSTF anodes have comparable performance to the dispersed anode. However, the dispersed anode has higher performance than NSTF anode at all H_2 concentrations. The biggest difference can be seen at 30% H_2 where there is a 25mV difference at 1.5 A/cm^2. On the other hand, the NSTF baseline and NSTF low loading are comparable on H_2 concentration sensitivity.

As presented in Figure 6.4, the major difference between the NSTF baseline and NSTF low loading is in the extended reversal tolerance.

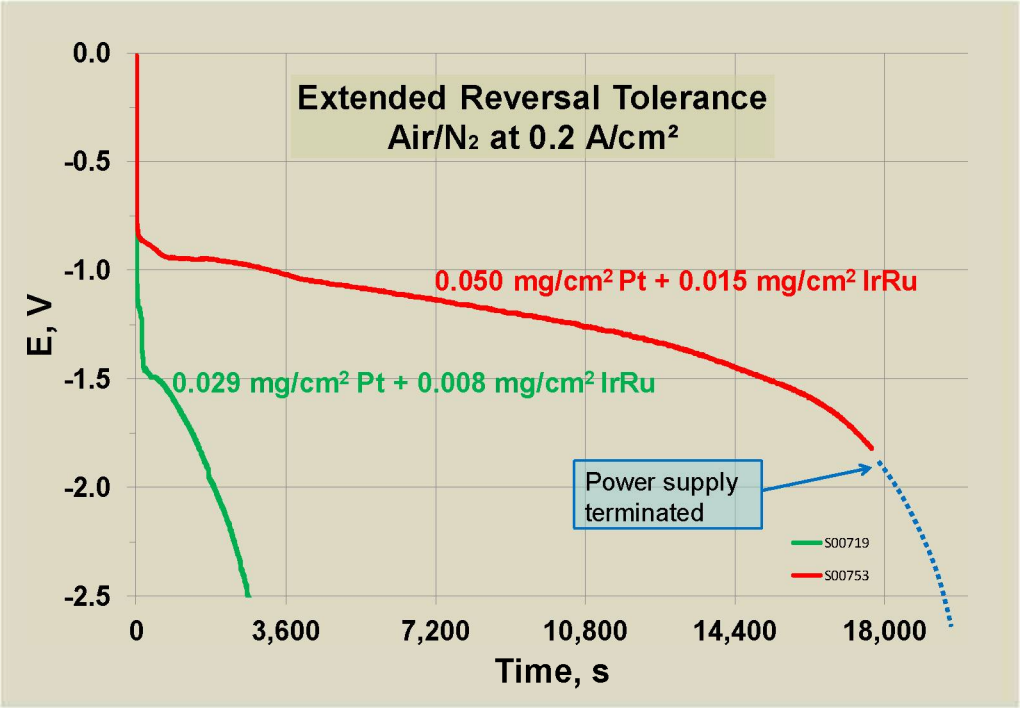


Figure 6.4. Stack Reversal Tolerance Comparison of baseline and low loading OER-Pt/NSTF anodes.

The time for the cell voltage to reach the limit of -2.5V at – 0.2 A/cm^2 while the anode is under nitrogen and the cathode under air for this test is used to represent reversal tolerance. As shown in Figure 6.4, NSTF has approximately 300 min reversal time before the cell voltage reached -2.5V, while NSTF with a low loading has only 43 min. The difference of the reversal time could be explained by the loading of OER catalyst for both designs. The NSTF baseline has 15 µg/cm^2 of OER catalyst, while the loading of the OER for the low-loaded NSTF anode is 8 µg/cm^2, which is half of that for the NSTF baseline. Therefore, the smaller amount of OER catalyst led to the significant reduction of reversal tolerance.

One of the benefits of the NSTF anode is the selectivity, which could provide protection of the cathode during SU/SD. The NSTF baseline has shown its selectivity in various small scale SU/SD tests. In this project, the low-loaded NSTF anode was selected to perform SU/SD testing on a full scale basis, in order to see if the lower Pt loading on anode maintains its selectivity.

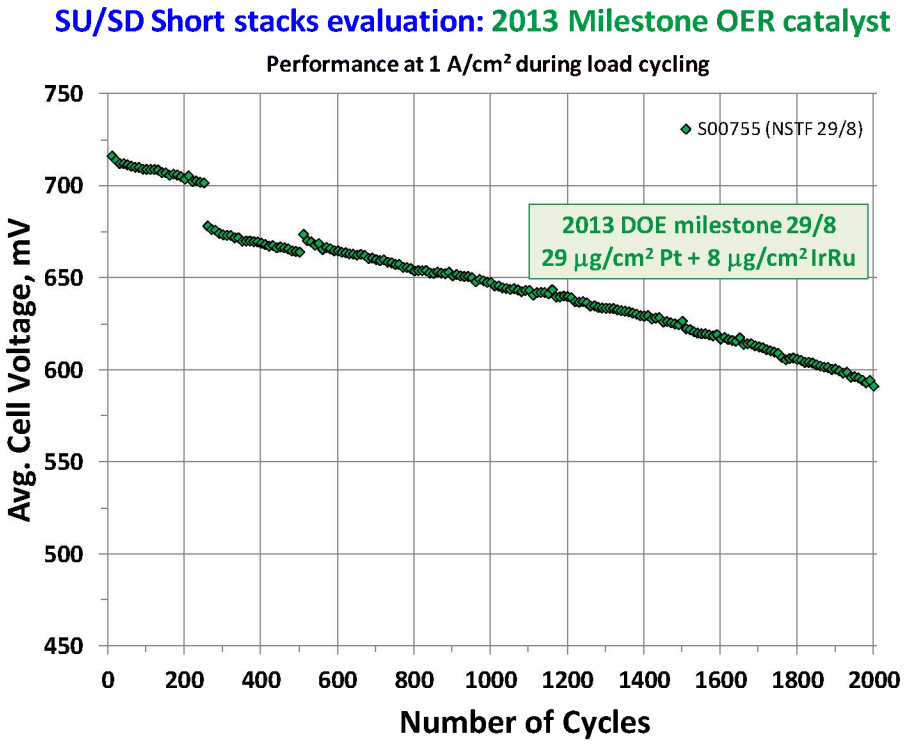


Figure 6.5. OER/NSTF durability cycling data at 1.03 A/cm^2 during SU/SD test for NSTF low loading anode

Figure 6.5 shows the cycling data at 1.03 A/cm^2 during the SU/SD test. The slope of the trend line is considered the degradation rate, which is 54 µV/cycle at 1.03 A/cm^2. This degradation rate at 1.03 A/cm^2 for the baseline NSTF (50/15) with similar a cathode was 78 µV/cycle, which is ~30% higher than that for the low loading NSTF anode. This finding suggests that the lower Pt loading on the anode provides more cathode protection during SU/SD.

The AFCC evaluation of the OER modified anode within the subcontract to this program can be summarized as follows:

- NSTF anode has comparable performance to the dispersed anode. NSTF anode might have some effect on performance under warm-up conditions. NSTF anode also shows more sensitivity to H_2 concentration, especially when H_2 concentrations are < 40%.
- NSTF with low loading has comparable performance and H_2 concentration sensitivity to the NSTF baseline loading anode. The reversal tolerance of low-loaded NSTF is significantly lower than the baseline. NSTF with low loading showed more selectivity than the NSTF baseline to protect the cathode during SU/SD cycling.
- Finally, NSTF anode with short whiskers (graphs not included) has comparable performance to NSTF with regular whiskers at all conditions, except under HOT condition at high current density, where NSTF with short whiskers has a lower performance. The NSTF short whisker anode and NSTF with regular whisker anode show similar cathode protection in SU/SD durability testing.

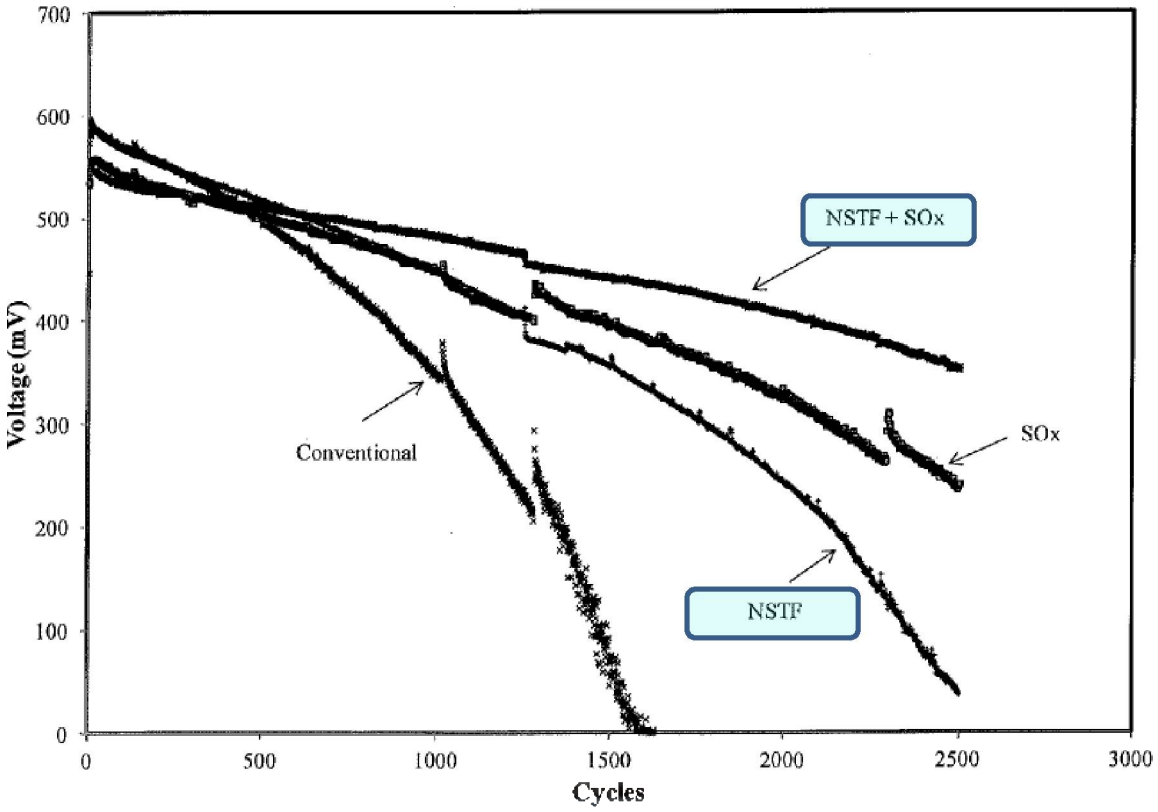


Figure 6.6. Plots of voltage vs. number of SU/SD cycles for various fuel cells illustrating the benefits incorporating a selectively conducting anode component (see text)

In general, the short stack evaluation of the OER modified anode by AFCC can be considered the biggest confirmation of the successful development of highly active and highly durable anode catalysts. To emphasize this point and conclude this section, in Figure 6.6 the NSTF SU/SD performance was even used by AFCC in one of their patent applications [Patent Application Publication US 2013/0236807 A1].

The effect of the selectively conducting anode component notwithstanding, the addition of OER modified NSTF improved the SU/SD durability of the fuel cell even further yet.

7. X-ray Photoelectron Spectroscopy and Scanning Transmission Electron Microscopy

XPS and STEM have played an important role in the development of IrRu OER catalysts. The extensive XPS and STEM efforts are summarized in this section. The work began with understanding the morphology and compositions in pure Ir, Ru, and Ti films on Pt-NSTF, then focused in on the $Ir_{0.9}Ru_{0.1}$ catalyst, both before and after electrochemical testing. This was followed by a detailed study into the underlying mechanisms for the enhanced stability of the OER catalyst over NSTF.

7. 1. Nature of sputter-coated Ir, Ru, and Ti films on Pt-NSTF

This section highlights the work which has been published in [28, 29]. Minute amounts of Ru, Ir, and Ti (2 and 10 $\mu g/cm^2$) were sputter-deposited over 3M Pt-coated NSTF substrate for evaluation as OER catalysts in a PEM environment. In tandem with electrochemical evaluation, the surface chemistry and the morphology of OER catalysts on Pt-NSTF were examined by XPS and STEM. Secondary electron (SE) STEM images, as shown in the left column of Figure 7.1, reveal a different structure and degree of coverage for each of the three overlayers. The three-dimensional nature of the large Pt grains is clearly observed in the Ir-coated whisker. The Ir took the form of small nanoparticles on the surface of the Pt grains. Ru overlayers partially filled the gaps between Pt grains, with some Ru nanoparticles also visible on the surfaces of the whisker. The higher Ru coverage is due to the fact that Ru has a lower density than Ir, thus consisting of more atoms per mass loading. Consequently, the lowest density element of the three, Ti, completely coated the whiskers as well as filled the gaps between the Pt grains.

Energy dispersive X-ray spectroscopy (EDS) and aberration-corrected STEM were also utilized to show the morphology of the catalyst surfaces. In addition, an ensemble of HAADF images, elemental maps, and high-resolution bright-field (BF) images are presented in the right column of Figure 7.1 to show the degree of coverage and atomically-resolved morphology of the surface for each element at a high and low loading. Ir was shown to grow both epitaxially on the Pt surface and as clusters of nanoparticles. Unlike Ir, Ru could be easily distinguished from Pt in HAADF images, especially at the whisker tips. High-resolution BF images showed a strong crystalline component in the 10 $\mu g/cm^2$ Ru, which was indexed as metallic Ru. For this loading, EDS maps showed a nearly continuous thin layer of Ru. However, only intermittent coverage of Ru was obtained at the lower 2 $\mu g/cm^2$ loading. In the case of Ti, a complete coating of the Pt surface was again observed. The EDS map also detected oxygen (not shown) throughout the Ti layer. This is unlike the Ru and Ir OER catalysts, which were mostly metallic. The oxidized Ti layer was mostly amorphous, although some crystallinity was observed in high-resolution BF images of the 10 $\mu g/cm^2$ over-coated sample. A very thin, continuous oxide layer was present on the surface of the lower-loaded whiskers.

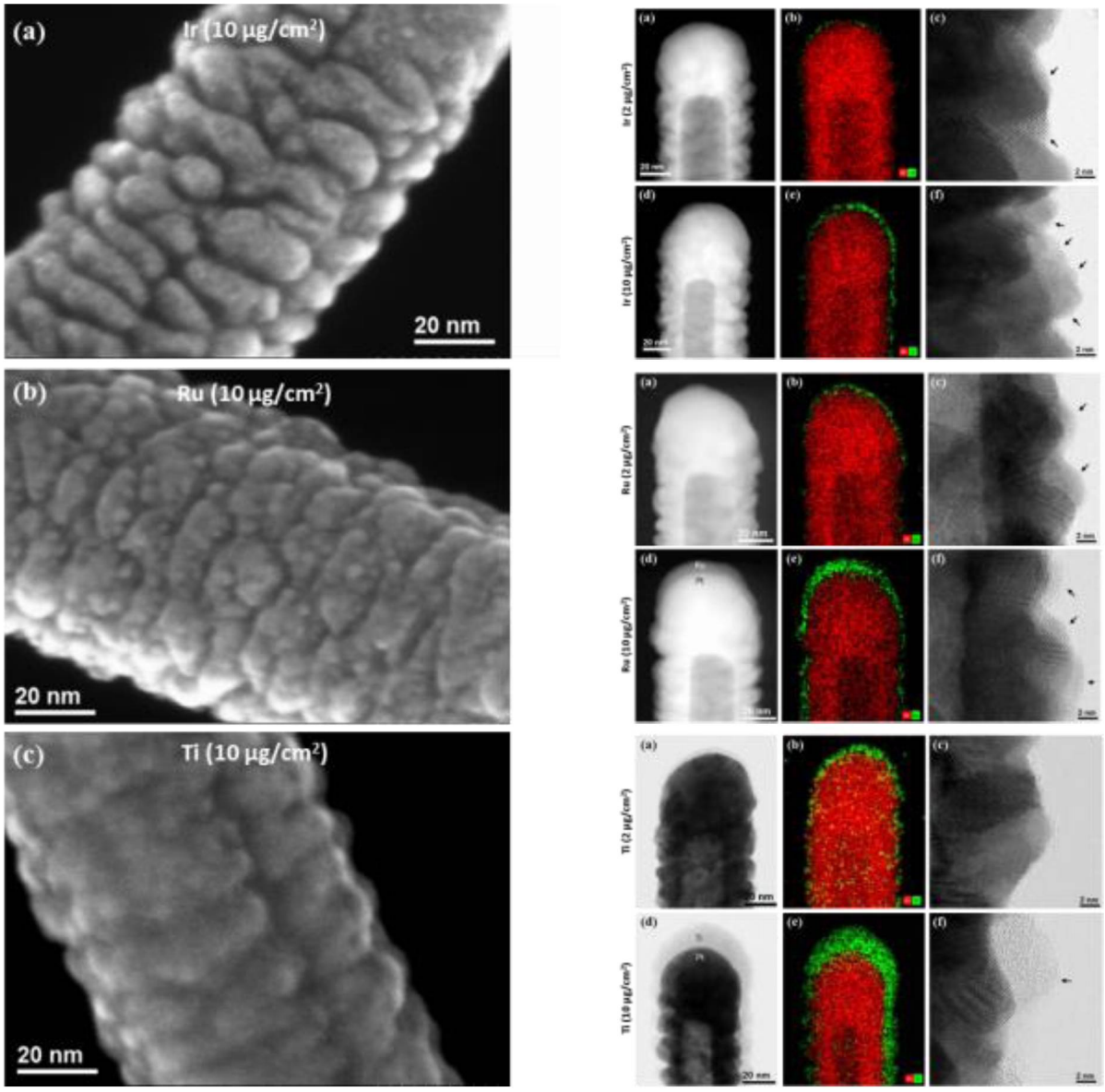


Figure 7.1. (left) SE-STEM images of Pt NSTF whiskers over-coated with a Ir, Ru, and Ti. (right) HAADF images with accompanying EDS maps and high-resolution BF images of Ir, Ru, and Ti-coated whiskers at the low and high loading. Arrows in the BF images mark the location of Ir/Ru/Ti on the Pt grains.

Further information about the composition of the OER catalyst layers was obtained by XPS. The results of careful and extensive curve fitting analysis are summarized in Table 7.1-Table 7.3. The surface of the Pt-NSTF substrate consists primarily of platinum with carbon and a trace level of oxygen. Even though oxygen was not deliberately introduced in the sputter-deposition chamber, the O/Ti, O/Ir and O/Ru ratios obtained for 2 µg/cm^2 loadings indicated that all the elements are present in the reacted/oxidized surface states. For the higher loading, the O/Ir and O/Ru ratios are noticeably lower, but the O/Ti ratio is still high. This suggests that Ti is present in the oxide form for both 2 and 10 µg/cm^2 loadings, which corroborates with STEM observations. In the case of Ir

and Ru, the reacted layer, which is formed at 2 $\mu g/cm^2$, becomes covered and attenuated at 10 $\mu g/cm^2$ by the outer layer of un-reacted Ir and Ru.

Since the carbon content varies between the coatings that were all prepared under the same PVD chamber conditions, it is not likely that contamination is the origin of the carbon. When sputter-deposited on a Si wafer substrate, similar carbon content, 15-18 % at., was detected for all three elements. This observation points to NSTF perylene red as the source of the carbon. Indeed, the 2 $\mu g/cm^2$ coatings formed from more reactive Ti and Ru elements have higher carbon contents than the one made from the more noble Ir. In addition, the attenuation of carbon photoemission by the thicker OER catalyst layers supports the hypothesis that the detected carbon comes from the perylene red substrate and not from contamination. Finally, because Iridium is nobler than Ru and Ti, there is less oxygen and carbon in the signal, which causes the Pt signal to be higher as a fraction of all atoms measured, even though the absolute Pt content is the same.

	C	O	Pt	Ti, Ir, Ru
Pt-NSTF substrate	26	4	70	
Overlayer: 2 $\mu g/cm^2$				
Ti	34	32	24	10
Ir	22	24	44	10
Ru	41	22	25	12
Overlayer: 10 $\mu g/cm^2$				
Ti	18	54	5	23
Ir	15	16	22	46
Ru	44	21	8	27

Table 7.1. XPS atomic concentrations (at.%): OER catalyst overlayer on Pt-NSTSF.

In order to obtain more detailed information about the nature of reacted Ir and Ru states at the interface with Pt-NSTF, high resolution XPS core level spectra were collected. The results based on the curve fitting analysis of the spectra are presented in Table 7.2 and Table 7.3. The curve fitting analysis for the 2 $\mu g/cm^2$ Ru sample shows that about 75 % of the detected ruthenium is in the reacted form, compared to 55% for Ir. As seen from Table 7.3, if the reacted ruthenium only exists in the RuO_2 form, almost all surface oxygen would have to be taken by ruthenium, which is not the case here. The stoichiometry balance suggests that both RuO_2 and organo-metallic Ru-O-C or Ru(CO)x bonds coexist at the interface. Therefore, it is reasonable to assume that the reacted Ru-II photoemission most likely incorporates Ru-(CO) bonds. The considerable surface content of the reacted ruthenium suggests a high ruthenium affinity for interaction with the perylene red. This was the first indication that that the presence of ruthenium on Pt-NSTF is preferentially attracting carbonyl functionalities from the NSTF perylene red. This phenomenon is explained in greater detail and will be summarized later on.

	Oxygen			Carbon			Iridium	
Total surface content (at.%)	24			22			10	
Functional group/valence state	Ether	Hydroxide + carbonyl	Oxide	Aliphatic C–C	Ether C–O	Carbonyl C=O	Ir^0	Ir^{4+}
% contribution of functional group to O 1s, C 1s and Ir 4f photoemission	28	51	21	75	14	11	45	55
Concentrations of functional groups (at.%)	7	12	5	16.5	3	2.5	4.5	5.5

Table 7.2. Stoichiometry for 2 µg/cm² Ir at the interface with Pt-NSTF.

	Oxygen			Carbon			Ruthenium	
Total surface content (at.%)	22			41			12	
Functional groups/valence states	Ether	Carbonyl	Oxide	Aliphatic C–C	Ether C–O	Carbonyl C=O	Ru^0	Ru^{4+}
% contribution of functional group to O 1s, C 1s and Ru 3d photoemission	25	46	29	65	10	25	25	75
Surface concentrations of functional groups (at.%)	6	10	6	27	4	10	3	9

Table 7.3. Stoichiometry for 2 µg/cm² Ru at the interface with Pt-NSTF.

7. 2. Effect of loading on structure of $Ir_{0.9}Ru_{0.1}$ OER catalysts

This section highlights the work which has been published in [30, 38]. Once the $Ir_{0.9}Ru_{0.1}$ catalyst was down selected, the material was thoroughly characterized by XPS and STEM for various loadings. The XPS atomic concentrations of Pt, Ir, C and Ru are plotted in Figure 7.2 as a function of the OER catalyst loading. As expected, the XPS concentration profiles show the expected rise in Ir with increased loading, which is mirrored by the decline in Pt. This can be explained by STEM (Figure 7.3), showing that Ir preferentially deposits over Pt. The increase in Ru, readily detectable by XPS, is visibly slower than that of Ir, and mirrors the decline in carbon, instead of platinum. This provides further evidence that Ru prefers to gather at exposed NSTF whisker sites, as suggested by the previous study.

The nature of the NSTF overlayers was further studied by STEM. Figure 7.3 shows a low magnification BF-STEM image of a pristine NSTF cathode, along with higher magnification images of a single whisker. The bare-Pt (Figure 7.3c) and OER catalyst-coated Pt-NSTF (Figure 7.3d) surfaces appear very similar, indicating that the IrRu catalyst grows epitaxially on the surface of Pt grains. Pt and Ir have the same face-centered-cubic crystal structure and very similar lattice parameters, and thus epitaxial growth would be expected. For the cathode catalyst, a non-continuous OER catalyst layer would be preferred over a continuous film, as complete coverage of the Pt-NSTF surfaces would block the Pt catalyst ORR sites, thus negatively impacting fuel cell performance. For the anode catalyst, a more complete film-like coverage is fine, provided that enough Pt sites are available to allow the HOR to take place uninhibited. The EDS maps presented in Figure 7.3 for various loadings used in this study show that a fully continuous coating of the Pt-coated perylene-red support is unlikely. Even for the highest OER loading, an even coating over the Pt-NSTF would result in layer thicknesses of only 1nm of Ir and a single monolayer of Ru.

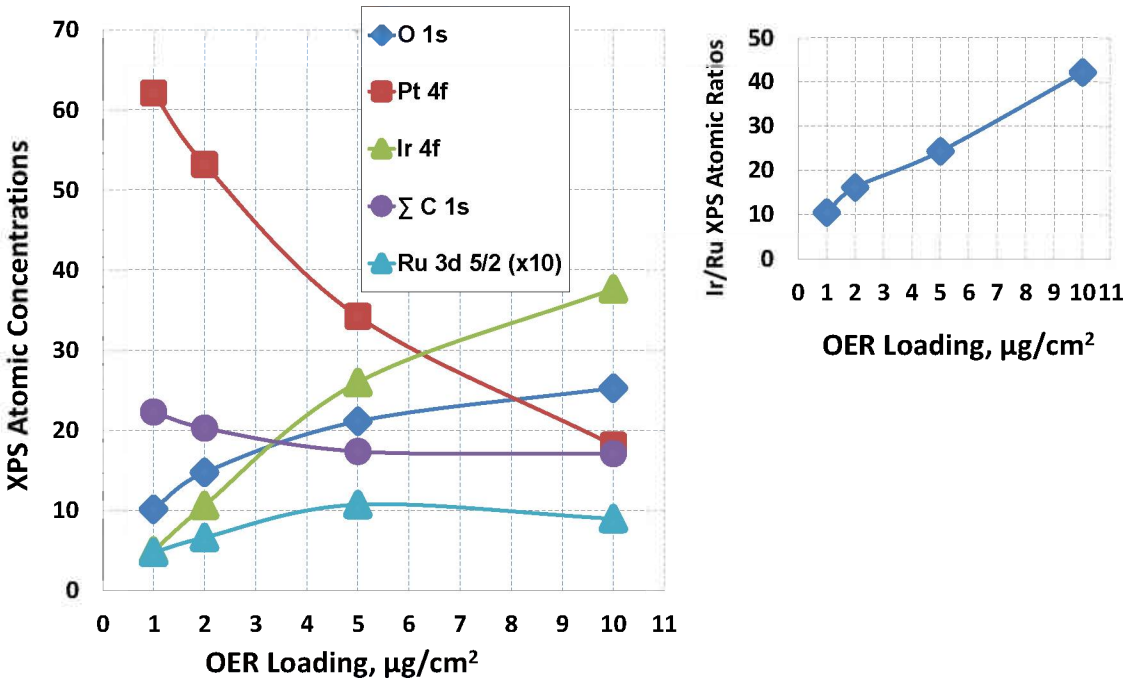


Figure 7.2. (left) Atomic concentration profiles derived from XPS survey spectra for varying IrRu loadings on Pt-coated NSTF; (right) XPS Ir/Ru atomic ratio vs. nominal OER catalyst loadings.

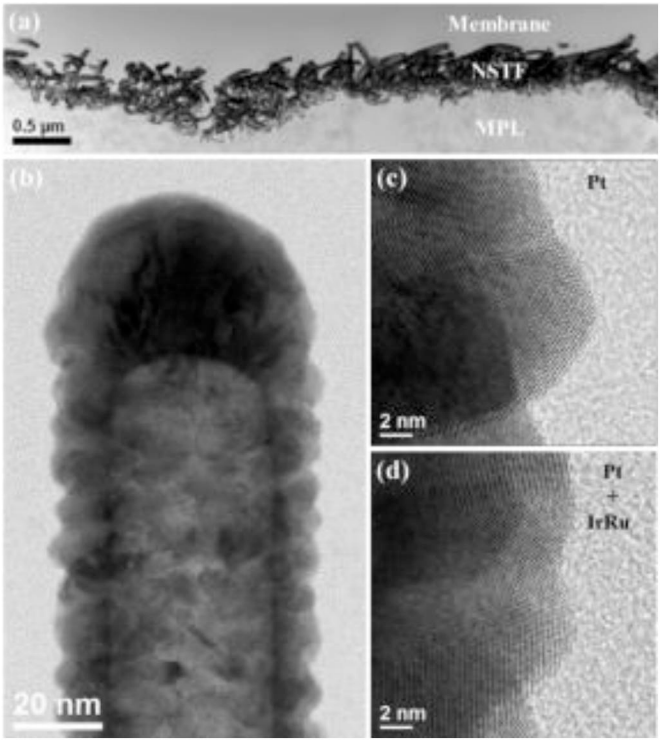


Figure 7.3. Bright-field STEM images of (a) Pt-NSTF cathode layer, (b) individual Pt-NSTF whisker and whisker surfaces (c) without and (d) with IrRu OER catalyst. In this formulation, the OER catalyst grows epitaxially on the surfaces of the Pt grains.

7. 3. Stability and Impact in Start-up/Shutdown and Cell Reversal Tests

This section highlights work published in [39, 40]. Electron microscopy was used to study the role of oxygen evolution reaction (OER) catalysts in mitigating degradation arising from SU/SD and CR events. Pt NSTF was coated with a $Ru_{0.1}Ir_{0.9}$ OER catalyst at loadings ranging from 1 to 10 μg/cm^2 and submitted to electrochemical tests simulating SU/SD and CR events within membrane electrode assemblies, as defined previously in chapters 3 and 4.

7.3.1. Start-up/Shutdown

Aberration-corrected STEM and EDS were used to observe the impact of the OER catalysts on Pt dissolution and migration through the membrane. As shown in Figure 7.4 (Compare the arrow/outline regions in BOL and EOL 0 μg/cm2 loading (pure-Pt)), the presence of the OER catalysts greatly reduced the smoothing of the Pt NSTF whiskers, which was been correlated with Pt dissolution and losses in electrochemically active surface area. Elemental mapping in Figure 7.4 also showed that a high percentage of the Ir catalyst was maintained on the NSTF whisker surfaces following testing. The Ir to Pt ratio of individual whiskers remained relatively constant following SU/SD, and alloying of Ir and Pt was not observed. The dissolution of both Ir and Pt led to the formation of IrPt nanoparticle clusters in the membrane close to the cathode, as well as the formation of a Pt band deeper in the membrane. The OER catalyst also limited the migration of dissolved Pt, as evidenced by the increased proximity of the Pt band to the cathode. Ruthenium, the least stable of the three catalyst components, was discovered in the MPL as nanoparticles. Crossover of the OER/ORR catalysts to the anode was not observed under any SU/SD test conditions.

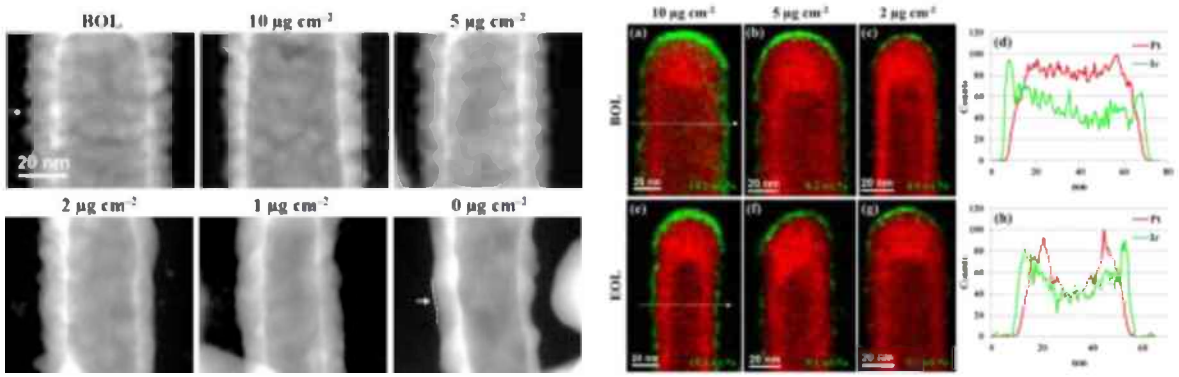


Figure 7.4. (left) HAADF-STEM images of individual whiskers after SU/SD testing for each OER catalyst loading, with a BOL image provided for reference.. (right) EDS maps (Ir: green, Pt: red) for (a-c) BOL and (e-g) EOL whiskers for different OER catalyst loadings showing retention of the Ir catalyst following SU/SD tests. EDS line scans in (d,h) correspond to lines in (a,e), and show that no alloying occurs between the Ir and Pt during SU/SD, nor does dissolved Pt redeposit over the OER catalyst.

7.3.2. Cell reversal

The stability of $Ru_{0.1}Ir_{0.9}$ OER catalysts deposited on Pt-coated NSTF under cell reversal conditions was also explored. Accelerated stress tests showed that the OER catalysts significantly improved the durability of the Pt under cell reversal conditions. High-resolution images of the end-of-life (EOL) NSTFs in Figure 7.5 showed significant Ir loss from the whisker surfaces, while no Pt loss was observed. The retention of the Pt indicated that the OER catalysts had protected the catalyst-coated whisker surfaces from degradation.

The EOL MEAs exhibited significant changes in morphology at the whisker surfaces and within the polymer membrane. Coarsening of the Pt whiskers was generally observed, but even more apparent was the presence of 1-2 nm particles within the membrane, as shown in Figure 7.5. These nanoparticles were identified as Ir by EDS maps, and were found as deep as 1 μm within the membrane. Some Ir was also observed in the GDL, although the penetration depth was limited to 250 nm. Additionally, EDS maps of individual whiskers showed residual Ir on the surface, which was often clustered in "tips" at the edge of Pt whiskers. Most importantly, only trace amounts of Pt were detected in the membrane. The retention of Pt indicated that the OER catalysts had fulfilled their role in protecting the Pt from oxidation and subsequent dissolution from the whisker surfaces.

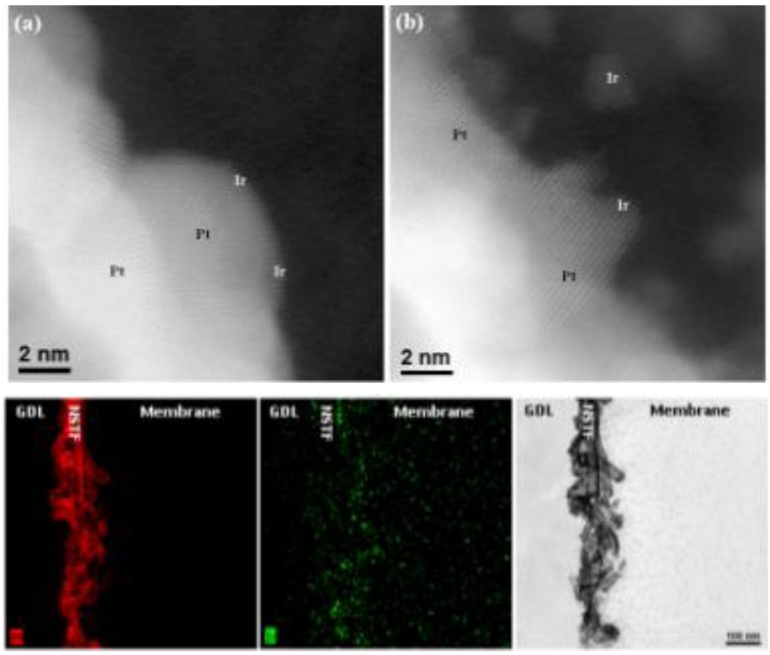


Figure 7.5. (top) Z-contrast images of the Pt/RuIr surface of NSTF whisker (a) before and (b) after cell reversal tests. Ir was found in clusters on the whisker surface and dissolved Ir had formed into nanoparticles in the polymer membrane. (bottom) EDS maps for Pt and Ir, with BF-STEM image of electrode after cell reversal testing. A significant portion of Ir had dissolved into the membrane, while little to no Pt had been lost from the NSTF. Some Ir was also detected in the microporous layer.

7. 4. *Understanding extraordinary stability of OER catalysts*

This section summarizes work which is described in more detail in [38]. The previous sections alluded to an interaction between Ru and perylene-red support which may contribute to the increase in stability and activity observed in electrochemical tests. The interface formation between nano-structured perylene red (PR) whiskers and OER catalysts ruthenium and iridium were studied systematically and extensively by XPS and STEM. The OER catalyst over-layers with thicknesses ranging from ~0.1 to ~50 nm were vapor deposited onto PR ex-situ.

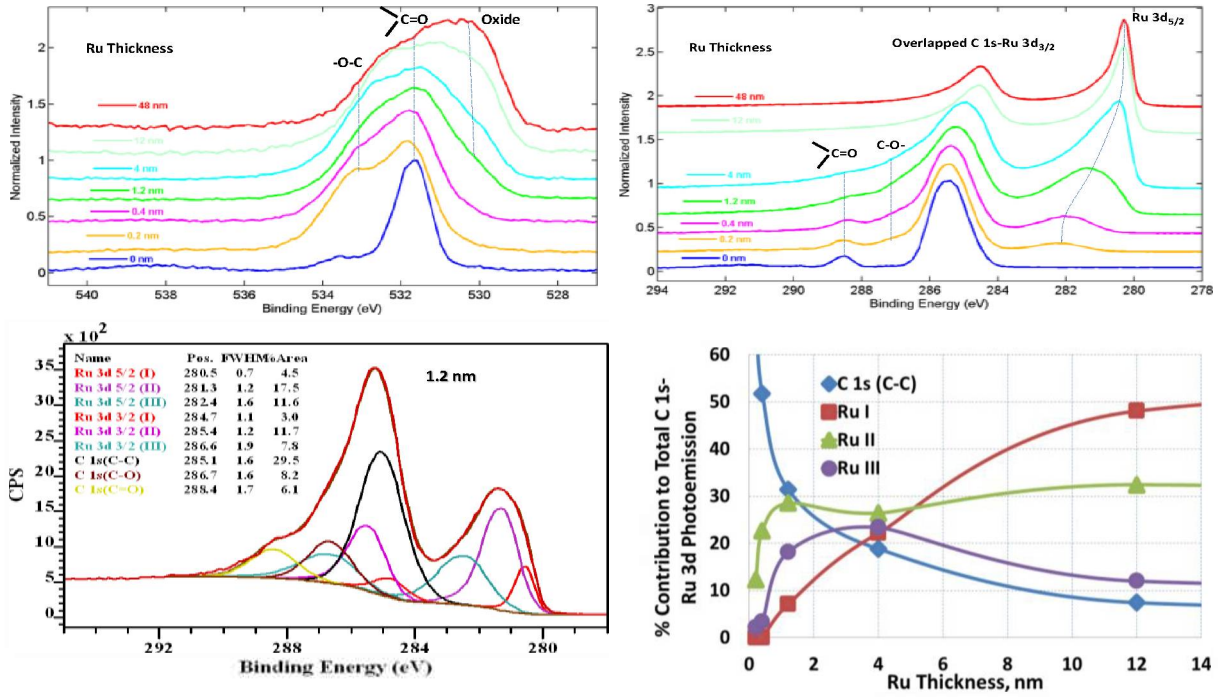


Figure 7.6 (top) C 1s core level spectra for bare PR substrate and C 1s-Ru 3d core level photoemission for Ru deposits from 0.2 to 48 nm. (bottom) Curve fitting analysis of C 1s-Ru 3d core level spectra for 1.2 nm Ru coverage and contribution of metallic and reacted Ru as a function of Ru thickness: Ru-I is un-reacted/metallic RuO, Ru-II is reacted Ru^{x+} and Ru-III is reacted Ru^{y+}

As summarized in Figure 7.6, XPS showed that a strong interaction of ruthenium with perylene red whiskers was found to the extent that no metallic ruthenium was present at low Ru coverage. The existence of Ru-O-C bonds could point out to the root cause of improved Ru OER catalyst stability on Pt-NSTF: the strong bonding of Ru to PR could increase the surface area of the deposited OER nanoparticles by preventing coalescence and reducing the rate of dissolution in the electrochemical environment. Possible bonding configurations are shown in Figure 7.7. STEM imaging demonstrated that, with increasing thickness, Ru and Ir transform from amorphous clusters to crystalline nanoparticles, which agglomerate with increased over-layer thickness are shown in Figure 7.8.

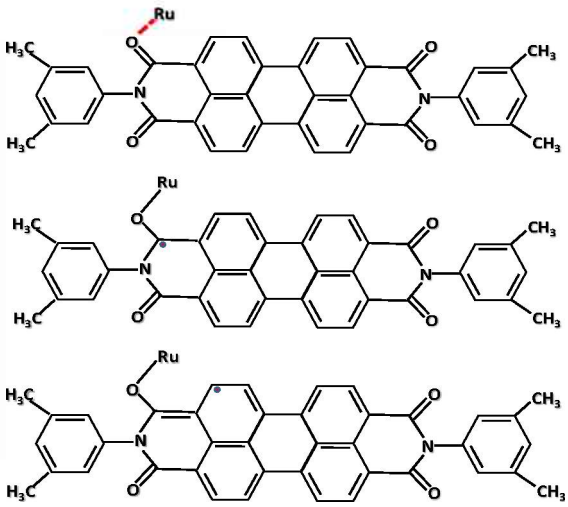


Figure 7.7. Perylene Red-Ruthenium Interaction: Ru-O-C complex formation and possible resonance hybrid structures.

Ir also interacts with PR although not to the extent seen for Ru. At low coverages the entire Ru deposit is in the reacted state while a small portion of the deposited Ir remains metallic. Ru and Ir bonding occur at the PR carbonyl sites as evidenced by the attenuation of carbonyl photoemission and the emergence of new peak assigned to C-O single bond.

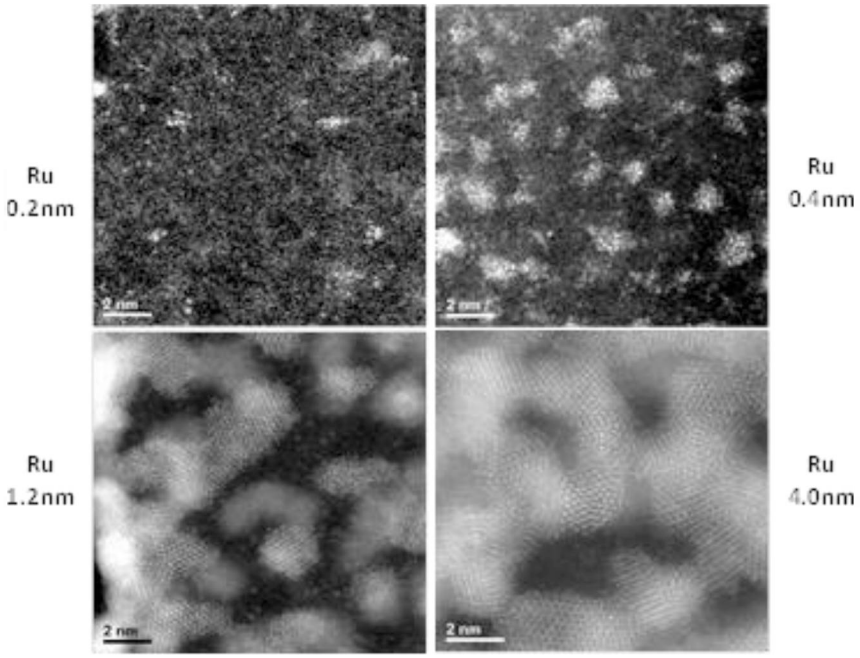


Figure 7.8. High-angle annular dark-field (HAADF) images of whiskers with Ru layer thicknesses of 0.2, 0.4, 1.2 and 4 nm taken at 10 Mx magnification.

As previously shown, the noticeable attenuation of Ru at the highest loadings may suggest that Ir also deposits on top of Ru. The change in the Ir/Ru atomic ratio with loading, shown in the right

panel of Figure 7.2, supports this interpretation. Thus, the stability of the OER catalysts may arise from anchoring of the Ru to the perylene red with additional enhancement provided by the formation of an Ir capping layer. These findings revealed a fundamental relationship which provides a basis for understanding the electrochemical behavior of these materials.

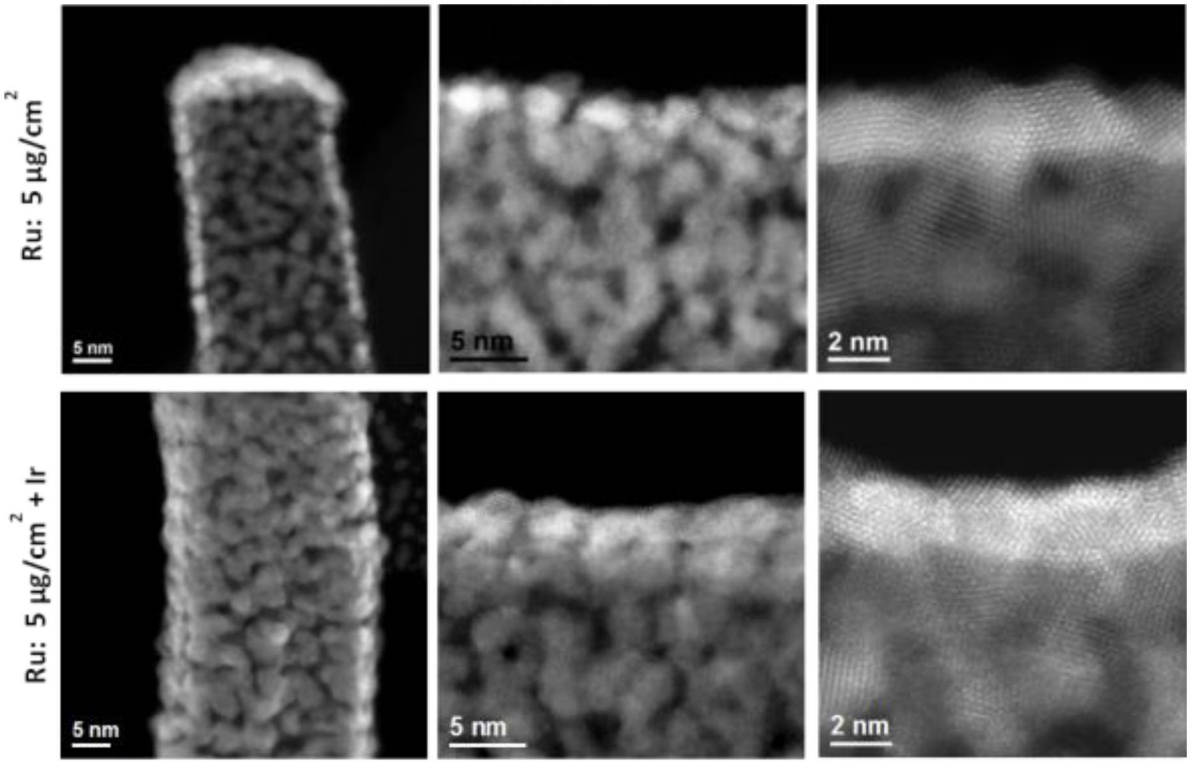


Figure 7.9. STEM images highlighting the morphology of 5 µg/cm^2 total loading, with and without Ir.

After the perylene-red/Ru interaction was confirmed, additional sample sets were created to explore the Ru-Ir and Pt-Ru-Ir interactions. The presence of an Ir capping layer showed a clear stabilizing effect in electrochemical tests. STEM images of one loading explored in this study are shown in Figure 7.9. The morphology of 5 µg/cm^2 total loading, with and without Ir, showed the clear capping effect of the Ir over the Ru. Further studies were performed with both a 5 and 10 µg/cm^2 Pt deposited between the peryelene-red and Ru. A few characteristic Z-contrast images are shown in Figure 7.10. Even at the higher loading, the Pt only partially coats the support surface. The Ru layer fills in the gaps between Pt nanoparticles, but become a full layer over the Pt at higher loadings. Again, the capping mechansim of the Ir is clearly observed at lower Ru loadings and is still evident, although to a lesser extent, at higher Ru loadings.

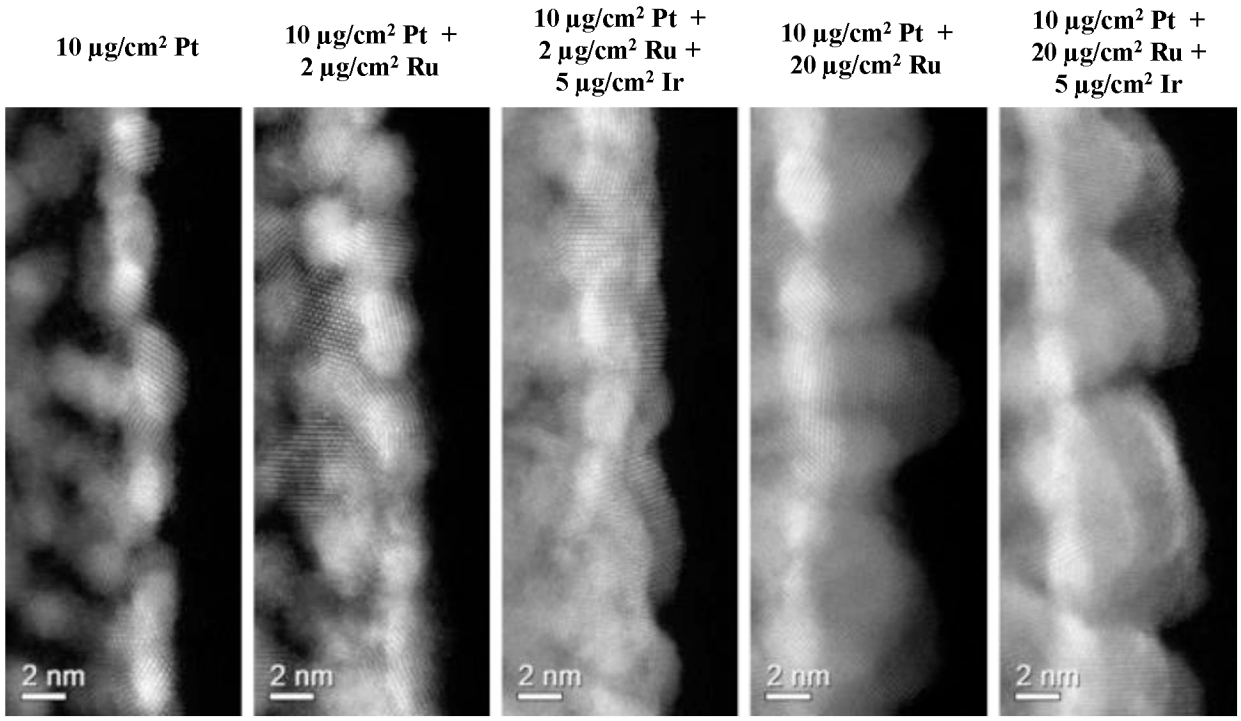


Figure 7.10. STEM images highlighting the morphology of various NSTF constructs.

The *XPS data* show the Ru 3d-C 1s core level spectra of Ru layers without and with both a 5 and 10 µg/cm^2 Pt deposited between the peryelene-red and Ru in Figure 7.11. The C 1s core level spectra of bare perylene red are included for comparison. The binding energy shift and the broad line-shape of Ru 3d 5/2 peak for 1 and 2 µg/cm^2 Ru clearly demonstrate that Ru interacts with perylene red through the Pt under-layer. This is not surprising considering the images in Figure 7.10, which show that Pt only partially covers the support surface, even at the higher loadings, allowing a direct Ru contact with perylene red between Pt nanoparticles. The contribution of reacted Ru can also be seen from the Ru 3d 5/2 peak shoulders for Ru loadings of 5 µg/cm^2 and higher. Furthermore, Figure 7.11 shows that for low Ru loadings the Pt presence has a noticeable effect on the Ru 3d 5/2 binding energy (BE) shift. The shift in BE location from reacted to metallic Ru is smaller for the 10 µg/cm^2 Pt, because there are fewer available bare perylene red sites between Pt nanoparticles, when compared to the 5 µg/cm^2 Pt.

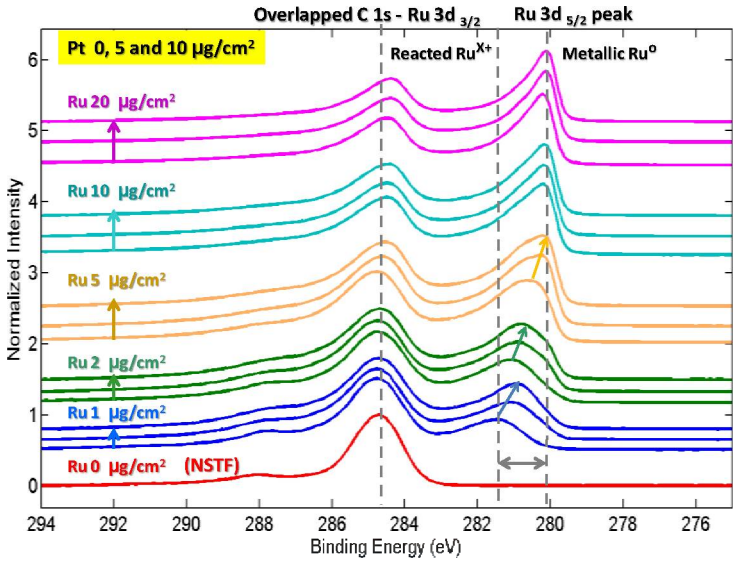


Figure 7.11. PtRu NSTF. Perylene Red-Ruthenium Interaction: Ru 3d5/2 shifts from metallic BE location

Figure 7.12 shows the Ru 3d-C 1s core level spectra of Ru deposits with and without a 5 and 10 µg/cm^2 Pt under-layer and with an Ir top layer. The spectra for the 0 µg/cm^2 Ru loading represent the C 1s core level photoemission of bare perylene red. In the presence of the Ir top layer, the Ru 3d 5/2 peaks are at the metallic BE locations and exhibit the line-shape narrowness for all Ru loadings without and with Pt under-layers. This is an indication of an Ir "reducing" effect on the reacted Ru. This Ir reducing effect observed by XPS correlates well with the stabilizing effect of an Ir capping layer observed in electrochemical tests.

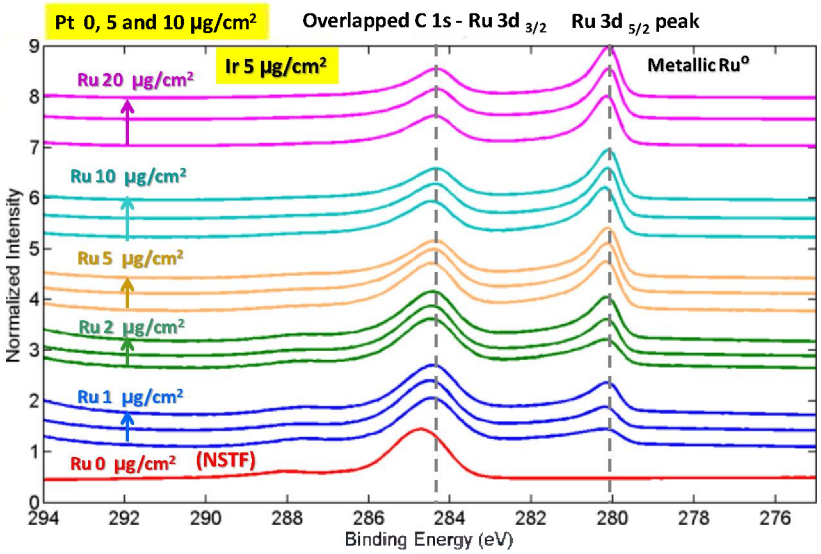


Figure 7.12. PtRuIr NSTF. Reducing effect of Ir top layer on ruthenium: Ru 3d5/2 peaks at metallic BE locations

8. Cell reversal durability of the anode during Start-up/Shutdown via gas switches

This section encompasses the work during the last 14 months of the project. The whole effort of the 3M core group and the subcontractors was entirely focused on understanding and solving the problem of the failure of the IrPt/NSTF catalyst due to the real life situation where the catalyst experiences gas switches rather than simulated electrochemical equivalent pulses. This effort was fully supported by the DOE management team. To facilitate the understanding of the fundamentals behind the proposed solutions, the DOE approved the engagement of ANL as a subcontractor for the use of the Advanced Photon Source. Due to the complexity of the problem and the originality in the proposed and accomplished solutions, a more comprehensive account of the last period of the program will be given.

The following fiscal year *2014 objectives* were formulated:

- Expand the catalyst evaluation towards 'real life' application with emphasis on hydrogen – air gas switching
- Perform root cause analysis and develop working hypothesis of the impact of gas switching
- Mitigate the impact of gas switching on the oxygen evolution reaction catalyst stability
- Synthesize modified OER catalysts and narrow composition and construction parameters
- Establish fundamentals of the modified OER catalysts activity and stability

8. 1. Technical Targets

DOE approved the technical target for the final year, with the following milestone:

- 2014 Milestone: After 200 Gas Switches achieve cell reversal of 10 hours at – 0.2 A/cm^2 at < 1.7 V with < 0.035 mg/cm^2 PGM.

We are listing the following major *accomplishments:*

- The final year project milestone has been achieved:
- Constructs with additional refractory metals have fulfilled the cell reversal requirement after gas switching within the 2014 Program milestone voltage limit, < 1.7 V, and PGM loading < 0.035 mg/cm^2.

In addition:

- Hypothesis that separating the OER catalyst from atomic proximity of Pt may alleviate the impact of gas switching was proven.
- As an added benefit of the separating layer, improved OER activity was achieved.
- Fundamental materials studies aimed at understanding the extraordinary durability of the new OER-Pt/NSTF constructs have converged to conclude that stabilizing the Pt and Ir oxides is paramount to increasing reversal endurance.

The performance of the OER catalyst developed in this Project was assessed based on data obtained in the testing of numerous lab-scale MEAs, with further 'real life' evaluation in over two dozen short stacks with full-size MEAs. It was established that, due to its unique composition and configuration, the IrRu catalyst on the anode provides:

- Extremely high inherent and mass activity towards the OER
- Unsurpassed durability at high positive potentials during cell reversal
- Sufficient HOR activity under a variety of operating conditions, including fully recoverable CO poisoning
- Possibility to lower the Pt loading without sacrificing performance
- ***Protection for the cathode during SU/SD*** due to ORR suppression on the anode, *an exclusive property unique to this catalyst*, owing to the synergy between the Pt NSTF film and OER catalyst in intimate contact.

As such, the OER catalyst modified Pt/NSTF anode was extensively evaluated for real life application by the Project collaborator/subcontractor – AFCC (see section 6). In the course of the evaluation, the OER catalyst modified anode has passed many gate reviews. While AFCC confirmed all the properties listed above, in one of the latest real life short stacks testing, a problem was identified that needed serious attention and a solution that required extension of the work in the Project. DOE granted a *no cost extension* during which the work was focused on this distinctively separate topic.

As evidence of the commitment to resolve this problem, during the final year of the program we have made over 50 varieties of catalysts and tested over 200 MEAs.

8. 2. Gas Switching

During the first four years we have developed and integrated Ir and IrRu OER components with Pt catalyst on 3M NSTF support (sections 2-4). The catalyst was tested via the electrochemical equivalent to start-up conditions sustaining up to 5,000 pulses to < 1.5 V. However, the *same catalyst when applied on the anode side for cell reversal mitigation lost its OER activity when exposed to real gas switching (GS) from hydrogen to air*. In Figure 8.1, the difference in the cell reversal durability is illustrated by comparing the baseline OER-Pt/NSTF (20 $\mu g/cm^2$ Pt + 15 $\mu g/cm^2$ Ir) after the 200 gas switching cycles with the same catalyst after the electrochemical equivalent of 200 pulses. It is obvious that the gas switches are detrimental to the OER. The initial hold potential of the GS cycled catalyst is about 50 mV higher than without the GS, and the decay to MEA failure happens 2.5 hours sooner. Clearly gas switches are damaging the MEA in a way that the electrochemical equivalent of 200 pulses (designed to simulate SU/SD cycles) did not predict.

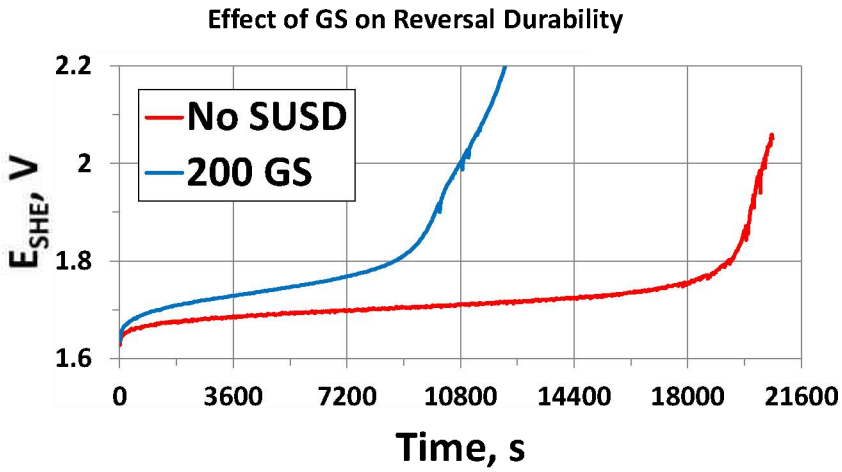


Figure 8.1. Potential as a function of time at 200 mA/cm^2 galvanostatic hold. The blue line represents reversal durability after 200 GS on $Pt_{20}Ir_{15}$ NSTF. The baseline without GS (but with the 200 current pulses at 200 mA cm^{-2}) is shown in red.

Root cause hypothesis. *High electrode potential* is usually the first cause to be associated with the catalyst failure during SU/SD. However, the *GS does not provoke a high anode potential;* the maximum potential that can be reached under air is about 1 V (Figure 8.2A). Numerous simulated SU/SD tests with integrated electrochemical pulses, performed during the initial four years of this project, have proven that the OER catalyst is stable up to 1.7 V (Figure 4.5). This precludes high potential during GS as the cause of the OER catalyst degradation.

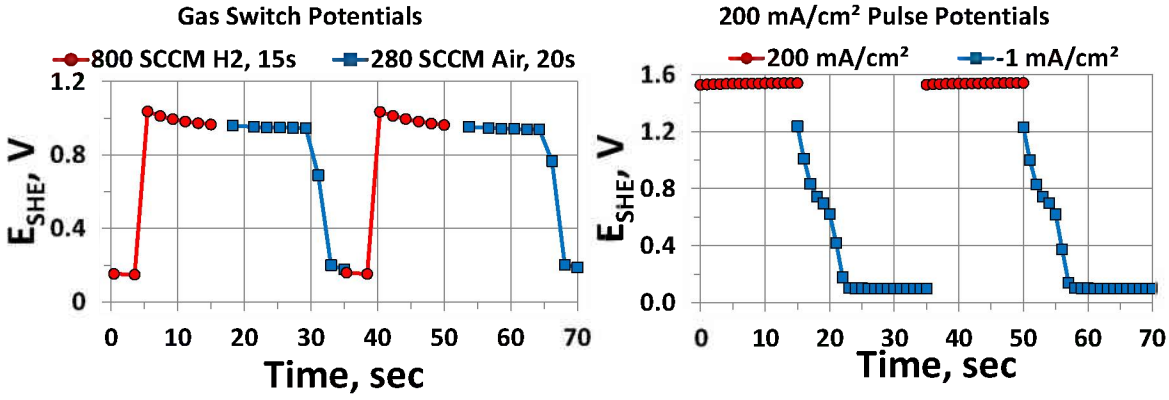


Figure 8.2. Potential profiles of the anode during gas switching (left), and during electrochemically simulated pulses (right)

The only other plausible explanation addresses the *hydrogen-air direct recombination on the anode catalyst.* This mechanism came into consideration based on the key observation that the otherwise inferior conventional, dispersed OER-added catalyst - *admixed* IrRu catalyst with dispersed Pt - did not lose much of its performance due to GS. As is well known, hydrogen and

oxygen (in the air) can spontaneously combust, which can be vigorous in the presence of platinum. This reaction produces *heat and a variety of radicals*. The OER-Pt/NSTF construct is such that the OER catalyst is in *atomic proximity* of the Pt reaction sites. Therefore, both the heat and the reactive radicals can directly impact the thin film OER catalyst before the heat is dissipated and the radicals recombined. This is in contrast to the dispersed catalyst where the two catalysts components, Pt/C for HOR and IrRu for OER, are well separated on the atomic scale. Therefore, the OER catalyst within the dispersed anode suffers very little from the SU/SD event, while the durability of the OER-Pt/NSTF is quickly compromised.

As an extension of this hypothesis, the concept and the strategy for diminishing the damaging effect of the gas switching were based on two principles:

1. *Slowing down the rate of the chemical reaction between hydrogen and oxygen,* while leaving the electrocatalytic HOR unaffected. This will decrease the rate of both the release of heat and the creation of radicals. The fact that the recombination of the two elements needs catalytic sites to proceed provides a theoretical background upon which this approach can be justified. Specifically, we would block a sufficient number of the platinum active sites in a fashion similar to the inhibition of the ORR (see section 5). Since the incoming hydrogen molecules during startup will react with the adsorbed oxygen, a substantial reduction in the number of the sites where oxygen can be adsorbed and where radicals can subsequently be formed will effectively reduce the rate of the hydrogen – oxygen reaction.
2. *Inducing a physical separation of Pt from the OER*, which will reduce both the number of radicals and the extent of heat transfer from the Pt sites where they are generated to the OER where they cause degradation.

This concept is material-based, just as with our OER-modified anode. The concept fits into the philosophy of a reliable protection from within the MEA, which is always 'on'. The success of the concept would depend on:

- finding a material that is stable when exposed to high potentials during cell reversal
- implementing an amount sufficient to inhibit the undesired $H_2 - O_2$ reaction without compromising the anode performance
- manufacturing feasible via processes compatible with the existing Pt/NSTF anode fabrication
- adding little, to the PGM loading; preferably nothing at all.

Materials with the required stability were found in *the group of transition elements known as refractory metals.* Due to the high affinity for oxygen, these metals form extremely inert oxide films on their surfaces, which is the source of their high stability. They are inexpensive compared to the PGMs and can be sputter-deposited in their metallic form in a vacuum, while their

compounds can be generated via reactive sputtering or by using a sputtering target of the desired composition.

Most of these elements and their oxides are known inhibitors for the ORR, therefore their application will not only inhibit the hydrogen – oxygen reaction but will also enhance the protection of the cathode during SU/SD. As we have shown in section 5, a relatively small coverage of Ta on Pt/NSTF reduces the ORR substantially without any noticeable adverse effect on the HOR.

Four elements from the group of refractory metals were selected for rather rigorous evaluation: Zr, Hf, Ti, and Ta. Ru was omitted as an OER component from these new constructs, because we lacked a fourth target in our deposition chamber. The catalyst fabrication and evaluation was intended to:

- Establish testing procedures and protocols
- Determine the effective loading range of added elements
- Ascertain the stability of the added element in PEM
- Evaluate the performance for cell reversal
- Understand the fundamentals of the impact of the added elements.

The cell reversal test protocol as described in section 4 was expanded by inclusion of:

- GS cycling (20 sec Air, 15 sec H_2)
- High current reversal hold up to 10 hours (-200 mA/cm^2, to 2.2 V)
- Conditions: 50-cm^2 MEAs at 70 °C, A/C N_2/1% H_2 @1,000 SCCM, 110% RH.

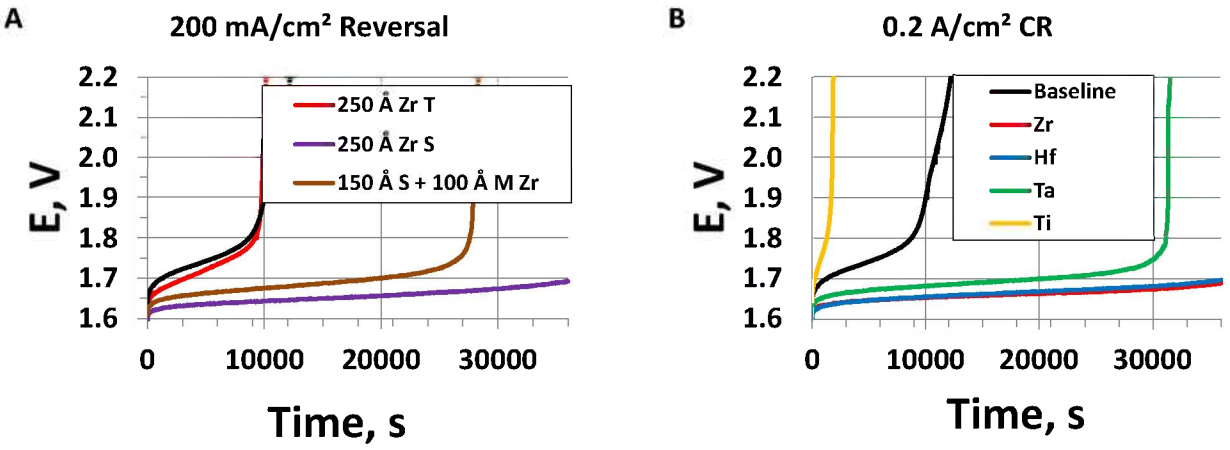


Figure 8.3. Potential responses during the 200 mA/cm^2 current hold after 200 gas switches. (A) Exploration of different constructs of 250Å Zr added to the OER-Modified Anode. Constructs include atop deposited Zr (T); Zr sandwiched between Pt and Ir (S); and 150Å Zr deposited on top of Pt, followed by 100Å Zr intermixed with Ir (M). (B) Reversal potential of the different refractory metals added to the OER-Modified Anode as a sandwich between Pt and Ir.

The screening of the refractory metal modified OER-NSTF anodes commenced with the *constructs with zirconium* and the results were such that eventually PtZrIr served as a *model system*. This material was studied in detail to understand the fundamentals of the mechanism with which the refractory metal oxides can mitigate the degradation through gas switching. It became clear from the Zr study that the layer thickness and position within the PtIr anode is of great importance. Fundamental characterization using advanced analytical techniques, such as XPS, XAFS and STEM, allowed for better understanding of the PtZrIr model system. This in turn generated experimental directions towards achieving improved durability.

The greatest impact on increasing reversal durability after GS appeared to be with Zr deposited between Pt and Ir (Figure 8.3A), forming a M-Ox 'sandwich' construction, validating our starting hypothesis that a physical separation of Pt from the OER catalyst is key in mitigating GS degradation. The best of class construct of each of the four elements is represented in Figure 8.3B, from which we concluded that both 250Å Zr and Hf gave the highest reversal durability performance, reaching 10 hours under 1.7 V.

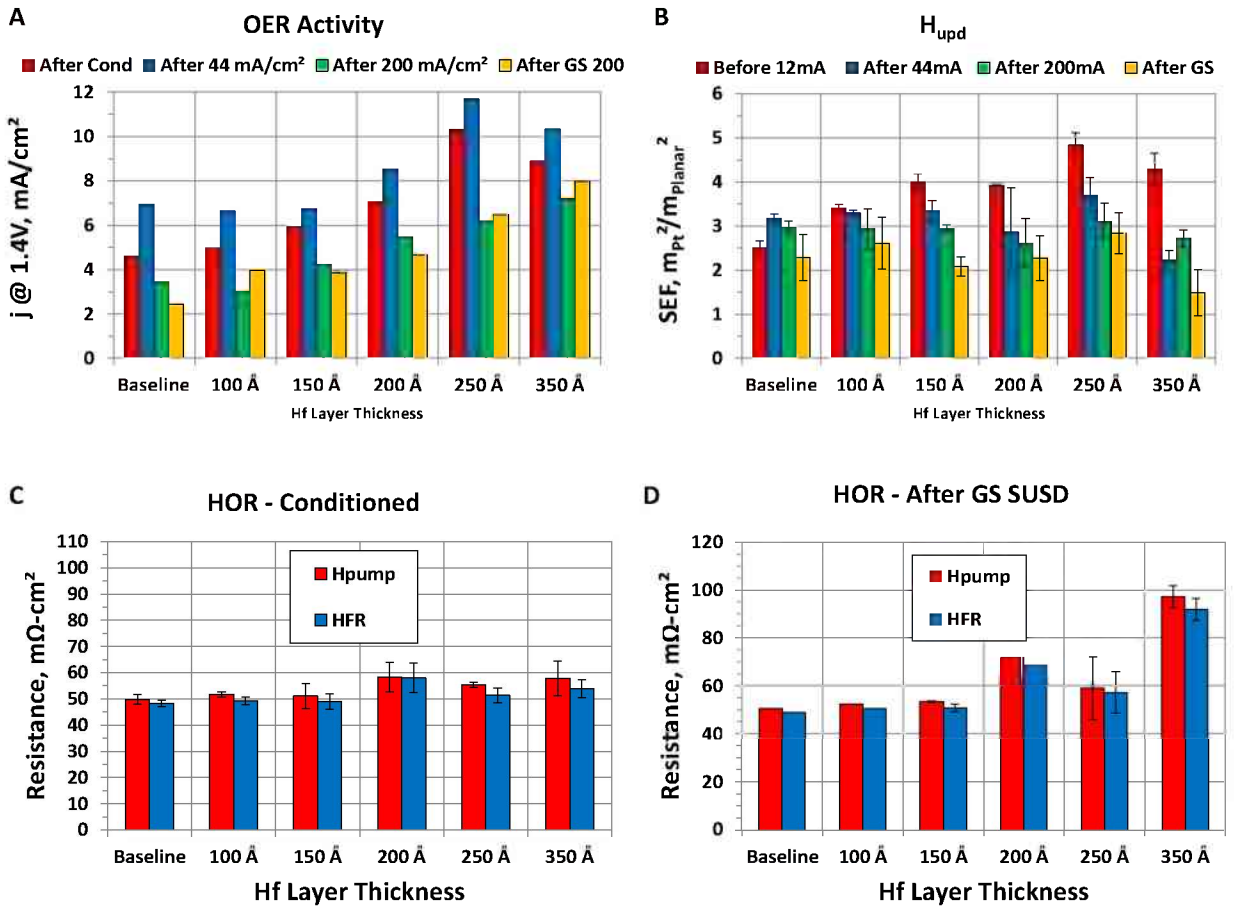


Figure 8.4. Effect of hafnium sandwich layer thickness on (A) OER activity; (B) Pt H_{upd}, expressed as an apparent surface enhancement factor with a H_{upd} charge of 210 µC assumed per cm_{Pt}^2; (C) initial HOR and (D) HOR after GS

As expected, Zr and Hf constructs behave very similarly. The mechanism by which Ta contributes to GS stability is significantly different, as evident from the smaller quantity of Ta (an order of magnitude lower in thickness) necessary to induce stability improvement for the GS compared to the baseline PtIr. The blocking of the direct recombination of $H_2 + O_2$ likely plays a larger role for Ta-modified PtIr than the physical separation. This diversity in the protective mechanism allows for greater exploration in future work. The addition of a Ti layer in the loading range of 25-250 Å did not prove to be beneficial.

The extensive experience gained during the initial Zr construct testing prompted us to efficiently and thoroughly screen the loading range for the Hf modified anodes. The results of these screens are presented in Figure 8.4. Clearly, the initial OER activity was superior with higher loadings of Hf, and more importantly, this activity was better preserved (Figure 8.4A). Although the Hupd decreases rapidly over the duration of the test, the HOR performance is maintained (Figure 8.4B-D).

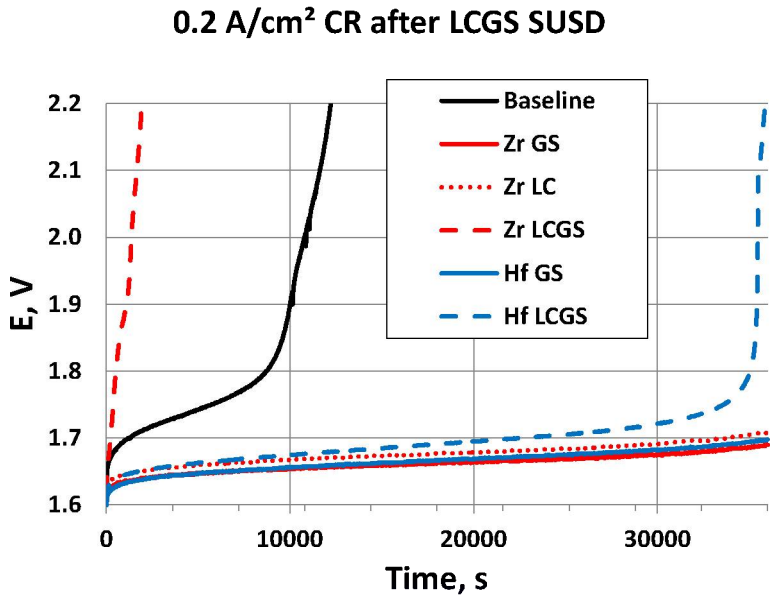


Figure 8.5. Effect of LCGS on reversal performance of Zr and Hf sandwich OER-Modified Anodes. Zr and Hf modified anodes after 200 gas switches shown in unbroken lines; after 200 LCGS shown in dashed lines Dotted red line indicated Zr modified anode after 200 Load Cycles without GS.

As mentioned earlier, in order to qualify the catalyst for 'real life' applications, it has to perform satisfactory in a more demanding durability protocol, which includes a load cycle (LC) during gas switching; a Load Cycle – Gas Switch (LCGS) combination. The screening target was set to perform 200 LCGS cycles, after which the catalyst still maintains 10 hours of reversal durability. The robustness necessary to endure such harsh conditions puts even the best of class Zr and Hf catalysts to the limit, as Figure 8.5 demonstrates. It is also clear from this figure that for the Zr sandwich, the combination of Load Cycles and Gas Switches is very damaging, whereas during the individual LC or GS treatments, the catalyst maintains its OER performance. Aiming

to reach 2,000+ LCGS cycles without reversal performance failure necessitates a vast amount of progress to be made in this area in order to meet 'real life' requirements.

Because of the introduction of a variety of new materials, we have initiated a *new stability test*. The purpose of the test is to evaluate the stability of the added/new materials in a realistic environment. Analysis of the blank cyclic voltammetry in MEA as a function of the upper limit potential has already revealed a link between the results as obtained by Fuel Cell Load Cycle, Gas Switch and Reversal tests and those obtained in the Synchrotron. Figure 8.6A shows how the standard PtIr exhibits the clear features of both elements (H_{upd} at 0-0.3 V, oxide formation at >0.6 V, oxygen evolution at 1.4 V, Pt oxide reduction at 0.7 V, Ir reduction at 0.7- 0.1 V). However, when Hf is added (Figure 8.6B), the resulting voltammetry after a single voltammogram to 1.4 V exhibits no H_{upd} features. All the typical Pt and Ir oxide signatures are still present; merely the proton adsorption is blocked.

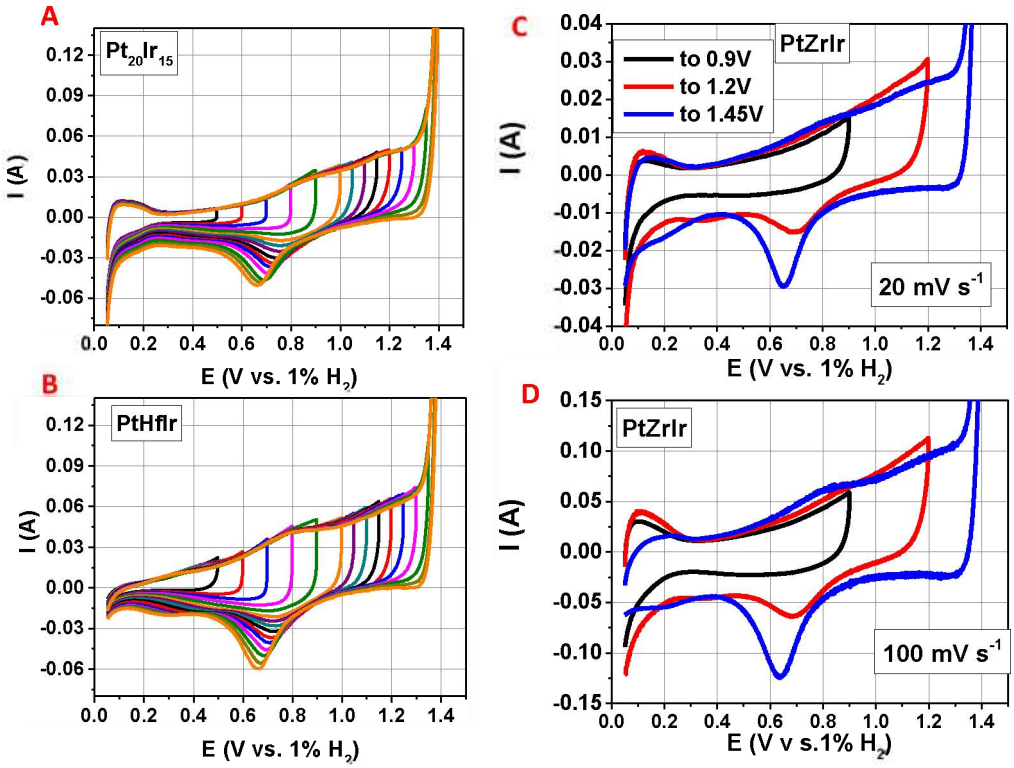


Figure 8.6. Comparison of the blank cyclic voltammetry of three constructs. (A) Standard PtIr NSTF; (B) PtHfIr after a single cyclic voltammogram to 1.4 V; (C & D) PtZrIr at slow (20 mVs^{-1}) and fast (100 mVs^{-1}) scan rates.

PtHfIr retained excellent reversal stability after the LCGS test, lasting over 9.5 hours under 1.8 V in the 200 mA/cm^2 hold, but had decreased HOR activity. On the other hand, addition of Zr resulted in great performance in reversal after GS, without significant performance loss, but much lesser performance after LCGS cycling (see Figure 8.5). Analysis of the PtZrIr cyclic voltammetry (Figure 8.6C&D) shows that the blockage of the H_{upd} can only be observed at high scan rates (or

lower temperatures, graph not shown). This result, however, validates our hypothesis that the added elements enhance durability by stabilizing oxides, which both separates the Pt from the Ir and diminishes the extent of direct recombination of H_2 and O_2 in GS. This also falls perfectly in line with the observed trend from XAFS (shown below), where is clearly shown that zirconium oxide increases the stability of the iridium oxide.

From these initial results it can be concluded that:

1. Cyclic voltammetry in the MEA can shed a clear light on the mechanics behind the function of the added refractory elements, and
2. The ideal solution of a construct with Load Cycle + Gas Switch stability without performance loss will require more than a single added element.

Fundamental studies played a crucial role in better understanding the phenomena involved during the gas switching and elucidating the role of the added materials. Besides the XPS and STEM characterization that have already proven valuable in understanding the catalyst constructs in the first years of the program, this task was further enhanced by using synchrotron-based techniques.

The incorporation of an interlayer to effectively separate the Ir over-layer from the Pt-NSTF substrate, while preserving the optimal synergy between Ir OER and Pt HOR requires systematic characterization of the formed interfaces. **XPS**, as a surface sensitive technique, is capable of providing quantitative information on the changes in elemental composition and chemical bonding at the evolving interfaces. The preliminary XPS evaluation of the 20 μg/cm² Pt-NSTF + 15 μg/cm² Ir samples separated by a Zr interlayer varying in thickness from 50 to 500 Å are in agreement with the intended construct of a Zr layer sandwiched between Pt-NSTF and Ir top layer. This is evident from the fact that the Ir level seems constant while Pt visibly attenuates with the increase of Zr interlayer thickness (see Table 8.1 and Figure 8.7).

Zr, Å	C 1s %	Ir 4f %	N 1s %	O 1s %	Pt 4f %	Zr 3d %
0	16.5	40.5	1.5	33.1	8.4	0.0
50	20.4	42.2	1.5	25.4	4.1	6.4
100	18.7	34.3	1.8	32.2	2.7	10.3
150	18.8	34.8	2.1	30.9	1.3	12.2
250	17.9	34.1	2.2	31.6	0.5	13.8
500	18.8	46.7	1.7	22.2	0.1	10.6

Table 8.1: XPS mean atomic concentrations derived from Survey Spectra at 3 random locations.

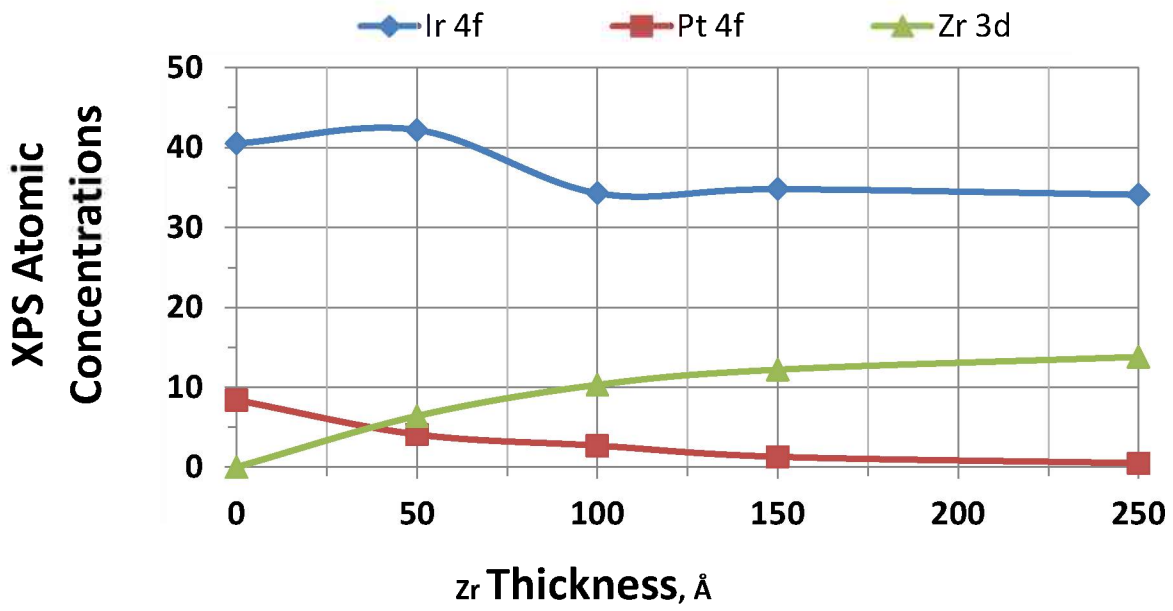


Figure 8.7. Mean Ir, Zr and Pt atomic concentrations as a function of Zr interlayer thickness

The Zr 3d core level spectra show the presence of Zr metal, Zr suboxide and ZrO_2 for all investigated Zr interlayer thicknesses (Figure 8.8). The BE location of the peak associated with the presence of Zr suboxide may also suggest a potential Zr-Ir interaction. The C 1s core level spectra show preferential attenuation of carbonyl carbon, possibly due to Zr interaction with the exposed bare PR sites. The O 1s core level spectra show the growth of oxide oxygen with increasing thickness of Zr interlayer.

Throughout the course of the *project*, STEM coupled with EDS has provided important insight into the nanoscale nature of catalyst overlayers tasks, and their evolving morphology during fuel cell testing. These efforts, carried out at Oak Ridge National Laboratory (ORNL), supported both the *catalyst fabrication and evaluation* and *fundamental studies*

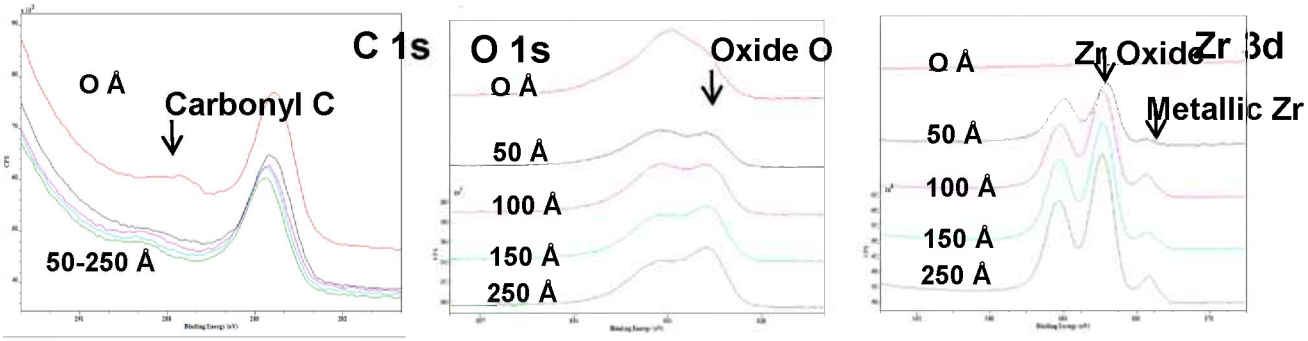


Figure 8.8. High resolution C 1s, O 1s and Zr 3d XPS core level spectra at a random location for each Zr interlayer thickness

Characterization of the PtZrIr NSTF series is highlighted in Figure 8.9. Owing to the lower atomic number of Zr, it is clearly distinguishable from both Pt and Ir in HAADF images. Mapping showed that Zr was relatively stable throughout various testing protocols. A direct comparison with a similarly tested PtIr NSTF series is essential if the more accurate mechanism by which the Zr interlayer improves the stability of the OER-modified anode catalyst is to be revealed. The synergistic combination of XPS and STEM has been a marquee success of our previous work, however, due to the surface sensitive nature of the technique, the highly insightful chemical bonding and surface composition information provided by XPS has been limited to as-grown materials. The addition of *ex-situ* X-ray absorption fine structure spectroscopy (XAFS) measurements allowed us to carry that same synergy into the embedded NSTF electrodes. The primary goal of these studies was to determine the mechanism by which the interlayer metals improve both the activity and performance durability of the NSTF-based anodes. XAFS provides the oxidation state (near edge region) and atomic coordination environment (extended region) of the absorbing atom. The effort was focused on XAFS characterization of the anodes with a zirconium interlayer in comparison with anodes of just platinum and iridium at various stages of fabrication and performance testing: as-deposited catalyst, the catalyst in an as-prepared CCM, and CCMs after conditioning, after applying an anodic current (200 mA/cm^2), after hydrogen-air GS, and after cell reversal. Special samples with palladium cathodes were manufactured for this series, in order to avoid interference of the anode Pt signal by cathode Pt.

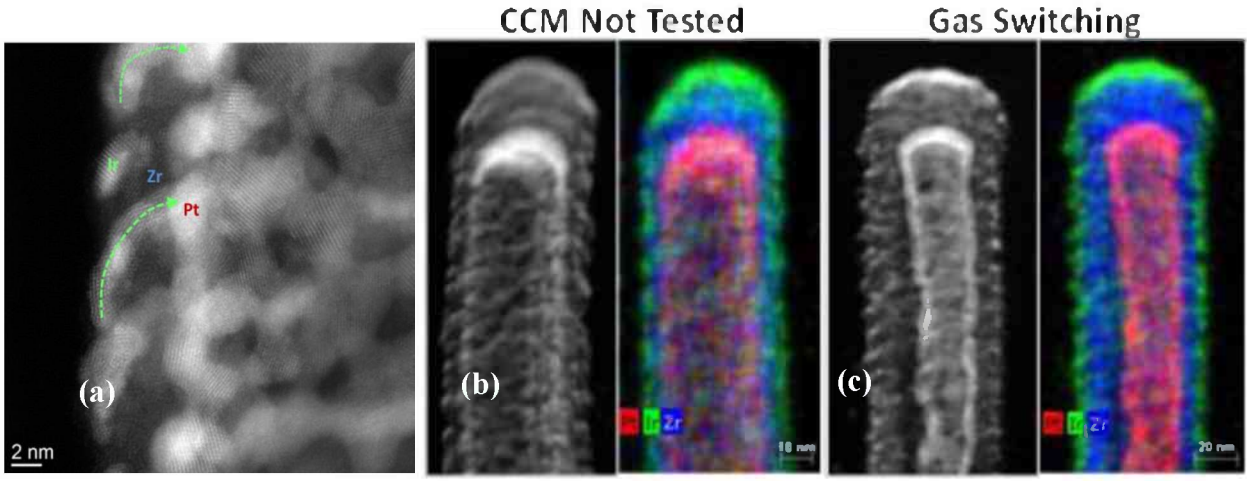


Figure 8.9. (a) STEM-HAADF image of surface of as-grown PtZrIr, with arrows indicating regions where Pt and Ir may be in contact. EDS maps of (b) an untested whisker and (c) a whisker following the gas switching phase showing the continued presence of Ir on the whisker surface, and the physical separation of Ir and Pt by the Zr layer.

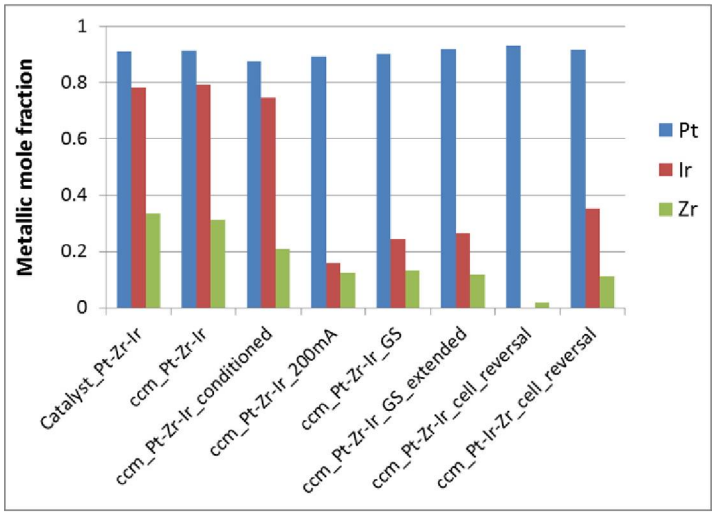


Figure 8.10. The extent of oxidation of Pt, Zr, and Ir in the as-prepared catalyst and after various steps in the CCM treatment and reversal tolerance testing. Extent of oxidation is represented as the fraction of the sample in the metallic form.

The extent of oxidation of Pt, Zr, and Ir of the Pt-Zr-Ir samples and of one sample with Ir deposited directly on the Pt and the Zr deposited on the top of the Ir (CCM: Pt-Ir-Zr_cell_reversal) are shown in Figure 8.10. These data show that the Ir and Zr are primarily oxides after the anodic current treatment (200 mA/cm^2) and that the Zr interlayer facilitates the complete oxidation of Ir upon cell reversal.

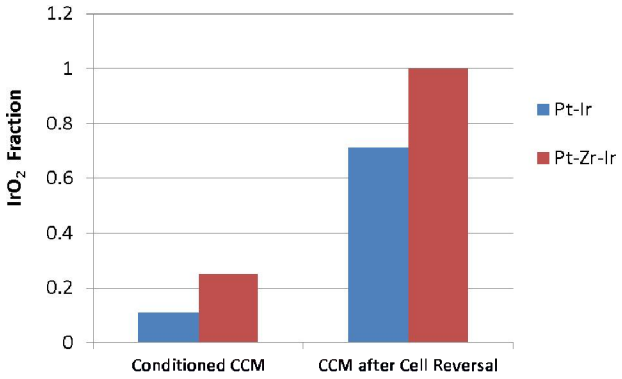


Figure 8.11. The extent of oxidation of Ir in Pt-Ir and Pt-Zr-Ir anode catalysts after conditioning and after cell reversal.

This is also supported by the data shown in Figure 8.11, which compares the extent of Ir oxidation of Pt-Ir anodes with and without the Zr interlayer after conditioning and after cell reversal. Analysis of the extended region of the XAFS spectra shows that Zr is incorporated into the Pt during Zr deposition to form a Pt-Zr surface alloy. It is postulated that the formation of this surface alloy during deposition inhibits the interaction between Pt and Ir, reducing the degradation of the OER catalyst due to the heat and radicals formed during GS. Based on these results, the

mechanism of the Zr protection is to facilitate the complete oxidation of Ir, while preventing its dissolution and loss from the anode at high potentials. This posed mechanism is supported by the observation from X-Ray fluorescence of the samples tested at the Synchrotron (Figure 8.12). It is clear from the figure that the ratio of Pt to Ir changes dramatically during the durability cycle when the Zr layer is absent, most likely caused by Ir dissolution. In contrast, the Pt:Ir ratio for the PtZrIr sandwich samples remain virtually unchanged, highlighting their stability.

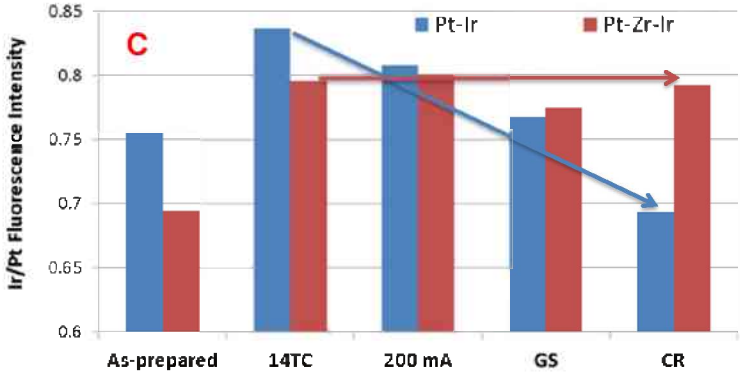


Figure 8.12. X-Ray Fluorescence of the MEAs at each stage of the testing. Pd counter electrodes ensure Pt signal is originating from the anode side.

In fact, STEM results support this mechanism wholeheartedly. As is evident from Figure 8.13, the Ir remains on the whisker throughout the gas switching for the PtZrIr construct, only to dissolve after 10 hours of cell reversal. On the other hand, Ir already dissolves after the 200 mA/cm^2 pulses for the unmodified PtIr catalysts. Indeed, both Pt and Ir are already removed from the whisker after gas switching, with complete whisker deformation taking place during CR.

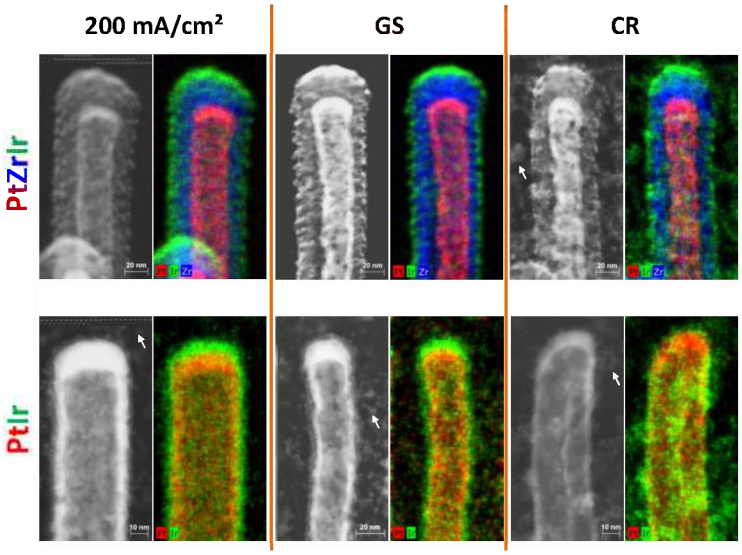


Figure 8.13. STEM analysis of the same MEAs on which XAFS analysis was performed, with palladium counter electrodes. Samples are show after three stages of the protocol: after the 200 mA cm^{-2} reversal pulses; after gas switching and after the 10 hours cell reversal hold.

8. 3. Durability under Load Cycle + Gas Switch (LCGS)

The synergy between the analysis techniques of the different project partners enables us to conclude with confidence that the key to the GS durability enhancement is the separation of the Pt from the Ir, in addition to the stabilization of the iridium oxides. Furthermore, a delicate balance has to be traversed in order to retain the HOR activity, which prefers a fully metallic surface, while improving oxide stability. One way to achieve this balance is to modify the PtIr catalyst by adding two elements (Zr and Hf), to combine the beneficial effects of both. Added Zr and Hf both improve GS stability, but Zr maintains HOR activity (where Hf shows inhibition) and PtHfIr has superior stability during load cycling in combination with the gas switches (where PtZrIr degrades).

The potential profile of a load cycle (LC) can be summarized as follows: during a load cycle, the MEA is operated normally, with alternating current demands set at 0.7 and 1.5 A/cm^2. The potential response of the cell is to cycle between approximately 1 V (at OCV), through 0.6 V (at 0.7 A/cm^2) and 0.2 V (at 1.5 A/cm^2). Therefore, rapid load changes are *de facto* performing potential cycles on the cathode, where the high Tafel slope for the ORR causes large potential variations during load cycles. However, this does not mean the anode is unaffected when load cycling is combined with gas switching, as is clearly shown in Figure 8.14. The curves in this figure show the cell reversal potential at 200 mA/cm^2, after 200 LCGS operations have been performed. The baseline PtIr NSTF reaches 1.8V (the failure point) in cell reversal after 4000 seconds, an order of magnitude faster than without LCGS (see section 4). Even more important is that the Zr-modified PtIr fails faster still; after a mere 500 seconds. On the other hand, Hf-modified PtIr survives for almost 10 hours after 200 LCGS. It is important to note here, that if the load cycle is disconnected from the gas switch, all of our anode formulations survive without problem. On its own, the load cycle is not damaging to the anode and the PtZrIr anode remains below 1.7V during the 10 hour reversal hold of 200 mA/cm^2. It is specifically the LCGS that is destructive to the zirconium constructs. The Hf containing anodes are stable throughout LC, GS and LCGS.

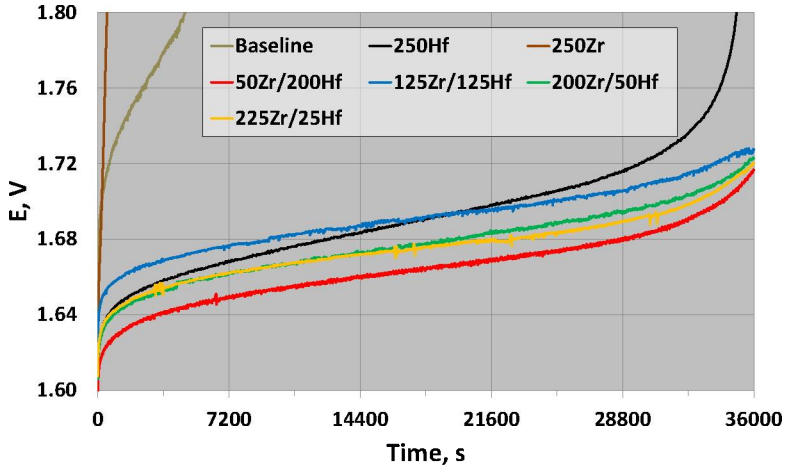


Figure 8.14. Cell Reversal durability of Zr and Hf modified PtIr OER-anodes after 200 LCGS.

This brings us to the point that was raised earlier: the beneficial properties of both the Hf and Zr can be combined to generate a robust OER-modified Anode catalyst that can withstand the harsh conditions during SU/SD and CR, including real life Gas Switching and Load Cycling. What is more, different ratios of Zr:Hf (Figure 8.14), and different deposition orders (graph not shown) have little effect on the durability of the PtZrHfIr quaternary catalyst. This is an important finding in regards to the manufacturing feasibility and cost, because it means that less refined ZrHf metals (they are each other's largest impurities in refined targets) can be used to generate the materials, without compromising durability and performance.

8. 4. Location/Site Separation of the OER Catalyst from Pt

The previously introduced, discussed and to a large degree proved hypothesis on the durability improvement towards gas switching stated that the physical separation of Pt from the OER via incorporation of minute amounts of inert materials is beneficial to the durability. To provide the ultimate proof that our hypothesis is correct, we took a step further and deposited the Pt and OER separately on a different component of the MEA: As usual, the Pt/NSTF was laminated to the membrane, and the OER (in the form of Ir) deposited on the GDL. The cell reversal results of the new constructs tested after LCGS are presented in fig. 8.15.

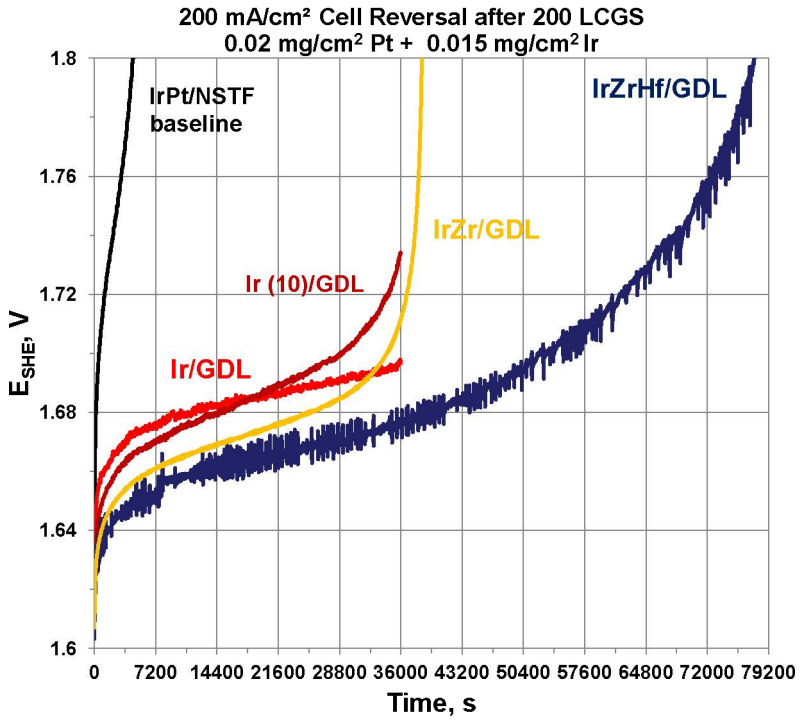


Figure 8.15. Cell Reversal potentials at 200 mA/cm² after 200 LCGS. All constructs contain 20 μg/cm² Pt and 15 μg/cm² Ir, except for the Ir(10)/GDL, which contains 10 μg/cm² Ir. Black line is the baseline PtIr on NSTF; red lines have Pt/NSTF and Ir on the GDL; yellow has Pt/NSTF and Ir + 250 Å Zr on the GDL; and blue has Pt/NSTF and Ir + 250 Å (ZrHf).

It is clear from Figure 8.15 that the function of the OER catalyst is not impaired when deposited on the GDL rather than in intimate contact with Pt. Indeed, the reversal performance after 200 LCGS is greatly enhanced. The potentials after 10 hours of 1.68 V, 1.70 V and 1.72 V for IrZrHf/GDL, Ir/GDL and IrZr/GDL, respectively, compare favorably to 1.72 V for the various PtZrHfIr/NSTF constructs (Figure 8.14). In fact, the lower loaded Ir(10)/GDL also made it to 10 hours (at 1.73 V), where most IrPt/NSTF constructs did not [the PtZrIr (orange trace) and PtHfIr (black trace) in Figure 8.14]. Astonishingly, an unsurpassed 21^{+} hours of cell reversal was recorded for the Pt/NSTF + IrZrHf/GDL sample before a cell potential of 1.8V was reached.

There are two important aspects of the location separation of the OER catalyst from the Pt:

- On a **fundamental level**, we have proven that the elimination of the intimate, atomic level proximity of Ir and Pt is the reason for the loss of the OER activity of the IrPt/NSTF catalyst.
- On a **practical level**, this implies that the hereby developed durability enhancement for fuel cell anodes may be a '**drop-in solution**' for stability improvement for a variety of MEAs with Pt nanoparticles on durable carbon supports.

9. Conclusion: Summary of Major Accomplishments

This project introduced two major novel approaches to solving durability issues during transient periods of FC operation that to our knowledge had not been reported thus far. The approaches are materials based and, as such, protection is provided from within the MEA and is therefore always "ON". These new concepts are original both in the *materials* that we are introducing into the catalysts and the *processes* through which we are incorporating these materials into the existing catalyst:

- Incorporating OER active particles onto/into the structure of the catalysts without interference with their basic function: catalyzing the ORR on the cathode and HOR on the anode.
- Over-coating or intimately mixing the anode catalyst with inert material that will selectively inhibit the ORR without interfering with the HOR.

We emphasize the fact that the additives to the existing anode and cathode NSTF catalysts are fully integrated and as such act as one catalyst. This is in contrast to approaches that have been proposed elsewhere in which OER catalysts more active than platinum have been introduced as additional layers or a mechanical mixture of two separate catalysts. The new integrated catalyst should be equally applicable for transient conditions in both automotive and stationary applications.

During the course of the program we developed a highly active OER catalyst that allowed us to accomplish the program milestones by adding marginal amounts of platinum group metals (PGM). This paves the way for the 2017 DOE target for durability and for 0.1 mg/cm^2 of PGM loading to be achieved. The OER enabled catalyst was successfully scaled up and its effectiveness was proven by several major automotive manufacturers both in their laboratories as well as in their more realistic 'real life' simulating testing in over two dozen short fuel cell stacks.

In general, the following are the key attributes of the OER modified catalysts:

- Extremely *high inherent and mass activity* towards the OER
- Unsurpassed *durability at high positive potentials* during cell reversal
- Sufficient HOR activity under a variety of operating conditions, including fully recoverable CO poisoning
- Possibility to lower the Pt loading without sacrificing performance
- *Protection for the cathode during SU/SD* due to ORR suppression on the anode, *an exclusive property unique to this catalyst*, owing to the synergy between the Pt NSTF film and OER catalyst in intimate contact.

On a programmatic level, all the milestones where accomplished and surpassed, both performance - and time- wise, as laid out in Table 9.1.

Task 1: OER Active Catalyst SU/SD (Cathode)	# of Cycles (>)	PGM (mg/cm²) (<)	End Voltage (<)	ECSA Loss (%) (<)	Status/Comments
2011	5,000	0.095	1.60 V	12%	Achieved 09/2011
Go/No Go	5,000	0.090	1.60 V	10%	Achieved 01/2012; End Voltage: 1.48 V
2013	**5,000**	**0.088**	**1.45 V**	**10%**	**Achieved** 11/2012; End Voltage: 1.44 V
Cell Reversal (Anode)					
2011	200	0.050	2.00 V		Achieved 09/2011
Go/No Go	200	0.045	1.80 V		Achieved 01/2012; End Voltage: 1.65 V
2013	**200**	**0.037**	**1.75 V**		**Achieved** 11/2012;End Voltage: 1.62 V
Task 2: Suppression of ORR (Anode)					
Go/No Go	A factor of 10 in the kinetic region				Achieved 01/2012; A factor > 100
2013	A **factor of >100** in the kinetic region				**Achieved** 02/2013; A factor > 1,000
Task 3: Scale-up					
2012	Scale up to full size cells (> 300 cm^2)				Evaluated in 2012: > 10 short stacks
2013	**"Real life"** evaluation – AFCC				**9 x (3 or 15)-cells short stacks**

Table 9.1. Milestones and Accomplishments.

Most of the work originally proposed and outcomes envisaged were realized by 3M, AFCC, ORNL, Dalhousie University and ANL. As presented in this report, there were numerous *accomplishments beyond the metrics*, some of which will be reemphasized here.

- OER/NSTF brought NSTF as a new catalyst concept very close to "real"/stack application
- Platinum dissolution is prevented satisfactory when the potential is maintained below 1.7 V.
- Original generic tests for SU/SD and Cell reversal were developed and implemented.
- Fully characterized coatings with XPS (ECSA) show indications of interaction of the OER catalysts with the NSTF substrate, potentially favorable from a durability point of view.
- Constructs with *additional refractory metals* have fulfilled the cell reversal requirement after gas switching and /or gas switching with load cycling.
- Hypothesis that separating the OER catalyst from atomic proximity of Pt may alleviate the impact of gas switching was proven with added benefit of improved OER activity.
- Fundamental materials studies aimed at understanding the extraordinary durability of the new OER-Pt/NSTF constructs have converged to concluding that stabilizing the Pt and Ir oxides is paramount to increasing reversal endurance.
- The constructs with a separating layer open up opportunities for use of a wider array of commercially acceptable materials to address both the OER performance and the application issues in general.
- Specific OEM requirements can be more readily addressed by the flexibility offered by the new constructs.

- 16 publications and 11 invited presentations are evidence of the recognition of this program and a testimony of the broad impact that the program had on the fuel cell community awareness of the durability during the transient conditions.

10. Publications, Presentations, Websites and Inventions

10. 1. Publications

1. Stevens, R.J. Sanderson, T.D. Hatchard, T.C. Crowtz, J.R. Dahn, G.D. Vernstrom, G.M. Haugen, T. Watschke, L. L. Atanasoska, and R.T. Atanasoski: *Development of Catalysts with Enhanced Tolerance to Fuel Cell Transient Conditions*, D.A., ECS Transactions, **33 (1)** 419 (2010).
2. T.D. Hatchard, J.E. Harlow, D.A. Stevens, Gary Chi-Kang Liu, R.J. Sanderson, N. van der Bosch, J.R. Dahn, G. M. Haugen, G.D. Vernstrom and R.T. Atanasoski,: *Rapid RDE Evaluation of Catalyst Performance and Durability During Transient Conditions: The Pt-Hf Binary System.* Electrochim. Acta. **56** (2011) 10436–10442
3. L.L. Atanasoska, G. D. Vernstrom, G. M. Haugen, and R. T. Atanasoski*: Catalyst Durability for Fuel Cells under Start-up and Shutdown Conditions: Evaluation of Ru and Ir Sputter-Deposited Films on Platinum in PEM Environment*, ECS Transactions, **41** (1) 785-795 (2011)
4. M. K. Debe, R. T. Atanasoski and A. J. Steinbach, *Invited presentation* "Nanostructured Thin Film Electrocatalysts – Current Status and Future Potential," ECS Transactions, **41** (1) 937-954 (2011)
5. D. A. Cullen, K. L. More, K. S. Reeves, G. D. Vernstrom, L. L. Atanasoska, G. M. Haugen, and R. T. Atanasoski: *Characterization of durable nanostructured thin film catalysts tested under transient conditions using analytical aberration-corrected electron microscopy,* ECS Transactions, **41** (1) 1099-1103 (2011)
6. David A. Cullen, Karren L. More, Radoslav T. Atanasoski, Sumit Kundu, and Wendy Lee: *"Comparison of quantitative electron microscopy methods for determining Pt-loss in PEM fuel cells"*, Fuel Cell Seminar, Orlando, Nov. 2011.
7. DA Cullen, KL More, RT Atanasoski: *"Towards quantifying catalyst losses from fuel cell electrodes: an electron microscopy study"*, Microsc Microanal. **17** (S2): 64544, 2012.
8. R.T. Atanasoski, L.L. Atanasoska, D.A. Cullen, G.M. Haugen, K.L. More, G.D. Vernstrom: *"Fuel Cells Catalyst for Start-up and Shutdown Conditions: Electrochemical, XPS, and TEM Evaluation of Sputter-Deposited Ru, Ir, and Ti on Pt-Nano-Structured Thin Film (NSTF) Support"*, Electrocatalysis **3,** 284 – 297, 2012.
9. R T Atanasoski, LL Atanasoska**,** DA Cullen: "*Efficient Oxygen Evolution Reaction Catalysts for Cell Reversal and Start/Stop Tolerance*" in M. Shao ed., "*Electrocatalysis in Fuel Cells: A Non and Low Platinum Approach*", Chapter 22, pp.637 – 663. Springer, March, 2013.

10. RT Atanasoski, DA Cullen, GD Vernstrom, GM Haugen LL Atanasoska:"*A Materials-Based Mitigation Strategy for SU/SD in PEM Fuel Cells: Properties and Performance-Specific Testing of IrRu OER Catalysts"*, ECS Electrochem. Lett, **2** (3) F25-F28, 2013.
11. LL Atanasoska, DA Cullen, AE Hester, RT Atanasoski: "*XPS and STEM of the interface formation between ultra-thin Ru, Ir and Pt layers and perylene red catalyst support whiskers*", ECS Transactions, 50,19 -33, 2013.
12. Vincent Lee, Darija Susac, Sumit Kundu, Viatcheslav Berejnov, Radoslav T. Atanasoski, Adam P. Hitchcock, Jürgen Stumper: "*STXM Characterization of Nanostructured Thin Film Anode Before and After Start-up Shut-down and Reversal Tests*", Transaction of the Electrochemical Society, **58** (2013) 473-479.
13. LL Atanasoska, DA Cullen, RT Atanasoski: "*XPS and STEM of the interface formation between ultra-thin Ru and Ir OER catalyst layers and Perylene Red support whiskers*", J. Serb. Chem. Soc. **78** (12) 1993–2005 (2013)
14. Vincent Lee, Adam P. Hitchcock, Marcia West, Viatcheslav Berejnov, Sumit Kundu, Darija Susac, Juergen Stumper, Radoslav Atanasoski and Mark Debe: "*STXM Investigations of Nano Structured Thin Film Catalysts for Proton-Exchange-Membrane Fuel Cell Applications*", J. Power Sources **263**, 163 - 174 (2014)
15. Timothy Crowtz, David Stevens, Robbie Sanderson, Jessie Harlow, George Vernstrom, Ljiljana Atanasoska, Greg Haugen, and Radoslav Atanasoski, Jeff Dahn: "*The effect of Ru or Ir addition on Nano-Structured-Thin-Film supported Pt fuel cell catalysts under rotating disk electrode simulated start-up shut-down*", J. Electrochem. Soc.**161** (10) F961-F968 (2014)
16. DA Cullen, KL More, LL Atanasoska, RT Atanasoski: "*Impact of IrRu Oxygen Evolution Reaction Catalysts on Pt Nanostructured Thin Films under Start-Up/Shutdown Cycling*", J. Power Sources, **269**, 671-681(2014)

10. 2. Invited Presentations

1. Radoslav Atanasoski: "*PEM Fuel Cells: Focus on Durability*", Electrochemical Section of the Chemical Soc., Belgrade, Serbia, Oct.13, 2009.
2. R. Atanasoski: *"Fundamental and practical aspects of Nano-structured thin film catalysts for PEM fuel cells*", Ulm ElectroChemical Talks 2010: *"2015" Technologies on Batteries and Fuel Cells*, June 2010.
3. R. Atanasoski: "*Durability of Thin Film Catalysts for PEM Fuel Cells*", *Key-Note Lecture*, "Electrochemical Energy Conversion and Storage" symposium , 61st Annual Meeting of the International Society of Electrochemistry, September 2010, Nice, France.
4. R. Atanasoski: "*Durable Catalysts for Transient Conditions",* 6th Annual International Conference, FUEL CELLS DURABILITY & PERFORMANCE 2010, Boston, Dec. 09, 2010.

5. R. Atanasoski: *"Role of catalysts durability in PEM Fuel Cells"*, *Key-Note Lecture,* "Role of Catalysis in Fuel Cells" Symposium, 241st Amer. Chem. Soc., Anaheim, CA, 03/29/2011.
6. R. Atanasoski: *"Role of catalysts durability in PEM Fuel Cells"*, *Key-Note Lecture,* "Role of Catalysis in Fuel Cells" Symposium, 241st Amer. Chem. Soc., Anaheim, CA, 03/29/2011.
7. R. Atanasoski: *"Catalyst Degradation during Transient Conditions focused on Durable Catalysts for Fuel Cell Protection during Transient Conditions"*, 2nd INTERNATIONAL WORKSHOP on DEGRADATION ISSUES OF FUEL CELLS, 21-23 SEPTEMBER, 2011, Thessaloniki, Greece (by DOE invitation).
8. R.T. Atanasoski, L.L. Atanasoska, D.A. Cullen, A. Hester: *"Oxygen Evolution Reaction on Minute Amounts of Ru and Ir Catalyst for Application in Fuel Cell Protection"*, I4 - *Electrocatalysis 6*, PRiME 2012, Honolulu, Hawaii, Oct. 08, 2012 (opening talk; # 3737).
9. R. Atanasoski: "*Catalysts Durability in PEM Fuel Cells focused on Durable Catalysts for Fuel Cell Protection during Transient Conditions*", Twin Cities Electrochemistry Symposium 2012, April 12, 2012.
10. R.T. Atanasoski, L.L. Atanasoska, D.A. Cullen, G.M. Haugen, G.D. Vernstrom: *"Catalyst Materials for Fuel Cell Voltages beyond 1.23 V"*, ILED 2012, Rome, May 30 – June 01, 2012.
11. R.T. Atanasoski,J.L. Wong, D. van der Vliet, L.L. Atanasoska, D. Cullen, and D.J. Meyers : *"Zr added Ir/Pt NSTF catalysts for Oxygen Evolution in Fuel Cells"*, ECAT 2014, Whistler, BC, Canada, October 26 – 29, 2014.

10. 3. Presentations

1. D.A. Stevens, A. Bonakdarpour, R.J. Sanderson, E. Marvel, S. Wang, R.T. Atanasoski, M.K. Debe and J.R. Dahn: *"Development of multi-component PEM fuel cell catalysts for enhanced stop-start protection"*, 217th Electrochemical Soc. Meeting, Vancouver, Canada, April 25 – 29, 2010.
2. D.A. Stevens, A. Bonakdarpour, R.J. Sanderson, E. Marvel, S. Wang, R.T. Atanasoski, M.K. Debe and J.R. Dahn: *"Development of multi-component PEM fuel cell catalysts for enhanced stop-start protection"*, 218th Electrochemical Soc. Meeting, Las Vegas, Oct, 2010.
3. D. Stevens, G. Vernstrom, R. Sanderson, G. Haugen, T. Hatchard, T. Crowtz, T. Watschke, M. Debe, R. Atanasoski, and J. Dahn: *"Development of Catalysts for Enhanced Tolerance to Fuel Cell Transient Conditions"*, Electrochemical Soc. Meeting, Las Vegas, Oct, 2010.
4. D. A. Cullen, K. L. More, K. S. Reeves, G. D. Vernstrom, L. L. Atanasoska, G. M. Haugen, and R. T. Atanasoski: "*Characterization of durable nanostructured thin film catalysts tested under transient conditions using analytical aberration-corrected electron*

microscopy", 220th ECS Meeting and Electrochemical Energy Summit, Boston, MA, October 9-14, 2011

5. L.L. Atanasoska, G. D. Vernstrom, G. M. Haugen, and R. T. Atanasoski*: "Catalyst Durability for Fuel Cells under Start-up and Shutdown Conditions: Evaluation of Ru and Ir Sputter-Deposited Films on Platinum in PEM Environment*", 220th ECS Meeting and Electrochemical Energy Summit, Boston, MA, October 9-14, 2011
6. D. A. Cullen, K. L. More, K. S. Reeves, G. D. Vernstrom, L. L. Atanasoska, G. M. Haugen, and R. T. Atanasoski*: "Analytical aberration-corrected electron microscopy study of the effects of transient operation on the stability of nanostructured thin film catalysts for PEM fuel cells"*, Microscopy and Microanalysis 2011, Aug 7th-11th, Nashville, TN.
7. Atanasoska LL, Cullen DA, Hester A, Atanasoski RT: *"XPS and STEM of the interface formation between ultra-thin Ru, Ir and Pt layers and perylene red catalyst support whiskers", PRiME 2012*, Honolulu, Hawaii
8. GM Haugen, GD Vernstrom, LL Atanasoska, and RT Atanasoski: *"SU/SD, a Materials Solution"*, 224th ECS Meeting, San Francisco, October 2013
9. T.C. Crowtz, D.A. Stevens, R.J. Sanderson, C.W. Watson, J.E. Harlow and J.R. Dahn: *"An RDE assessment of sputtered Ir-Ru-Pt overlayer nanostructured thin film catalysts for protection of PEMFC cathodes against start-up and shut-down: The durability of oxygen reduction activity"*, San Francisco, October 2013
10. Vincent Lee, Darija Susac, Sumit Kundu, Viatcheslav Berejnov, Radoslav T. Atanasoski, Adam P. Hitchcock, Jürgen Stumper: *"STXM Characterization of Nanostructured Thin Film Anode Before and After Start-up Shut-down and Reversal Tests"*, 224th ECS Meeting San Francisco, October 2013

10. 4. Web sites

1. Atanasoski RT (2009) *Kickoff Meeting for New DOE Fuel Cell Projects.* Washington, D.C. Online at: ww1.eere.energy.gov/hydrogenandfuelcells/pdfs/atanasoski_kickoff.pdf.
2. Atanasoski RT (2010) *DOE Hydrogen Program Review*. Washington, D.C. Available online at: www.hydrogen.energy.gov/ pdfs/review10/fc006_atanasoski_2010_o_web.pdf.
3. Atanasoski RT (2010) *DOE Annual Progress Report*. Available online at: www.hydrogen.energy. gov/pdfs/progress10/v_e_6_atanasoski.pdf.
4. Atanasoski RT (2010) *DOE Hydrogen Program Review*. Washington, D.C. Available online at: http://www.hydrogen.energy.gov/pdfs/review11/fc006_atanasoski_2011_o.pdf.
5. Atanasoski RT (2011) *DOE Annual Progress Report*. Washington, D.C. Available online at: www. hydrogen.energy.gov/pdfs/progress11/v_d_3_atanasoski_2011.pdf.
6. Atanasoski RT (2012) *DOE Hydrogen Program Review*. Washington, D.C. Available online at: http://www.hydrogen.energy.gov/pdfs/review12/fc006_atanasoski_2012_o.pdf.

7. Atanasoski RT (2012) *DOE Annual Progress Report*. Washington, D.C. Available online at: http://www.hydrogen.energy.gov/pdfs/progress12/v_d_3_atanasoski_2012.pdf.
8. Atanasoski RT (2013) *DOE Hydrogen Program Review*. Washington, D.C. Available online at: http://www.hydrogen.energy.gov/pdfs/review13/fc006_atanasoski_2013_o.pdf.
9. Atanasoski RT (2013) *DOE Annual Progress Report*. Washington, D.C. Available online at: http://www.hydrogen.energy.gov/pdfs/progress13/v_a_1_atanasoski_2013.pdf.
10. Atanasoski RT (2014) *DOE Hydrogen Program Review*. Washington, D.C. Available online at: http://www.hydrogen.energy.gov/pdfs/review14/fc006_atanasoski_2014_o.pdf.

10. 5. Presentations to DOE

1. "Durable Catalysts for Fuel Cell Protection during Transient Conditions" Proposal presented to DOE, July 1, 2009, St. Paul, Minnesota.(internal)
2. "Durable Catalysts for Fuel Cell Protection during Transient Conditions" presented at the DOE Kickoff meeting, Sept. 30, 2009, Washington, DC.
3. "Durable Catalysts for Fuel Cell Protection during Transient Conditions" presented at the FC Tech Team, Detroit, April 14, 2010.
4. "Durable Catalysts for Fuel Cell Protection during Transient Conditions" presented at the DOE 2010 AMR, June 8, 2010, Washington, DC.
5. "Durable Catalysts for Fuel Cell Protection during Transient Conditions" Project progress Review, presented to DOE, Nov. 08, 2010, St. Paul, Minnesota. (internal)
6. "Durable Catalysts for Fuel Cell Protection during Transient Conditions" presented at the FC Tech Team, Detroit, April 27, 2011
7. "Durable Catalysts for Fuel Cell Protection during Transient Conditions" presented at the DOE 2010 AMR, May 10, 2011, Washington, DC.
8. "Durable Catalysts for Fuel Cell Protection during Transient Conditions" Project Go/No go Review, presented to DOE, Feb. 08, 2012, Golden, Colorado. (internal)
9. "Durable Catalysts for Fuel Cell Protection during Transient Conditions" presented to the FC Tech Team, Detroit, April 18, 2012
10. DOE 2012 AMR, May 15, 2012, Washington, DC.
11. DOE " Project Progress Review, Sept. 18, 2012, St. Paul, Minnesota. (internal)
12. Durability Work Group Workshop, Feb. 28, 2013, Washington, DC.
13. DOE Project progress Review , April 9, 2013. Vancouver, CA (internal)
14. Presentation to the FC Tech Team, Detroit, April 17, 2013.
15. DOE 2012 AMR, May 14, 2012, Washington, DC.
16. "Durable Catalysts for Fuel Cell Protection during Transient Conditions" Project progress Review, presented to DOE , November, 2013, St. Paul, Minnesota. (internal)
17. "Durable Catalysts for Fuel Cell Protection during Transient Conditions" Project progress Review, presented to DOE (internal), Web conf., April, 2014 (internal).

18. "Durable Catalysts for Fuel Cell Protection during Transient Conditions" presented at the FC Tech Team, Detroit, April, 2014.
19. "Durable Catalysts for Fuel Cell Protection during Transient Conditions" presented at the DOE 2014 AMR, June, 2014, Washington, DC

10. 6. Inventions

Title	Investigators	Reported to DOE	Patent Application #
Method for Evaluating Fuel Cell Catalyst and Gas Diffusion Layers	**Atanasoski**	**06-03-2011**	
Durable OER Catalysts	**Atanasoski, Haugen, Vernstrom and Atanasoska**	**08-01-2011**	**US Provisional, 61/739410 (WO 2014/099790, US 61/769950)**
Durable Anode for Fuel Cell During Start Up/Shut-down	**Atanasoski, Atanasoska, Haugen**	**02-12-2012**	**US Provisional, 62/096097 (WO 2014/189637)**
A New Additive – OER/Pt/NSTF Construct for Mitigating Failure Under Gas Switching during SU/SD	**Atanasoski, Atanasoska, Haugen, Armstrong, Van der Vliet, Wong**	**09-15-2014**	**PCT/US2014/034757**
Membrane Electrode Assembly	**Haugen, Atanasoski, Atanasoska, Haug, Van der Vliet, Wong.**	**09-15-2014**	**U.S. Appl. No. 62/096097**

11. References:

1. M. K. Debe, S. M. Hendricks, A. K. Schmoeckel, R. T. Atanasoski, G. D. Vernstrom, G. M. Haugen: "*Durability Aspects of Nanostructured Thin Film Catalysts for PEM Fuel Cells*", ECS Transactions, **1**, (8) 51, 2006.
2. M. K. Debe, A. K. Schmoeckel, G. D. Vernstrom, R. Atanasoski, "*High Voltage Stability of Nano-Structured Thin Film Catalysts for PEM Fuel Cells*," J. Power Sources, **161**, 1002, 2006.
3. M. K. Debe, "*Novel catalysts, catalyst supports and catalyst coated membrane methods*," in Handbook of Fuel Cells – Fundamentals, Technology and Applications, W. Vielstich, A. Lamm, H. A. Gasteiger, Eds., Wiley & Sons, 2003, Ch. 45.
4. K.L. More, R. Borup and K.S. Reeves, *"Identifying Contributing Degradation Phenomena in PEM Fuel Cell Membrane Electrode Asemblies Via Electron Microscopy"*, ECS Transactions **3**[1] 717-33 2006.
5. K.S. Reeves, K.L. More, L.R. Walker, and J. Xie, *"TEM Evaluation of Aged PEMFCs,"* in Microscopy & Microanalysis, **10**[2] 2004
6. US Patent US-2002-0076582-1A.
7. C.A. Reiser, L. Bregoli, T.W. Patterson, J.S. Yi, J.D. Yang, M.L. Perry, T.D. Jarvi: "*A Reverse-Current Decay Mechanism for Fuel Cells*", Electrochem. Solid-State Lett. **8**, A273, 2005.
8. R Makharia, S. S. Kocha, P. T. Yu, M. A. Sweikart, W. Gu, F. T. Wagner and H. A. Gasteiger, *"Durable PEM Fuel Cell Electrode Materials: Requirements And Benchmarking Methodologies"*, ECS Transactions, **1** (8) 3, 2006.
9. K. Kinoshita, "*Electrochemical Oxygen Technology*", Wiley, 1992.
10. S. Trasatti and W. E. O'Grady: "*Properties and Application of Ru-Based Electrodes*" in H. Gerischer and C. W. Tobias eds., "Advances in Electrochemistry and Electrochemical Engineering" vol. 12, Wiley, 1981.
11. S. Trasatti and W. E. O'Grady: "*Properties and Application of Ru-Based Electrodes*" in H. Gerischer and C. W. Tobias eds., "Advances in Electrochemistry and Electrochemical Engineering" vol. 12, Wiley, 1981.
12. S. Trasatti: *"Physical electrochemistry of ceramic oxides"*, Electrochim. Acta **36**, 225, 1992.
13. C. Angelinetta, S. Trasatti, Lj. Atanasoska, Z. Minevski and R. Atanasoski, "*Effect of Preparation and the Surface and Electrocatalytic Properties of RuO_2 + IrO_2 Mixed Oxide Electrodes*" Mater. Chem. Phys., **22**, 23, 1989.
14. Lj Atanasoska, R. Atanasoski, S. Trasatti, "*XPS and AES study of mixed layers of RuO_2 and IrO_2*", Vacuum, **40**, 91, 1990.
15. R. Koetz, S. Stucki, "*Stabilization of RuO_2 by IrO_2 for anodic oxygen evolution in acid media*", Electrochim. Acta **31**, 1311, 1986.
16. S. Trasatti, ed.: "*Electrodes of conducting metallic oxides*", Parts A and B, Elsevier, 1980 and 1981.
17. Lj. Atanasoska, R. Atanasoski, F. Pollak and W. E. O'Grady: "*Single Crystal RuO_2\|Ti and RuO_2\|TiO_2 Interface: LEED, Auger and XPS Study*", Surface Science, **230**, 95, 1990.

18. B. Wessling, A. Besmehn, W. Mokwa, U. Schnakenberg: *"Reactively sputtered iridium oxide"*, J. Electrochem. Soc. 154, F83, 2007.
19. E. Slavcheva, U. Schnackenberg, W. Mokwa: "*Deposition of sputtered iridium oxide – Influence of oxygen flow in reactor on the film properties"*, Appl. Surf. Sci., **253**, 1964, 2006.
20. E. Slavcheva , I. Radev, S. Bliznakov, G. Topalov, P. Andreev, E. Budevski: "*Sputtered iridium oxide films as electrocatalysts for water splitting via PEM electrolysis*", Electrochim. Acta, **52,** 3889, 2007.
21. G. Chen, D. A. Delafuente, S, Sarangapani, T. E. Mallouk: *"Combinatorial discovery of bifunctional oxygen reduction – water oxidation electrocatalysts for regenerative fuel cells"*, Catalysis Today **67**, 341, 2001.
22. A. G. Dokoutchaev, F. Abdelrazzaq, M. E. Thompson: "*Multicomponent Electrodes for Water Oxidation: From Combinatorial to Individual Electrode Study*", Chem. Mater., **14**, 3343, 2002.
23. US Patent US-2002-0076582-1A.
24. M. B. Vukomirovic, P. Liu, J. T. Muckerman, R. R. Adzic: "*Electrodeposition of Pt onto RuO_2(110) Single-Crystal Surface"*, J. Phys. Chem. C, **111**, 15306, 2007
25. A. Bonakdarpour, R. Lobel, S. Sheng, T.L. Monchesky and J.R. Dahn, *"Acid stability and oxygen reduction activity of magnetron-sputtered $Pt_{1-x}Ta_x$ (0 <= x <= 1) films"*, J. Electrochem. Soc., **153** (12), A2304 (2006).
26. D.A. Stevens, J.M. Rouleau, R.E. Mar, A. Bonakdarpour, R.T. Atanasoski, A.K. Schmoeckel, M.K. Debe, and J.R. Dahn., *"Characterization and PEMFC testing of $Pt_{1-x}M_x$ (M=Ru,Mo,Co,Ta,Au,Sn) anode electrocatalyst composition spreads"*, J. Electrochem. Soc. **154**, B566, 2007.
27. S. Kinoshita, "*Anode Overpotential at Low Pt Loadings for Pure H_2*", ECS Transactions, **11** (1) 309, 2007.
28. R.T. Atanasoski, L.L. Atanasoska, D.A. Cullen, G.M. Haugen, K.L. More, G.D. Vernstrom: *"Fuel Cells Catalyst for Start-up and Shutdown Conditions: Electrochemical, XPS, and TEM Evaluation of Sputter-Deposited Ru, Ir, and Ti on Pt-Nano-Structured Thin Film (NSTF) Support"*, Electrocatalysis **3,** 284 – 297, 2012.
29. R T Atanasoski, LL Atanasoska**,** DA Cullen: "*Efficient Oxygen Evolution Reaction Catalysts for Cell Reversal and Start/Stop Tolerance*" in M. Shao ed., "*Electrocatalysis in Fuel Cells: A Non and Low Platinum Approach*", Chapter 22, pp.637 – 663. Springer, March, 2013.
30. RT Atanasoski, DA Cullen, GD Vernstrom, GM Haugen LL Atanasoska:"*A Materials-Based Mitigation Strategy for SU/SD in PEM Fuel Cells: Properties and Performance-Specific Testing of IrRu OER Catalysts"*, ECS Electrochem. Lett, **2** (3) F25-F28, 2013.
31. R. Koetz, S. Stucki, "O*oxygen evolution on ruthenium-iridium alloys*", J. Electrochem. Soc, **132**, 103, 1985.
32. Fuentes RE, Farell J, Weidner JW: "*Multimetallic electrocatalysts of Pt, Ru, and Ir supported on anatase and rutile TiO2 for oxygen evolution in an acid environment*". Electrochem Solid St Lett **14** (3): E5-E7, 2011.

33. Mattos-Costa FI, de Lima-Neto P, Machadoa SAS, Avaca LA: *"Characterization of surfaces modified by sol-gel derived RuxIr11-x O_2 coatings for oxygen evolution in acid medium"*, Electrochim Acta **44** (8):1515-1523,1998.
34. N. Danilovic, R. Subbaraman, K.-C. Chang, S.H Chang, Y. J. Kang, J. Snyder, A.P. Paulikas, D. Strmcnik, Y.-T Kim, D. Myers, V.R. Stamenkovic, N.M. Markovic: "*Activity–Stability Trends for the Oxygen Evolution Reaction on Monometallic Oxides in Acidic Environments"*, J. Phys. Chem. Lett., **5**, 2474–2478, 2014.
35. S.H Chang, J.G. Connell, N. Danilovic, R. Subbaraman, K.-C. Chang, V.R. Stamenkovic, N.M. Markovic: "*Activity-Stability Relationships in the Surface Electrochemistry of the Oxygen Evolution Reaction"*, Faraday Discuss., 2014, DOI: 10.1039/C4FD00134F
36. Jang SE, Kim H: *"Effect of water electrolysis catalysts on carbon corrosion in polymer 803 electrolyte membrane fuel cells"*, J Am Chem Soc **132**(42):14700–14701, 2010
37. T.D. Hatchard, J.E. Harlow, D.A. Stevens, Gary Chi-Kang Liu, R.J. Sanderson, N. van der Bosch, J.R. Dahn, G. M. Haugen, G.D. Vernstrom and R.T. Atanasoski,: *Rapid RDE Evaluation of Catalyst Performance and Durability During Transient Conditions: The Pt-Hf Binary System.* Electrochim. Acta. **56** (2011) 10436–10442
38. DA Cullen, KL More, LL Atanasoska, RT Atanasoski: "*Impact of IrRu Oxygen Evolution Reaction Catalysts on Pt Nanostructured Thin Films under Start-Up/Shutdown Cycling*", J. Power Sources, 269, 671-681(2014)
39. D. A. Cullen, K. L. More, K. S. Reeves, G. D. Vernstrom, L. L. Atanasoska, G. M. Haugen, and R. T. Atanasoski: *Characterization of durable nanostructured thin film catalysts tested under transient conditions using analytical aberration-corrected electron microscopy,* ECS Transactions, **41** (1) 1099-1103, 2011
40. LL Atanasoska, DA Cullen, AE Hester, RT Atanasoski: "*XPS and STEM of the interface formation between ultra-thin Ru, Ir and Pt layers and perylene red catalyst support whiskers*", ECS Transactions, **50**, 19 -33, 2013.